

SUPERCONDUCTING SUPER COLLIDER (SSC)
ACCELERATOR MAGNET
CRYOSTAT PREDESIGN

Report Number SSC-LBL-306-RWB
1 May 1985

Revision date 5-16-85

Prepared for

LAWRENCE BERKELEY LABORATORY
University of California
One Cyclotron Road
Berkeley, CA 94720

Contract No. 4531210
GDC PIN No. 84-P-0205

Prepared by

GENERAL DYNAMICS CONVAIR DIVISION
P. O. Box 85377
San Diego, CA 92138

Approved by



R. W. Baldi
Program Manager

FOREWARD

This report documents the preliminary design of a 55-foot-long cryostat cryostat for the Superconducting Super Collider (SSC) accelerator magnet system. The work was sponsored by the Department of Energy under the direction of the University of California -- Lawrence Berkeley Laboratory subcontract 4531210. This work was performed during the five-month period beginning December 1984.

ACKNOWLEDGEMENTS

The Lawrence Berkeley Laboratory personnel who made significant contributions to this program are:

K. L. Mirk	Technical Director
C. Taylor	Technical Director
R. Wolgast	Technical Director

General Dynamics Convair Division personnel who made significant contributions to this program are:

K. L. Agarwal	Materials & Processes
R. W. Baldi	Program Manager
K. R. Dawson	Structural Analysis
J. E. Burgeson	Design
M. A. Hilal	Electromagnetic Analysis
T. E. Johnson	Manufacturing/Producibility
A. Mancuso	Structural Analysis
S. D. Peck	Thermodynamic Analysis
J. L. Pickering	Structural Analysis
S. D. Zullo	Design

TABLE OF CONTENTS

<u>SECTION/TITLE</u>	<u>PAGE</u>
SUMMARY	
1.0 INTRODUCTION	1-1
2.0 TRADE STUDY	2-1
2.1 ALTERNATIVE CONCEPTS CONSIDERED	2-1
2.2 ALTERNATIVE CONCEPT DESCRIPTION AND EVALUATION	2-4
2.2.1 DESIGN DESCRIPTION	2-4
2.2.2 STRUCTURAL ANALYSIS	2-14
2.2.3 THERMODYNAMICS ANALYSIS	2-44
2.2.4 PRODUCIBILITY CONSIDERATION	2-50
2.3 SUMMARY OF THE SELECTED SUPPORT CONCEPT	2-52
3.0	
3.1 DESIGN DESCRIPTION	3-1
3.1.1 INTRODUCTION	3-1
3.1.2 COLD MASS SUPPORT	3-1
3.1.3 THERMAL RADIATION SHIELDS	3-4
3.1.4 FLUID TRANSPORT LINES	3-6
3.1.5 MULTILAYER INSULATION	3-8
3.1.6 VACUUM VESSEL	3-8
3.1.7 MAGNET INTERCONNECT REGION	3-9
3.2 STRUCTURAL ANALYSIS	3-10
3.2.1 INTRODUCTION	3-10
3.2.2 DESIGN CRITERIA	3-10
3.2.3 MATERIALS PROPERTIES	3-11
3.2.4 COLD MASS - HELIUM SUPPORT VESSEL AND SUPPORT ANALYSIS	3-11
3.2.5 BELLOWS ANALYSIS	3-22
3.2.6 VACUUM VESSEL ANALYSIS	3-23
3.2.7 VACUUM VESSEL/CLEVIS ANALYSIS	3-26
3.2.8 ANALYSIS OF THE HELIUM SUPPLY AND RETURN LINES	3-29
3.2.9 THERMAL SHIELDS ANALYSIS	3-30
3.2.10 REFERENCES	3-33

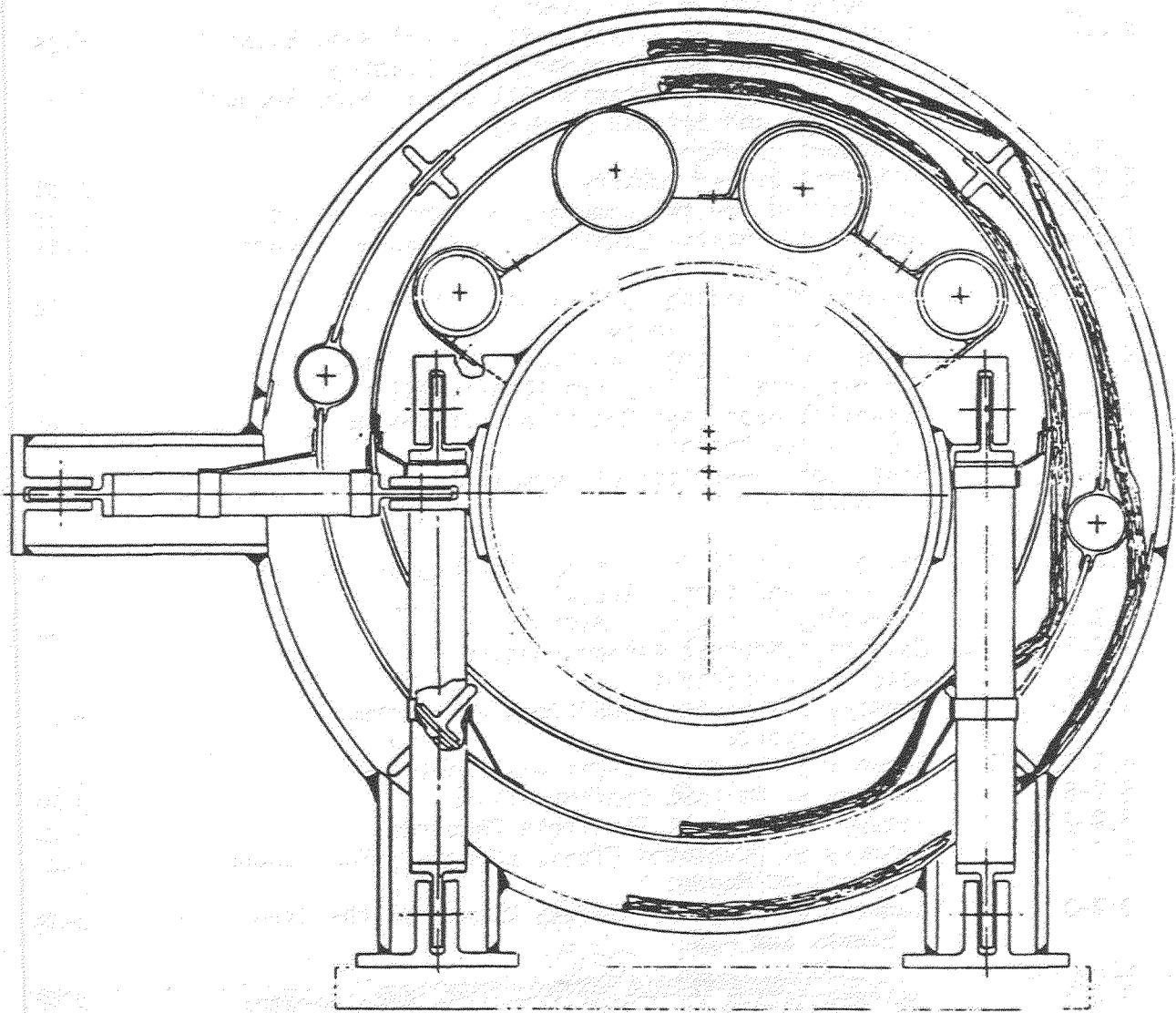
3.3	THERMODYNAMICS ANALYSIS	3-34
3.3.1	LIFE CYCLE COST OF REFRIGERATION	3-34
3.3.2	THERMAL INTERCEPT LOCATIONS	3-39
3.3.3	MLI TRADE STUDY	3-41
3.3.4	BASELINE DESIGN THERMAL ANALYSIS	3-48
3.3.5	SUMMARY	3-58
3.4	EDDY CURRENTS ANALYSIS	3-59
3.4.1	INFINITELY LONG CONDUCTING PLATE	3-59
3.4.2	EDDY CURRENT IN TWO-DIMENSIONAL SURFACES	3-60
3.4.3	DISCUSSION	3-61
3.5	MATERIALS AND PROCESSES	3-64
3.5.1	INTRODUCTION	3-64
3.5.2	SPECIFIC CRITERIA USED IN SELECTION OF MATERIALS	3-66
3.6	PRODUCIBILITY ANALYSIS	3-68
3.6.1	COLD-MASS SUPPORTS	3-68
3.6.2	THERMAL RADIATION SHIELDS	3-68
3.6.3	FLUID LINES	3-69
3.6.4	MULTILAYER INSULATION	3-69
3.6.5	VACUUM VESSEL AND FINAL ASSEMBLY	3-69
4.0	CONCLUSIONS AND RECOMMENDATIONS	4-1
4.1	STRUCTURAL ANALYSIS	4-1
4.2	THERMODYNAMIC ANALYSIS	4-1
4.3	MANUFACTURING/PRODUCIBILITY	4-1

LIST OF FIGURES

<u>FIGURE NUMBER</u>	<u>TITLE</u>	<u>PAGE</u>
2.1-1a	Design Concepts	2-2
2.1-1b	Design Concepts	2-3
2.2-1	Compression Strut Arrangement	2-5
2.2-2	Tension Strut Arrangement	2-7
2.2-3	Double-Ring Support	2-9
2.2-4	Elliptical Titanium Support	2-10
2.2-5	Elliptical G-10 Support	2-11
2.2-6	Titanium "J" Support	2-13
2.2-7	Test Specimen - Elliptical Ring	2-15
2.2-8	Instrumentation Layout for G-10CR Elliptical Ring Creep Test	2-18
2.2-9	Average Creep Response of G-10CR Elliptical Ring Support	2-19
2.2-10	Thermal Expansion of 6Al-4V Titanium	2-20
2.2-11	Temperature Dependence of K_{Ic} for Ti-6Al-4V Alloys	2-21
2.2-12	Elliptical Ring Support Configuration	2-28
2.2-13	Finite-Element Model of Elliptical Ring	2-29
2.2-14	Node Identification on Elliptical Ring Model	2-30
2.2-15	Double-Ring Support	2-34
2.2-16	Section A-A J-Support Geometry Titanium	2-35
2.2-17	J-Support Model and Boundary Conditions	2-36
2.2-18	Compression Strut Supports for the Cold Mass	2-38
2.2-19	Tension Strut Supports for the Cold Mass	2-39
3.1-1	Cryostat Cross Section	3-2
3.1-2	Cold-Mass Support Strut	3-3
3.1-3	80°K Thermal Shield	3-5
3.1-4	20°K Thermal Shield	3-7
3.2-1	Cold-Mass Geometry	3-14
3.2-2	Cold-Mass Deflection Between Supports and Load at the Supports	3-15
3.2-3	Compression Strut Supports for the Cold Mass	3-19
3.3-1	Generalized Support for Intercept Location Analysis	3-39
3.3-2	Combined Material and Refrigeration Costs for a 300K-80K Blanket	3-46
3.3-3	Combined Material and Refrigeration Costs for a 80K-5K Blanket	3-47
3.3-4	Thermal Parameters for Baseline Support Analysis	3-50
3.3-5	Geometry and Nomenclature of Shield Thickness Analysis	3-54
3.4-1	Infinitely Long Shield	
3.4-2	Two-Dimensional Surface for Eddy Current Calculations	3-63

LIST OF TABLES

<u>TABLE NUMBER</u>	<u>TITLE</u>	<u>PAGE</u>
2.2-1	G-10CR Material Properties	2-17
2.2-2	Mechanical and Physical Properties of 6Al-4V Titanium Alloy	2-17
2.2-3	Elliptical Ring Support Loading	2-23
2.2-4	Stress Summary of G-10CR Elliptical Ring Support (Dead Weight and Transportation Loading)	2-24
2.2-5	Stress Summary of G-10CR Elliptical Ring Support (Thermal and Seismic Loading)	2-25
2.2-6	Stress Summary of Titanium Elliptical Ring Support (Dead Weight and Transportation Loading)	2-26
2.2-7	Stress Summary of Titanium Elliptical Ring Support (Thermal and Seismic Loading)	2-27
2.2-8	J-Support Loading	2-32
2.2-9	J-Support Stress Summary	2-33
2.2-10	Rod Loading for the Compression Configuration	2-37
2.2-11	Summary of Loading Conditions - Titanium Support - Five Supports	2-41
2.2-12a	Summary of Loading Conditions - Titanium - Fiberglass - 4 Supports	2-42
2.2-12b	Summary of Loading Conditions - Titanium - Fiberglass - 4 Supports (Continued)	2-43
2.2-13	Potential Heat Leak Reduction for Design Evolution Options	2-46
2.2-14	Heat Leak Comparison of Support Concept Candidates	2-48
3.2-1	Design Criteria for the LBL SSC Magnet Support System and Vacuum Vessel	3-10
3.2-2	Operating Pressure Conditions	3-12
3.2-3	Cold-Mass Support Design Loading	3-13
3.2-4	Material Properties	
3.2-5a	Summary of Loading Conditions - Titanium - 4 Supports	3-20
3.2-5b	Summary of Loading Conditions (Continued)	3-21
3.2-6	Summary of Bellows Configurations	3-24
3.2-7	Vacuum Vessel Wall Thickness Required	3-25
3.2-8	Summary of Developed Clevis Loading - Four Support Locations/Magnet	3-27
3.2-9	Summary of Margin-of-Safety Values on the Strut Clevis and Pin	3-28
3.3-1	Representative Values of Cryogenic Refrigerator Coefficients of Performance (COP)	3-36
3.3-2	Thermal Conductivity Integrals for Titanium and G-10	3-42
3.3-3	Baseline Design Heat Leak Summary	3-57
3.5-1	Structural Material Selection for LBL Cryostat	3-67
3.6-1	Vacuum-Vessel Material Cost Comparison	3-70



SUMMARY

The overall objective of this study was to produce a preliminary engineering design of a 55-foot long cryostat for the dipole magnets to be used in the Superconducting Super Collider (SSC) program. Principal components of the cryostat include the thermal radiation shields, multilayer insulation, fluid transport lines, cold-mass supports, and the vacuum vessel. Design of the dipole magnet interconnect region was also included. The scope of this engineering study included overall assembly layouts, detailed structural analyses, and thermodynamic, electromagnetic analysis of key components of the cryostat.

This study was based on the "1-in-1", cold iron, 6.5 tesla, cosine theta, superconducting dipole magnet designated reference D. The reference D design evolved during 1984 and early 1985 from the collaborative efforts of Brookhaven National Laboratory, Fermi National Laboratory, and Lawrence Berkeley Laboratory.

A cross section of the cryostat design produced as part of this study is shown on the facing page. Key features of this design are described below:

- o A compression strut arrangement was selected for the cold-mass support. A major advantage of this design arrangement is the exceptional access it provides for installation of the cryogenic plumbing and other cryostat components. These struts are stationed at four positions along the length of the magnet. In order to maintain less than 0.5 mm (0.020 inch) sag between the supports, the 304L stainless-steel helium vessel thickness was increased to 6.4 mm (0.25 inch).
- o Titanium alloy was selected as the baseline material for the struts since it can sustain all strength and long-term alignment requirements. However, other material options with lower heat leak characteristics, such as fiberglass epoxy, can be substituted if their long-term creep behavior and strength characteristics are proven to meet the operational requirements for SSC. It is highly probable that fiberglass epoxy could be used for the side and axial struts.
- o 6061-T6 aluminum alloy was selected for the 80K thermal radiation shield. To reduce eddy currents in this shield during a rapid discharge of the magnet, radial slots are to be cut through the shield at 40.6 cm (16.0 in) intervals along its length.
- o 304L stainless steel alloy was selected for the intermediate temperature thermal radiation shield. Stainless steel provides sufficient thermal conductivity at the lower temperature with greatly reduced eddy current forces due to its high electrical resistivity. It also is directly compatible with stainless-steel plumbing which eliminates the need for intermetallic transition joints for the bellows connections that are required for the aluminum shield.

- o Aluminized mylar separated by Dacron scrim was selected for the multi-layer insulation. A total of 20 layers was selected to cover the intermediate temperature shield and a total of 30 layers was selected to cover the 80K shield. These numbers of layers were determined by minimizing the combined estimated cost of the installed MLI plus the magnet operating costs attributed to radiation losses. For ease of installation, these MLI blankets are designed to be a large rectangular shape.
- o A 6061-T6 aluminum alloy was selected for the vacuum vessel. Aluminum was selected over stainless steel due to its lower cost. Mild steel would provide an even greater cost savings if its ability to safely sustain a cryogenic leak within the cryostat were proven. However, some of the savings for substituting mild steel would be partially offset by the added cost of corrosion protection and future maintenance.
- o The operational requirements for the bellows in the interconnection region are very stringent. To meet cyclic life requirements, and to minimize bellows length, Inconel 625 alloy material was selected for all bellows except for the beam-line bellows for which type 321 stainless steel was sufficient. In addition, a double-walled bellows with vacuum guard provision was selected for the beam line to insure leak-tight integrity. To meet the squirm pressure requirements, two in-line bellows were specified in all locations except for the helium vessel for which one bellows was sufficient. Adequate support will have to be provided between these bellows for the final design. Overall deflections of the vacuum vessel can be accommodated with bellows in special areas, such as the spool regions; therefore, no bellows were included in the dipole magnet interconnect regions. Instead, a low-cost welded aluminum sleeve has been included.

Although further optimization and design improvements must be performed, our analysis indicates that the preliminary design presented herein is highly producible and cost effectively meets all performance objectives.

1.0

INTRODUCTION

The cryostat preliminary design study was performed in essentially two phases. In the initial phase, a total of six alternative cold-mass support concepts were studied. Based on this study, a compression strut arrangement was selected. Details of the concepts considered and the analysis performed to arrive at this choice are documented in Section 2.0 of this report.

Selection of the support arrangement was a major milestone for this study. Once this selection was made, the second phase of this study was initiated. In this phase, the arrangement and design of the other cryostat components was further refined. These components include an intermediate temperature radiation shield, an 80K radiation shield, multi-layer insulation, fluid transfer lines, electrical busings, and a vacuum vessel. Details of the design and analysis of these components, as well as further refinements of the strut components, are described in Section 3.0 of this report.

Section 4.0 of this report provides conclusions regarding this preliminary design and recommendations for future programs.

The preliminary design presented herein was developed in accordance with the design criteria provided in Reference 1.0-1. The essence of all requirements was met with the exception of the heat load as described in Section 3.5 of this report.

References

- 1.0-1. SSC Design D Cryostat Design Criteria, Initial Release, FNAL Memo dated 15 February 1985.

SECTION 2.0

SUPPORT CONCEPT TRADE STUDY

2.1 ALTERNATIVE CONCEPTS CONSIDERED. The initial phase of this design study consisted primarily of engineering trade studies of alternative support concepts for the cold mass. A total of six different design concepts were evaluated.

- o Compression struts
- o Tension struts
- o Double ring
- o Titanium elliptical beam
- o Fiberglass/epoxy elliptical beam
- o Titanium J's

Each of these support concepts are illustrated in the upper portion of Figures 2.1-1a and 2.1-1b. A summary chart highlighting the relative advantages and disadvantages identified for each concept is provided in the lower portion of Figures 2.1-1a and b. These relative merits were subjectively evaluated in terms of operational performance, producibility, cost, and potential for improvement. Based on this evaluation, the compression strut arrangement was selected for further refinement under this study. The following sections provide an in-depth description of each of these approaches and the supportive analyses of them.

Figure 2.1-1a. Design Concepts

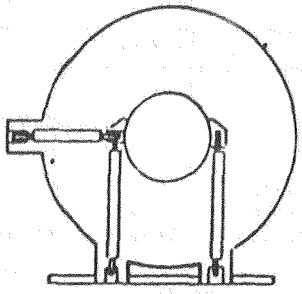
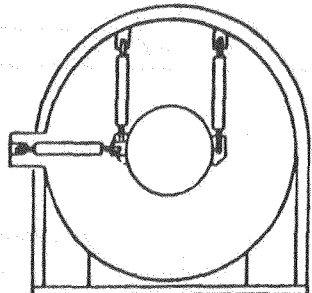
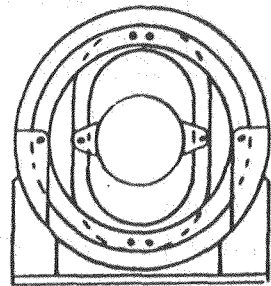
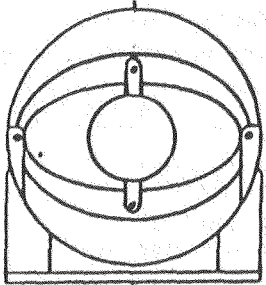
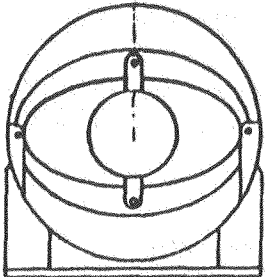
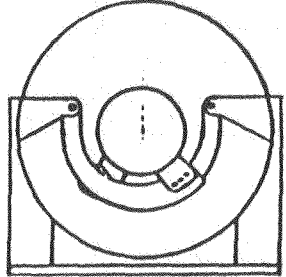
COMPRESSION STRUTS		TENSION STRUTS		DOUBLE RING	
					
DESIGN CONSIDERATIONS		DESIGN CONSIDERATIONS		DESIGN CONSIDERATIONS	
ADVANTAGES	DISADVANTAGES	ADVANTAGES	DISADVANTAGES	ADVANTAGES	DISADVANTAGES
<p>Small 22.0-inch O.D. vacuum vessel.</p> <p>Easy to assemble.</p>	<ul style="list-style-type: none"> Requires 5.5-inch extension on vacuum vessel for the side support. 	<ul style="list-style-type: none"> Small 22.0-inch O.D. vacuum vessel. Smaller dia. rods required for tension load than compression. 	<ul style="list-style-type: none"> Requires outside reinforcing ring. Requires 5.5-inch extension on vacuum vessel for the side support. 	<ul style="list-style-type: none"> Lowest stress for G-10. High axial flexibility. 	<ul style="list-style-type: none"> Complex geometry. Very large 26.0-inch O.D. vacuum vessel. Multiple parts. Poor material utilization.
THERMAL		THERMAL		THERMAL	
<p>Lowest 4.5K heat load; < .12 watts per magnet.</p> <p>High intercept efficiency.</p> <p>Easy to place shields.</p>	<ul style="list-style-type: none"> St. stl. rod ends contribute to LHe heat leak. Heat leak penalty to size rods for buckling. Internal radiation shield will be req'd. 	<ul style="list-style-type: none"> Lowest 4.5K heat load; < .12 watts/magnet. Easy to place shields. High intercept efficiency. 	<ul style="list-style-type: none"> St. stl. rod ends increase heat leak. Internal radiation shield required. 	<ul style="list-style-type: none"> Potential for very low heat leak. 	<ul style="list-style-type: none"> Difficult to place shields. Limited room for cryogen plumbing.
MANUFACTURE		MANUFACTURE		MANUFACTURE	
<p>Moderate assembly cost.</p> <p>Less tooling - use optics.</p> <p>Non-recurring tooling costs.</p>	<ul style="list-style-type: none"> More welding. High tooling costs. 	<ul style="list-style-type: none"> Difficult to assemble. Additional tooling. More machined parts. More welding. 	<ul style="list-style-type: none"> Additional tooling. High fabrication cost. High material cost. Additional parts increase fabrication costs. 		

Figure 2.1-1b. Design Concepts

TITANIUM ELLIPSE		G-10 ELLIPSE		TITANIUM J's	
					
DESIGN CONSIDERATIONS		DESIGN CONSIDERATIONS		DESIGN CONSIDERATIONS	
ADVANTAGES	DISADVANTAGES	ADVANTAGES	DISADVANTAGES	ADVANTAGES	DISADVANTAGES
<ul style="list-style-type: none"> o Symmetrical distribution. o Lower bending moment. o Simple construction - can be split into upper and lower halves. 	<ul style="list-style-type: none"> o Large 24.0-inch O.D. vacuum vessel. 	<ul style="list-style-type: none"> o Symmetrical distribution. o Simple construction. 	<ul style="list-style-type: none"> o Poor material utilization. o Material creep limits long-term load capabilities. o Requires two supports per location due to creep problem. 	<ul style="list-style-type: none"> o Stable configuration. o Provides a long heat path between the cold mass and vacuum vessel. 	<ul style="list-style-type: none"> o Higher stress than full ring. o Large 25.0-inch O.D. vacuum vessel. o More displacement for lateral seismic o High local stress. o Stress limited by fracture mechanics uncertainty.
THERMAL		THERMAL		THERMAL	
<ul style="list-style-type: none"> o Lowest overall heat leak. - .70 KW at compressor. o High intercept efficiency. 	<ul style="list-style-type: none"> o Correct placement of shields will be difficult. 	<ul style="list-style-type: none"> o Low conductivity material. 	<ul style="list-style-type: none"> o Intercept efficiency not as good as titanium. o Correct placement of shields will be difficult. 	<ul style="list-style-type: none"> o Longer heat path. 	<ul style="list-style-type: none"> o Difficult to analyze. o Not significantly better than titanium ellipse. o Shields very difficult to locate properly.
MANUFACTURE		MANUFACTURE		MANUFACTURE	
<ul style="list-style-type: none"> o Low fabrication cost. o Simple assembly. 	<ul style="list-style-type: none"> o Lack of adjustment. o High tooling cost. o Moderate matl. cost. 	<ul style="list-style-type: none"> o Simple assembly 	<ul style="list-style-type: none"> o High material cost. o Lack of adjustment. o High tooling cost. o Must assemble from end. 	<ul style="list-style-type: none"> o Simple assembly. o Low fabrication cost. 	<ul style="list-style-type: none"> o Moderate matl. cost. o moderate tooling cost.

2.2 ALTERNATIVE CONCEPT DESCRIPTION AND EVALUATION

2.2.1 DESIGN DESCRIPTION. The six (6) support concepts for the cold mass that were studied are described in this section. In addition, the relative advantages and disadvantages of each support system are described.

All the support concepts studied were sized to meet all anticipated handling, manufacturing, and operational requirements, such as:

- o Gravity (long-term alignment)
- o Handling
- o Shipping
- o Seismic
- o Thermal-induced deflection
- o Alignment features

Detailed criteria for requirements can be found in Sections 2.2.2 and 3.2 of this report.

2.2.1.1 Compression Struts. Each magnet has four (4) sets of struts, as shown in Figure 2.2-1. This arrangement results in a total of eight (8) compression struts, four (4) side struts, and one (1) axial strut per magnet. The struts are made from titanium tubing and have titanium end fittings welded to the tube. The titanium alloy is Ti-6AL-4V ELI in the annealed condition. This titanium is a special low interstitial grade for use at low cryogenic temperatures.

Use of compression struts to support the cold mass provides exceptional access for installation of the cryogenic plumbing as well as other cryogenic components. Also, the problems associated with flaw growth and possible tension failures are eliminated. Due to buckling considerations, compression struts have a larger cross-sectional area than tension struts. This results in a small heat leak penalty, but is considered acceptable because of the other producibility and operational benefits.

The vacuum vessel design associated with the compression strut arrangement has a 22-inch outside diameter, which is smaller than the other type support systems. Less aluminum alloy will be required to manufacture the vacuum vessel, resulting in lower material costs. However, a cylinder-shaped extension is required on the side of the vacuum vessel to accommodate the side strut.

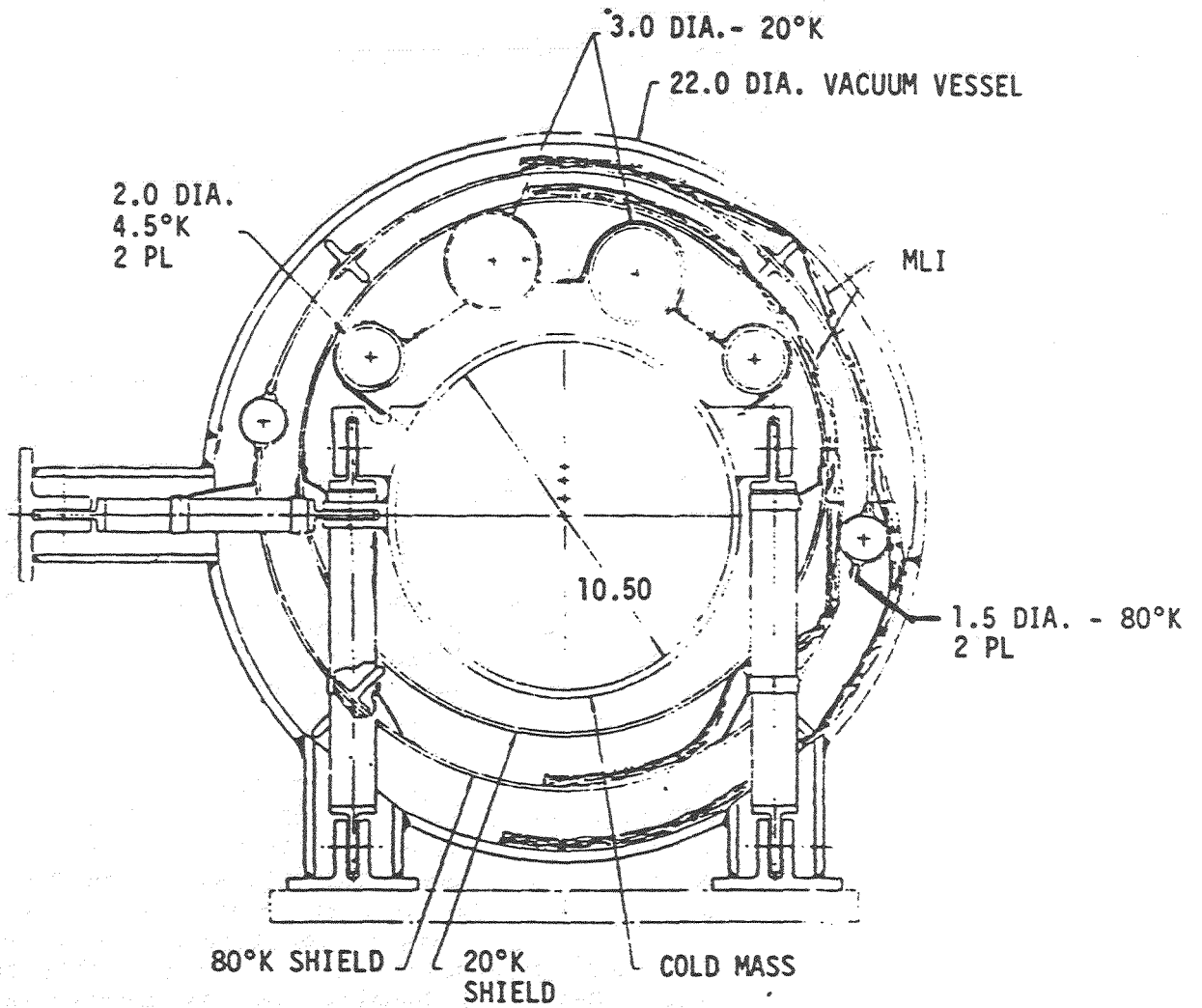


Figure 2.2-1. Compression Strut Arrangement

The LN₂ and He radiation shield have a smaller circumference than the shield circumference for the other support systems. This results in reduced heat load to the radiation shields.

The radiation shields and the MLI insulation are easy to install, since the top portion of the vacuum vessel is open. The struts are first installed in the lower part of the vacuum vessel and the cold mass lowered into place and the bolts installed. Installing the cold mass is a relatively easy operation, however, substantial tooling is required in order to align the strut bolt holes.

A further reduction in the heat load can be obtained by having the side strut and axial strut tubes made of epoxy/glass laminate. These tubes are not normally subjected to sustained loads and, therefore, they are not subject to creep.

2.2.1.2 Tension Struts. The strut support system for this arrangement is similar to the compression strut arrangement described in 2.2.1.1. The tension arrangement for support of the cold mass is shown in Figure 2.2-2. There are a total of eight (8) tension struts, four (4) side struts, and one (1) axial strut per magnet. The struts are made of titanium tubing and have titanium end fittings welded to the tube. The titanium alloy is annealed Ti-6AL-4V ELI. The tension struts have the minimum cross-section area for heat leak to the cold mass.

The vacuum vessel for the tension support arrangement requires an outside reinforcing ring to react the vertical strut loads. Also, a cylinder-shaped extension is required on the side of the vacuum vessel to accommodate the side strut. This requires a total of four (4) rings and four (4) cylinders per magnet, adding to the manufacturing cost.

Assembly of the cold mass within the vacuum vessel is difficult because the cold mass and vacuum vessel must be upside down in order for the bolts to be installed on the struts. The LN₂ and He radiation shields and MLI insulation are similar to the compression struts described in section 2.2.1.1. While the coil is upside-down, the lower portion of the vacuum vessel is welded in place. Then the magnet is rotated 180° to its normal position.

The tension strut approach was not selected, primarily due to the four (4) added reinforcing rings required for the vacuum vessel and the handling problems associated with rotating the magnet during assembly.

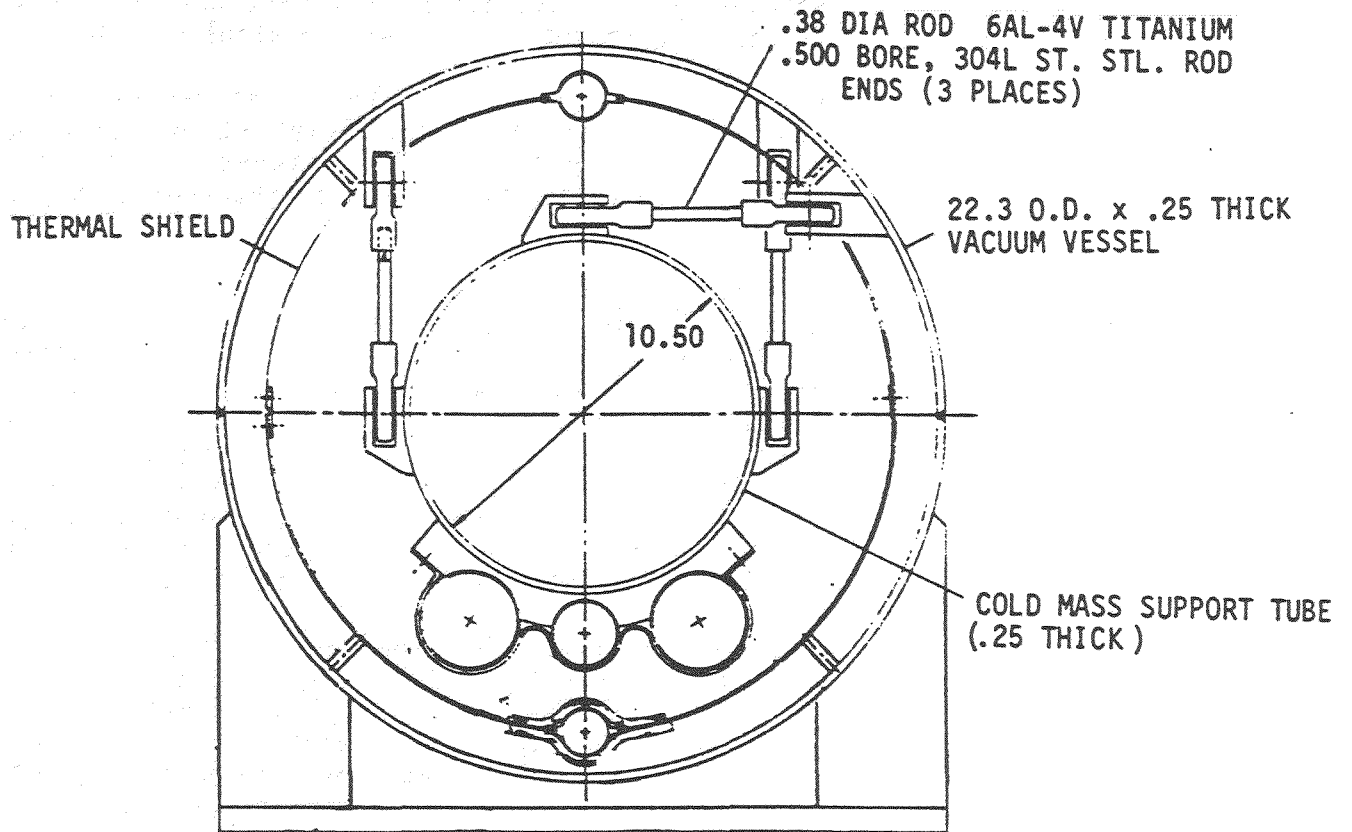


Figure 2.2-2. Tension Strut Arrangement

2.2.1.3 Double Ring. Each magnet has four (4) sets of double rings supporting the cold mass, as shown in Figure 2.2-3. This results in four (4) G-10 epoxy/glass fabric laminate cold mass support rings, four (4) 304L stainless-steel support rings, and a titanium alloy axial strut.

The LN₂ radiation shield and the He radiation shield are complex due to the double ring supports. The radiation shields, MLI insulation, and plumbing are difficult to install due to limited available space. The vacuum vessel outside diameter is a relatively large 26 inches.

The double ring support concept was not selected because of its high parts count, high fabrication cost, high material cost, and the fact that the vacuum vessel diameter exceeds the allowable space envelope.

2.2.1.4 Titanium Ellipse. There are four (4) elliptical titanium cold mass support frames and one titanium axial load strut for each magnet. The titanium alloy is annealed Ti-7AL-4V ELI. Figure 2.2-4 shows the elliptical titanium support system.

The elliptical support frames make the LN₂ radiation shield and He radiation shield complex. The radiation shields, MLI insulation, and plumbing are difficult to install due to the support frames, and the design lacks adjustment and requires expensive tooling in order to hold the required tolerances. The vacuum vessel outside diameter is a relatively large 24 inches.

The elliptical titanium support system was not selected. With this support concept, the radiation shields and MLI are difficult to position and install. Also, the vacuum vessel diameter is larger than desired.

2.2.1.5 G-10 Ellipse. This design is similar to the titanium ellipse design described in section 2.2.1.4. There are four (4) elliptical G-10 epoxy/glass fabric laminate cold mass support frames and one titanium axial load strut for each magnet. Figure 2.2-5 shows the elliptical support system. The LN₂ and He radiation shields are complex due to the elliptical support frames and the radiation shields, MLI insulation, and plumbing are difficult to install and position. Tests run at General Dynamics on a G-10CR elliptical frame to determine long-term creep capability have shown excessive creep and inability to maintain acceptable alignment of the cold mass. The outside diameter of the vacuum vessel is a relatively large 24 inches. Due to the above problems, this design was not selected.

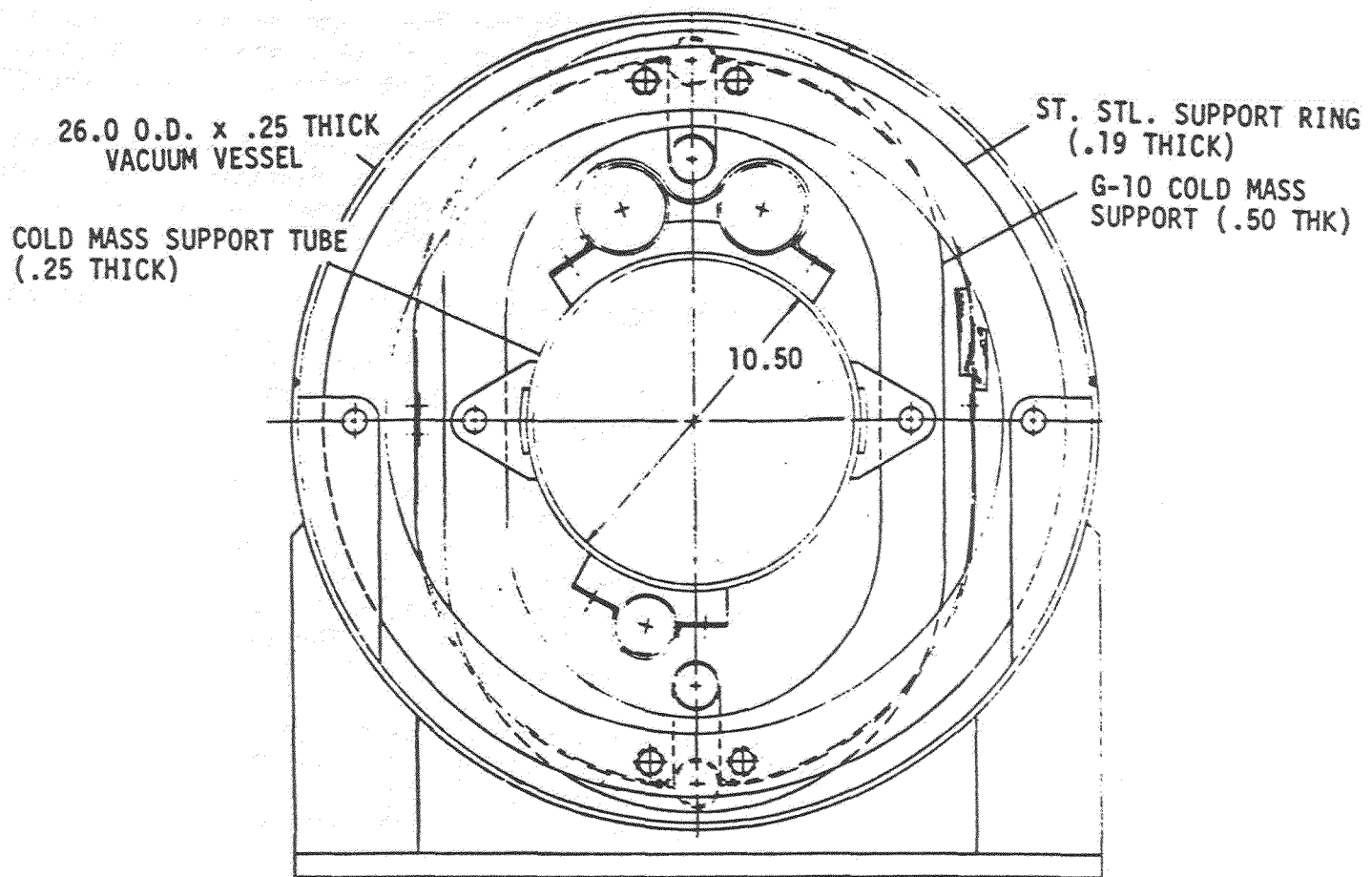


Figure 2.2-3. Double-Ring Support

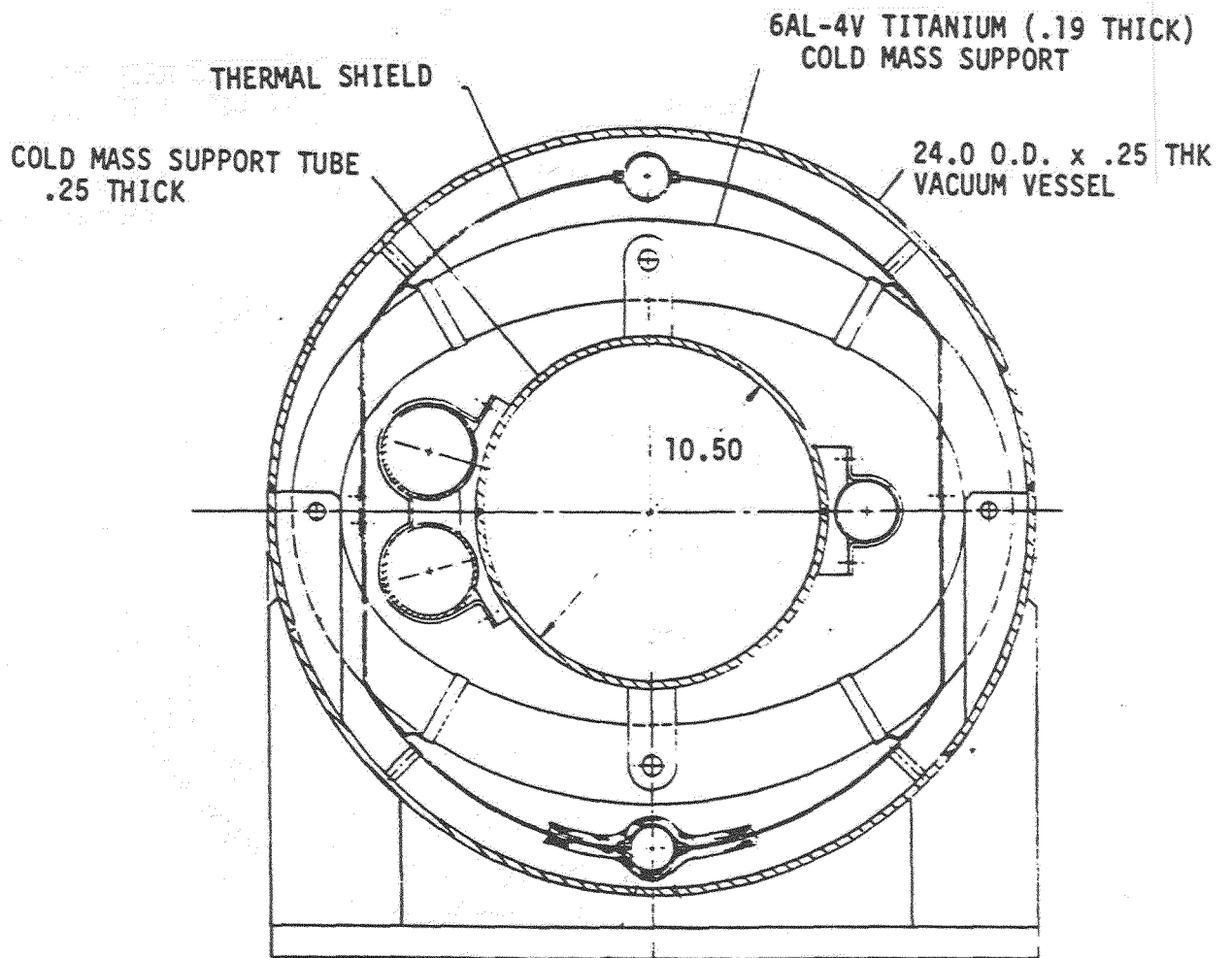


Figure 2.2-4. Elliptical Titanium Support

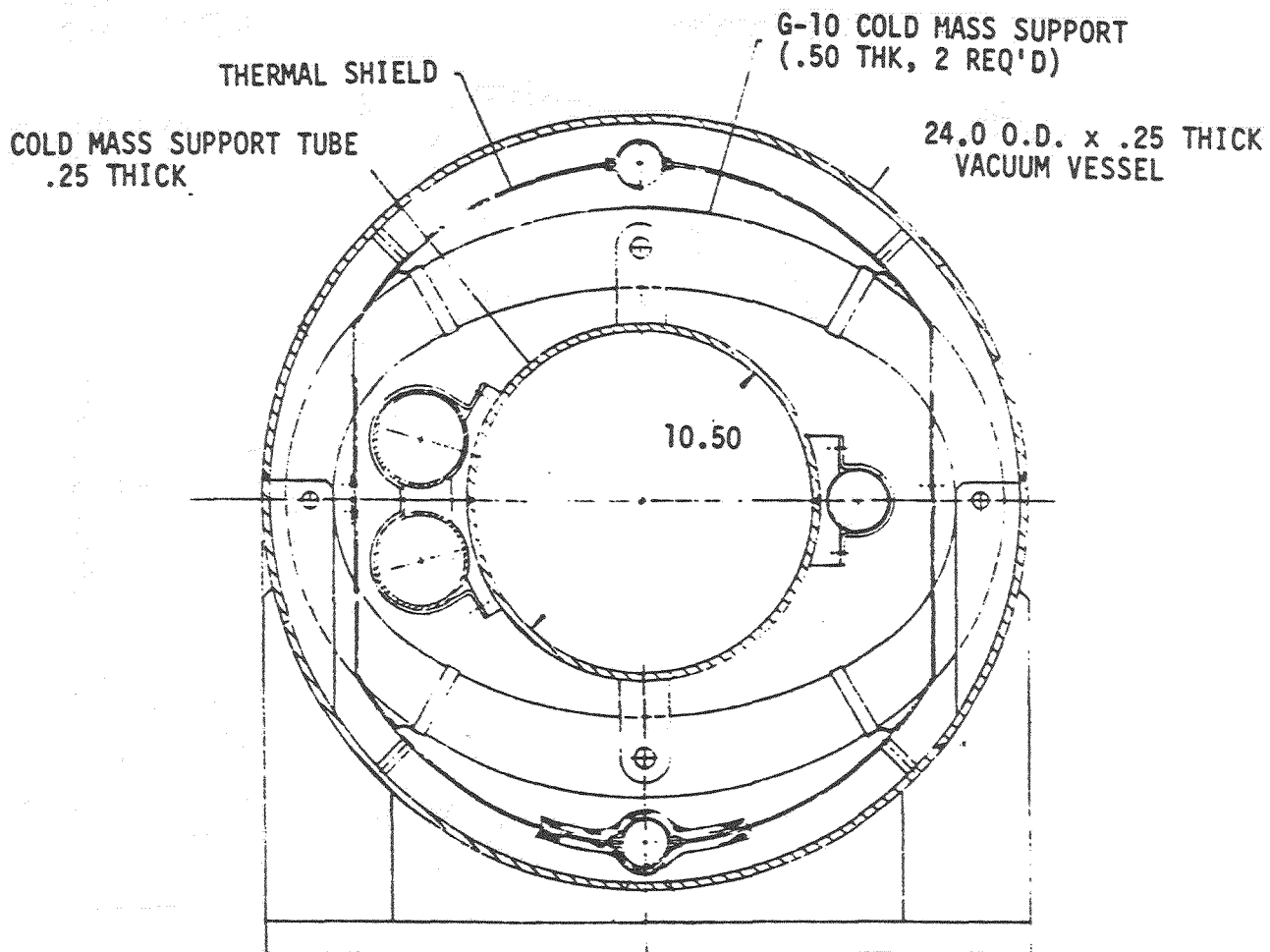


Figure 2.2-5. Elliptical G-10 Support

2.2.1.6 Titanium J's. There are four (4) pairs of titanium cold mass support "J" fittings and one titanium axial load strut for each magnet. The titanium alloy is annealed Ti-6AL-4V ELI. Figure 2.2-6 shows the "J" support of the cold mass.

The LN₂ and He radiation shields are fairly simple and straight-forward in this design. Installation of the radiation shields, MLI, and plumbing is easier than with the ellipse or double ring types. Fabrication and tooling costs are moderate. However, deflections will be larger than in most versions and the 25-inch outside diameter of the vacuum vessel exceeds the allowable space envelope.

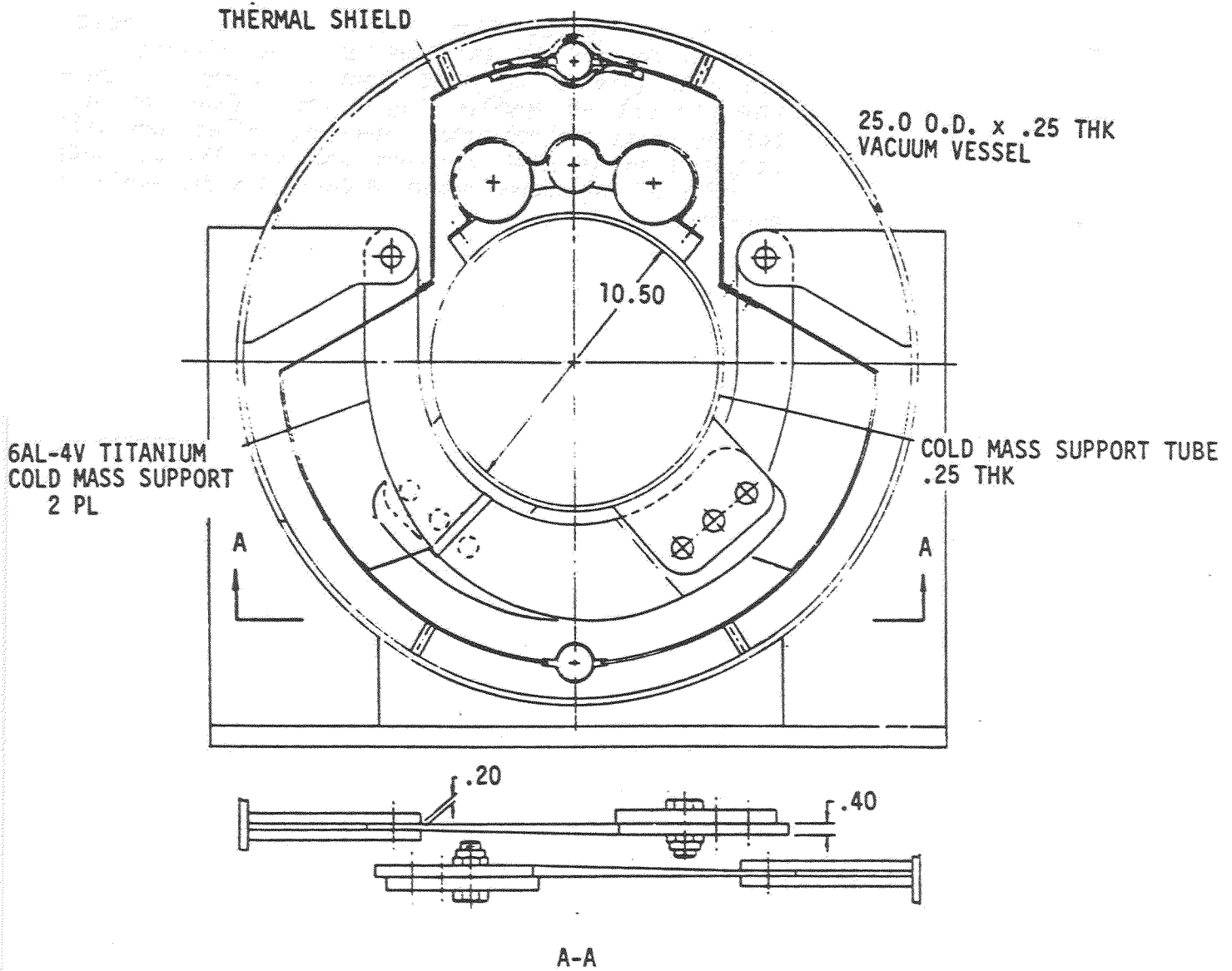


Figure 2.2-6. Titanium "J" Support

2.2.2 STRUCTURAL ANALYSIS.

2.2.2.1 Material Considered for Support Concepts. The materials considered included:

- 1) G-10CR
- 2) Titanium 6AL-4V (ELI)
- 3) Fiberglass - Ohio Brass

G-10CR Material Characteristics. The following is a discussion of the material properties of G-10CR.

The G-10CR material is an industrial high-pressure, glass-reinforced epoxy laminate. It is commonly used for electrical and thermal insulation in superconducting magnets. The CR grade rating implies a predictable cryogenic-radiation performance. The material consists of woven glass-reinforced laminates with epoxy resin developed for their high strength-to-weight ratios, low thermal and electrical conductivity, and ease of processing, and a glass laminate with polyimide resin for radiation resistance. The glass fabric is a plain weave produced in a conventional loom by interlacing warp (length) threads (43 +/- 3 per inch) and fill (width) threads (32 +/- 2 per inch). The standard material laminate is developed with layers of fabric orientated in the same direction (90°). The material properties are dependent upon the orientation of the threads because of the different numbers of threads in the warp/fill directions.

A special G-10CR laminate lay-up is used in this study in order to establish a more isotropic material behavior. The laminate has a lay-up of 135°/90°/45°/0°. The material characteristics of this material are not available in literature and have to be developed using the standard (90°) characteristics. The characteristics are expected to be more directionally uniform and are, therefore, termed "pseudo-isotropic."

One of the primary concerns regarding the use of this material for the cold mass support application was its creep characteristics under dead-weight loading over time. GDC discretionary funding was used to perform a creep response test on a prototype G-10CR elliptical ring support. The test specimen configuration is shown in Figure 2.2-7. The support thickness is 0.475 inches and

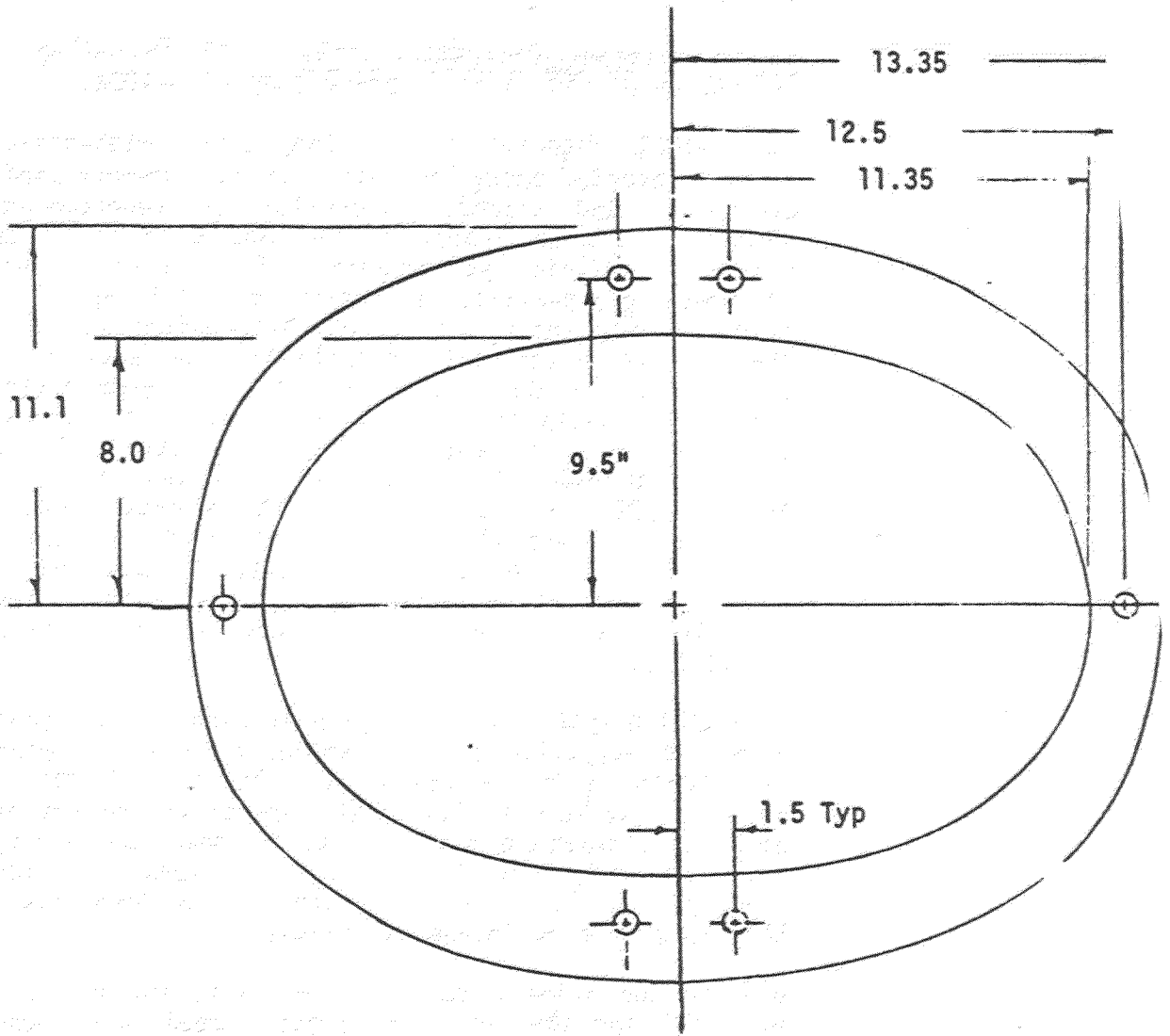


Figure 2.2-7. Test Specimen - Elliptical Ring

made of the G-10CR pseudo-isotropic material previously described. The test fixture that is to be used for this test is illustrated in Figure 2.2-8. The fixture is constructed of 12.25-inch by 12-inch wide flange "erector" beams. The test specimen is attached to the test fixture using shear pins into the steel clevis. Aluminum channel is bolted to the test specimen simulating the attachment of the cold mass and is also used to load the specimen (dead weight).

The entire test fixture was enclosed with 1-1/2-inch insulation panels. Thus, a chamber was provided in which temperature could be controlled.

Results of G-10CR Creep Test. The results of the creep test are given below. The average of the two linear variable displacement transformers (LVDT) versus time is shown in Figure 2.2-9. The results indicate that the creep response is very sensitive to temperature. The creep rate at 20°C (68°F) is shown to be 50.7 μ in/day (or 0.0185 in/yr). The temperature in the test chamber was then raised to 34-35°C (93-95°F) and the corresponding creep rate increased to 375.8 μ in/day (or 0.137 in/yr). The temperature was then allowed to cool to 18°C (64°F) and the corresponding creep rate reduced to 11.4 μ in/day (or 0.0042 in/yr). It appears from this test that the creep rate can be minimized by keeping the temperature at or below room temperature.

Results of other material properties of G-10CR that are available are listed in Table 2.2-1.

Material Characteristics of Titanium. Titanium was selected as a possible support material because of its high strength and relatively low conductivity characteristics, as listed in Table 2.2-2 and Figure 2.2-10. The extra-low interstitial (ELI) grade was chosen because of the toughness characteristics for cryogenic application as shown in Figure 2.2-11. This figure also shows a transition from high to relatively low fracture toughness values occurs in the ELI grade at approximately 125K. This increases the risk of brittle fracture dictating that fracture analysis be performed during the detailed design phase on the selected support structure if it is made from titanium.

Table 2.2-1. G-10 CR Material Properties

	Ultimate ⁽¹⁾ KSI		CTE (RT-4K) (2) 10 ⁻⁶ in/in/°F	Youngs Modulus MSI	
	RT	4K		RT(3)	4K
Warp (90°)	60	125	4.5	3.84	5.0
(45°)	--	--	--	1.6	--
Fill (0°)	43	78	5.1	3.39	4.8
Normal	-61	-109	14.0	--	3.2

(1) Ref. 2.2-1, PMS-II Final Design Review, GDC report dated 15 Nov 1984.

(2) Ref. 2.2-2, Laminates for Superconducting Magnets, J. Benzinger.

(3) GDC Test Results, 1 specimen each direction at RT.

Table 2.2-2. Mechanical and Physical Properties
6AL-4V Titanium Alloy

ρ (lb/in ³)	Ultimate (ksi)	Yield (ksi)	E (MSI)	CTE (RT-4K) 10 ⁻⁶ in/in/°F
0.16	130	120	16.0	3.7

Ref. 2.2-3, Bruhn pg. B2.35.

. Annealed condition.

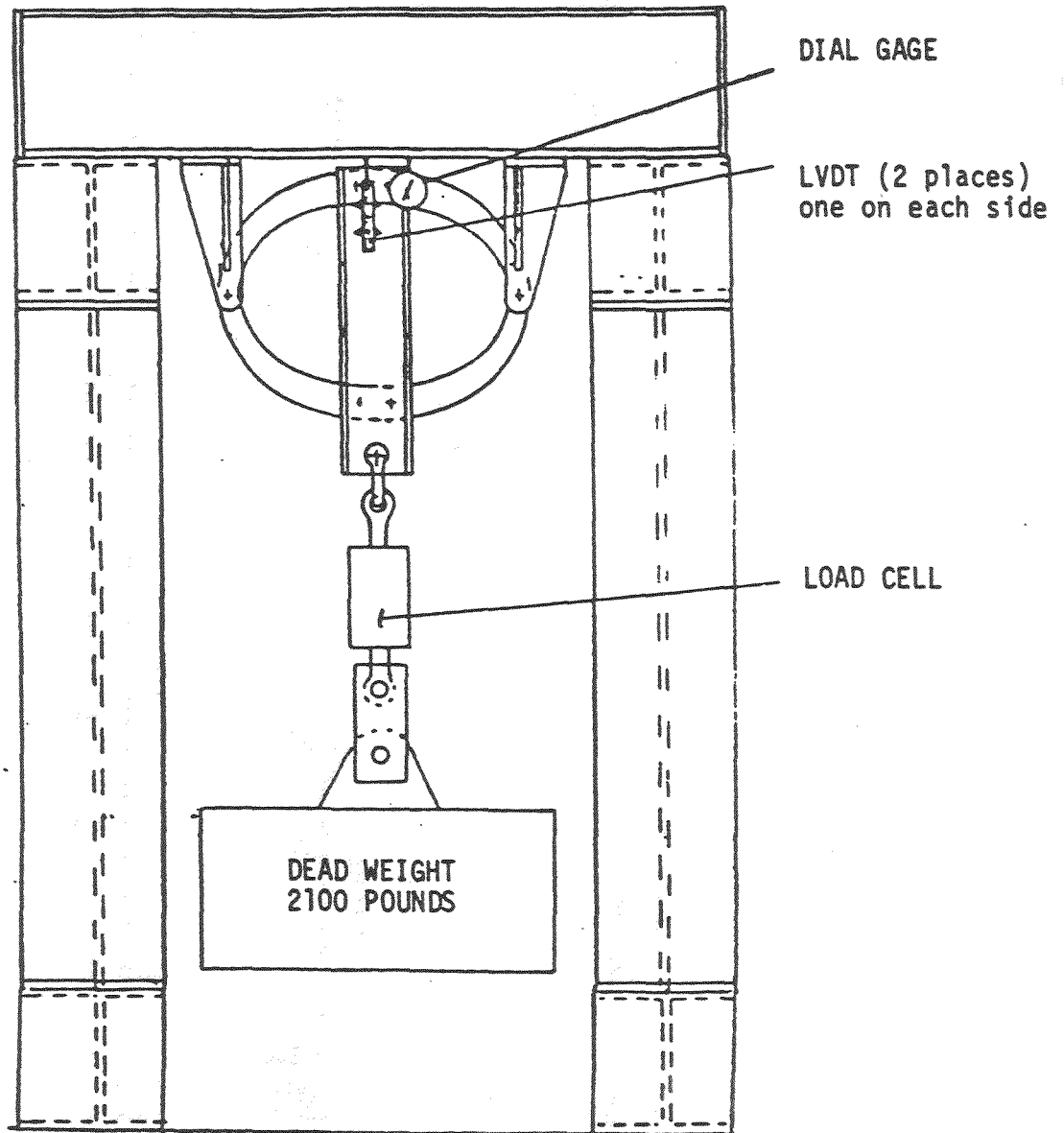


Figure 2.2-8. Instrumentation Layout for G-10CR Elliptical Ring Creep Test

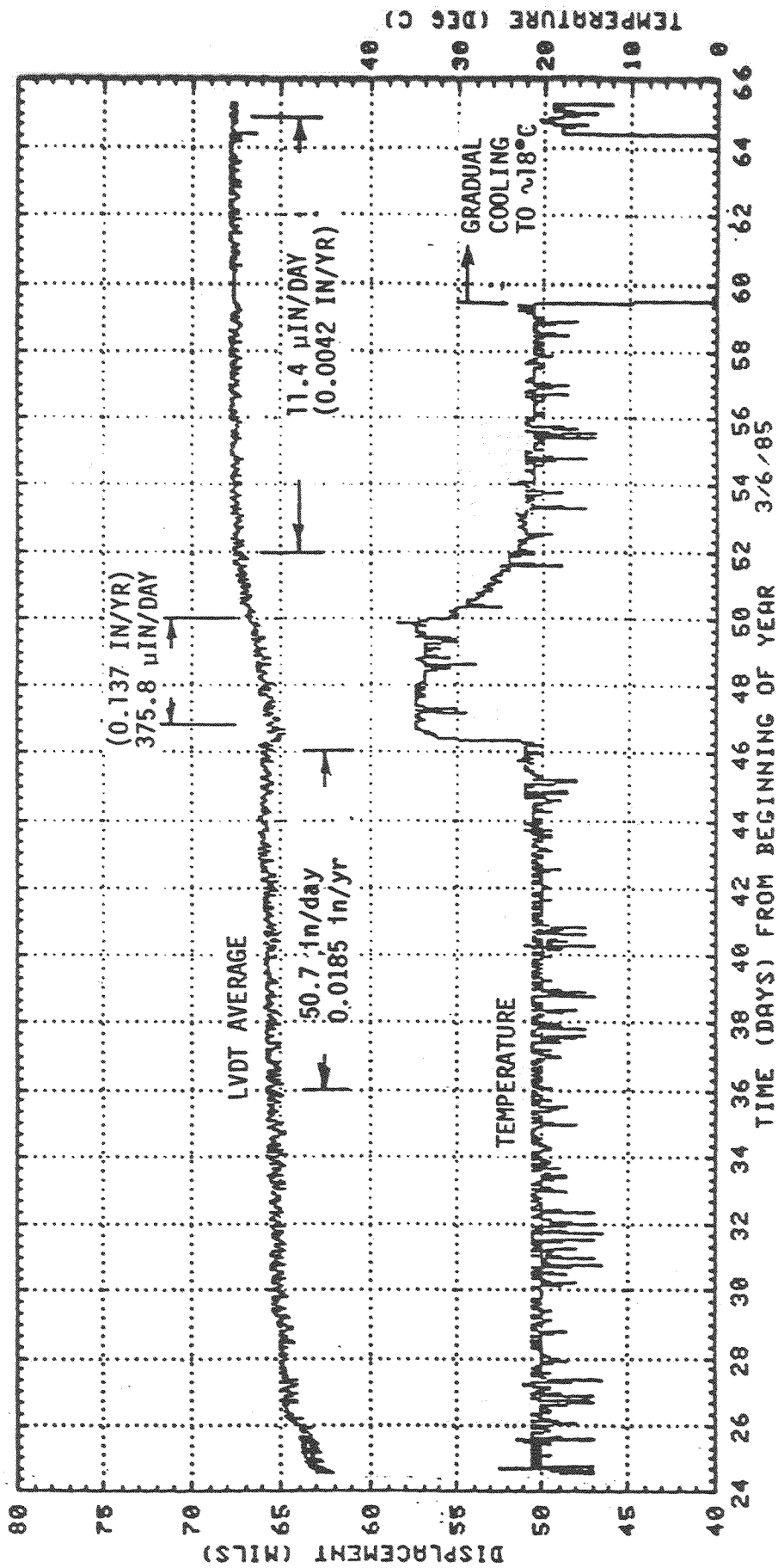


Figure 2.2-9. Average Creep Response of G-10CR Elliptical Ring Support

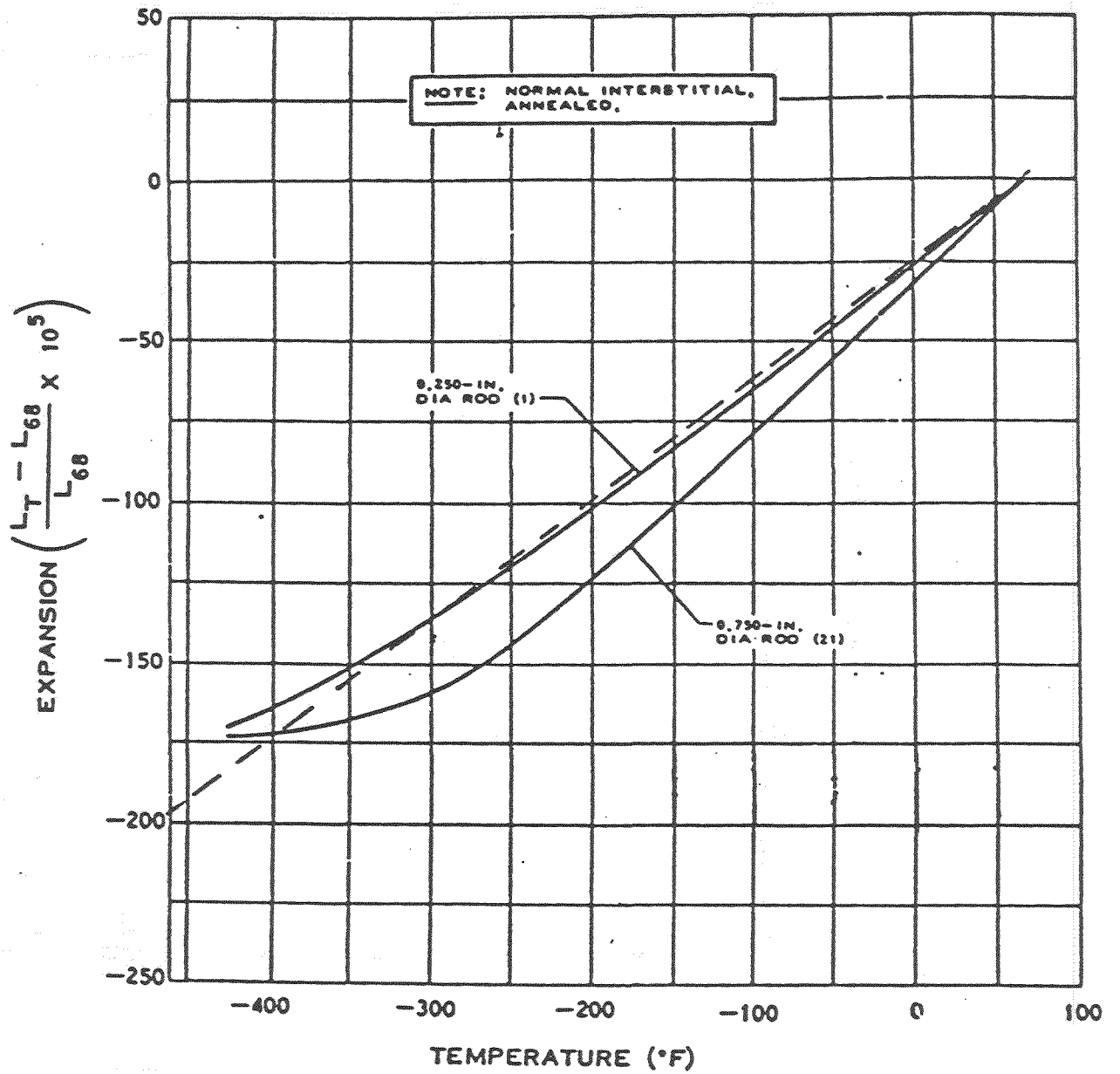
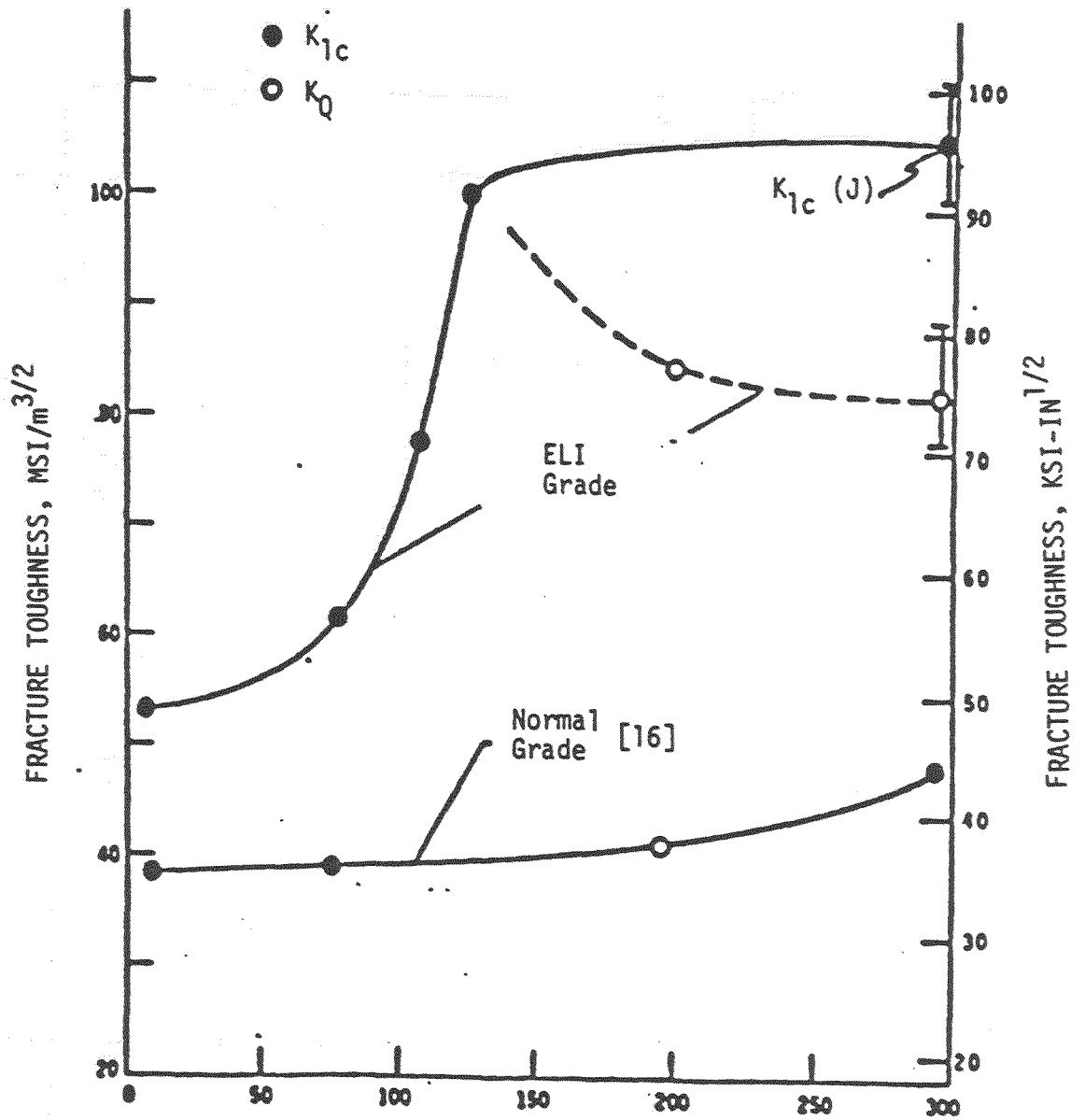


Figure 2.2-10. Thermal Expansion of 6Al-4V Titanium



Taken from Ref. 2.2-4. Tobler R1. Fatigue Crack Growth and J - Integral Fracture Parameters of Ti-6Al-4V Ambient and Cryogenic Temperatures, STP-601, 1976.

Figure 2.2-11. Temperature Dependence of K_{1c} for Ti-6Al-4V Alloys

2.2.2.2 Support Configurations. The geometries/material combinations that were investigated as possible configurations for the SSC cold-mass support system are:

-- Based on 5 supports/cold mass

- 1) G-10CR elliptical ring configuration
- 2) Titanium elliptical ring configuration
- 3) Titanium "J" support configuration
- 4) Titanium strut support-tension configuration
- 5) Titanium strut support-compression configuration

-- Based on 4 supports/cold mass

- 6) Titanium strut support-compression configuration.
- 7) Fiberglass strut support-compression configuration.

Elliptical Ring Supports. The elliptical ring geometry and relationship to the cold mass/vacuum vessel is illustrated in Figure 2.2-12. Two G-10CR rings are being considered at each support location with each ring being 0.5 inch thick. One titanium ring at a thickness of 0.90 inch is the alternative for this configuration.

The loading conditions imposed on the elliptical ring supports are listed in Table 2.2-3. The G-10CR loading is based on two rings per support location while the titanium is based on one.

A finite-element computer model of the elliptical ring was created to use in the analysis. The ring was modeled as shown in Figure 2.2-13. The boundary conditions imposed on this model are illustrated in Figure 2.2-14.

A summary of stress results for the G-10CR and the titanium elliptical rings are presented in Tables 2.2-4 to 2.2-7. The creep characteristics of G-10CR is a major concern. Therefore, two rings per support location were adopted in order to minimize the stress state during potential long-term elevated temperature (above operating) storage loading condition. This design approach produces relatively low stresses in the operating condition and also in the higher loaded (short-time load case).

Table 2.2-3. Elliptical Ring Support Loading

CASE	CONDITION	LOADING PER SUPPORT*	
		G-10CR	TITANIUM
①	<u>THERMAL</u> **		
	Steady State	ΔT Grad. 4K/80K/RT	ΔT Grad. 4K/80K/RT
	<u>MECHANICAL</u>		
②	DW	$F_{VER} = -2000 \text{ lb}$	$F_{VER} = -4000 \text{ lb}$
③	Manufact. (+2G/ -3G/±1G)	$F_V = 6000 \text{ lb}/F_H = 2000 \text{ lb}$	$F_V = 12000 \text{ lb}/F_H = 4000 \text{ lb}$
④	Transpor. (+4G/ -5G/±1G)	$F_V = -10000 \text{ lb}/F_H = 2000 \text{ lb}$	$F_V = 20000 \text{ lb}/F_H = 4000 \text{ lb}$
⑤	Seismic (+.7G/ -1.7G/±.7G)	$F_V = 3400 \text{ lb}/F_H = 0$	$F_V = 6800 \text{ lb}/F_H = 0$
		$F_V = 2000 \text{ lb}/F_H = 1400 \text{ lb}$	$F_V = 4000 \text{ lb}/F_H = 2800 \text{ lb}$
	<u>OPERATIONAL</u>		
	Steady-State Case ① + Case ② + $\Delta_{AXIAL} = 0.9$		
	Low Prob. Event Case ① + Case ⑤ + $\Delta_{AXIAL} = .9$		

* Based on 5 supports per 55' cold mass length (4000 lb/support location.)

** Cold mass shrinkage on the ring was not included because the difference in movement between the support and cold mass was relatively small.

Table 2.2-4. Stress Summary of G-10CR Elliptical Ring Support
(Dead Weight and Transportation Loading)

NODE*	STRESS, PSI			
	DEAD WEIGHT ⁽¹⁾		TRANSPORTATION ⁽²⁾	
	σ_x	σ_y	σ_x	σ_y
1	-27	-2777	-112	-9827
7	106	1754	401	4910
267	-3164	-133	-16200	-756
273	2796	208	13620	987
533	-39	-2729	-230	-17633
539	97	2010	604	14172

* See Figure 2.2-9.

(1) Input Deck: NASM3D; RUN4H, DW = -1000 lb (ON Model, 1/2 Sym)

(2) Input Deck: NASM3D; RUN5H, F_{VERT} = -5000 lb, F_{HOR} = 1000 lb

= Max. Stress

Table 2.2-5. Stress Summary of G-10CR Elliptical Ring Support
(Thermal and Seismic Loading)

STRESS, PSI						
NODE	THERMAL (1)		DW+SEISMIC+0.9"(2)		SUMMATION (1) + (2)	
	σ_x	σ_y	σ_x	σ_y	σ_x	σ_y
1	903	6476	-5032/4942	-5200/-4240	-4130/5845	-1276/2240
7	215	-4570	1890/-1530	-20392/26355	2100/-1315	-24962/21785
267	-181	-2018	2711/-13470	2196/-2650	2530/-13650	178/-4668
273	-243	1844	26659/-17153	-3481/4187	26420/-17396	-1640/6030
533	-173	5426	-3540/3400	-7372/-1900	-3713/3227	-1946/3526
539	685	-4125	4850/-4530	-25275/32110	5545/-3845	-29400/27985

(1) Input Deck: NASTG4; TRANSVERSE GRADIENT - 450°F to RT with
RUN 1 with intercept

(2) Input Deck: NASM3D; $F_{VERT} = -1700$ lb, plus $\Delta_{AXIAL} = 0.90$ "
RUN 7H (Top Surface/Bottom Surface)

- Max. Stress

Table 2.2-6. Stress Summary of Titanium Elliptical Ring Support
(Dead Weight and Transportation Loading)

NODE*	STRESS, PSI			
	DEAD WEIGHT (1)		TRANSPORTATION (2)	
	σ_x	σ_y	σ_x	σ_y
1	142	-34500	530	-124120
2	1230	15644	4664	39530
267	-34094	-1280	-170500	-6410
273	30353	2050	151800	10250
533	143	-34500	898	-220930
539	1230	15664	7620	117113

* See Figure 2.2-9.

(1) Input Deck: NASM4TA; RUN 4H, DW = 2000 lb (on Model - 1/2 sym)

(2) Input Deck: NASM4TA; RUN 7H, F_{VERT} = 10000 lb, F_{HOR} = 2000 lb

- Max. Stress

Table 2.2-7. Stress Summary of Titanium Elliptical Ring Support
(Thermal and Seismic Loading)

STRESS, PSI						
NODE	THERMAL (1)		DW+SEISMIC+0.90 (2)		SUMMATION (1) + (2)	
	σ_x	σ_y	σ_x	σ_y	σ_x	σ_y
1	3447	22253	603/-117	-66500/-50800	4050/3330	-44250/-28500
7	930	-15075	2140/2040	18413/34844	3070/2970	3340/19770
267	-6830	-703	-49300/-66620	-1340/-3020	-42470/-59800	-2043/-3720
273	6014	-940	67200/36000	2040/4930	61200/30000	1100/4000
533	-673	18220	600/100	-66500/-50800	0/-600	-48280/-32600
539	2731	-13360	2140/2040	18400/34850	4870/4771	5040/21500

(1) Input Deck: NASTT3, RUN 1, TRANSVERSE GRADIENT - 450°F
to RT - with intercept

(2) Input Deck: NASM4TA, RUN 7H, $F_{VER} = 3400$ Lb, plus $\Delta_{THERM} = 0.90$
(Top Surface/Bottom Surface)

- Max. Stress

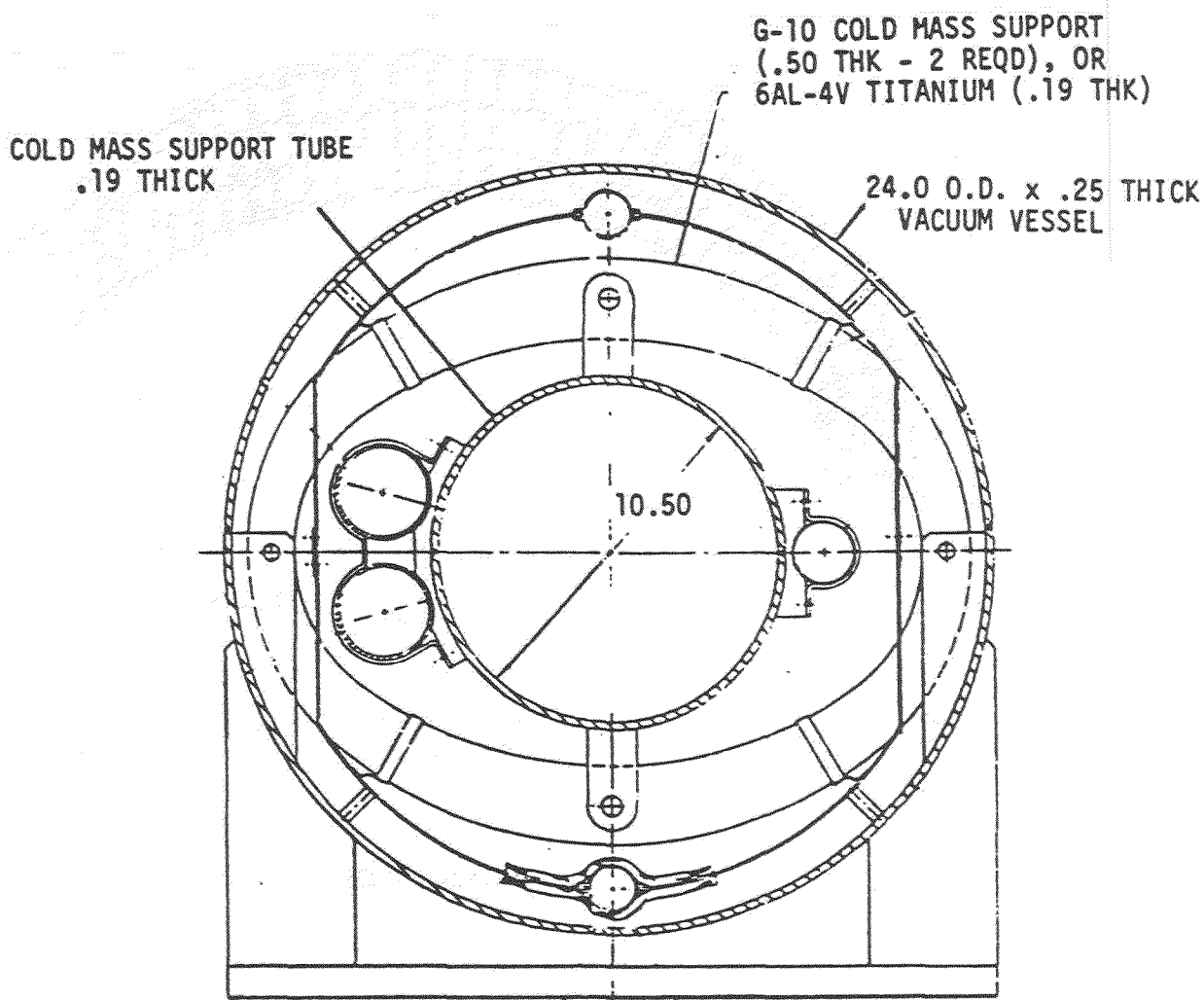
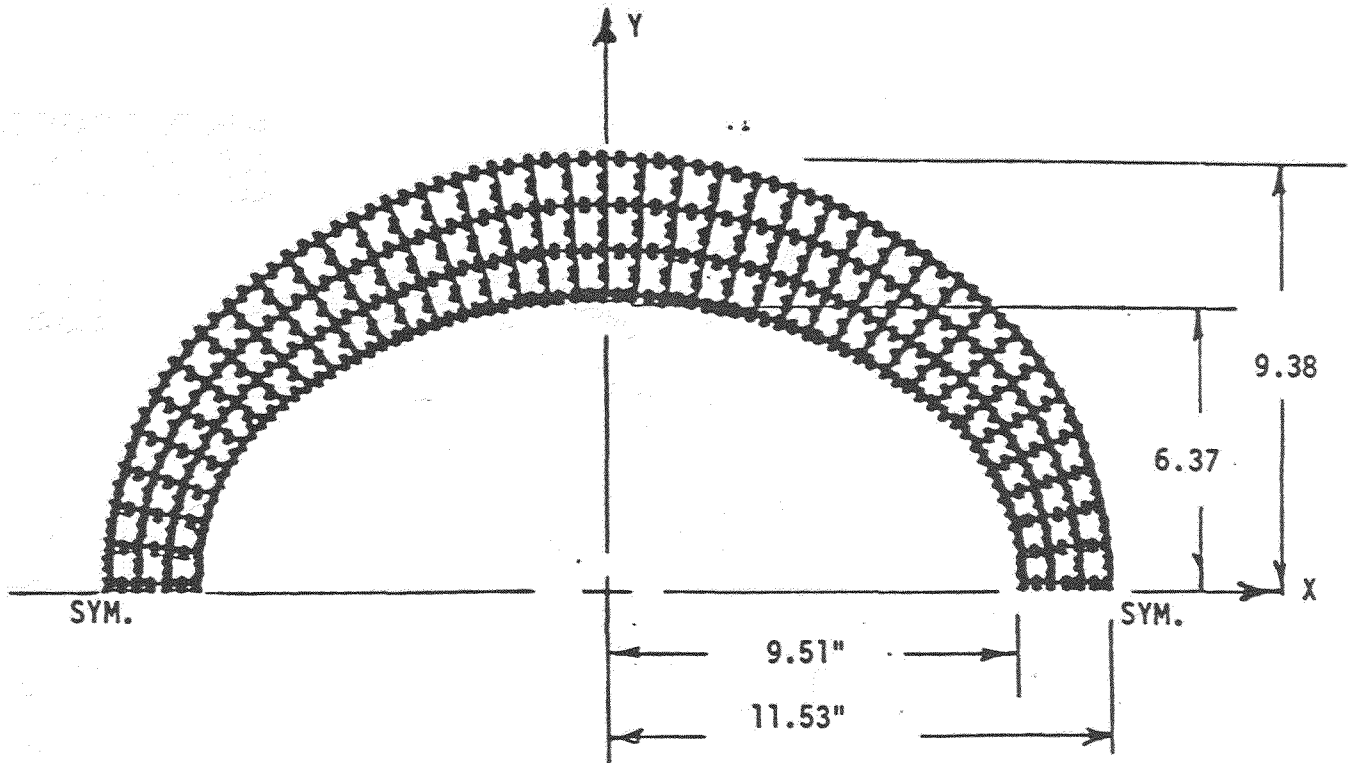


Figure 2.2-12. Elliptical Ring Support Configuration

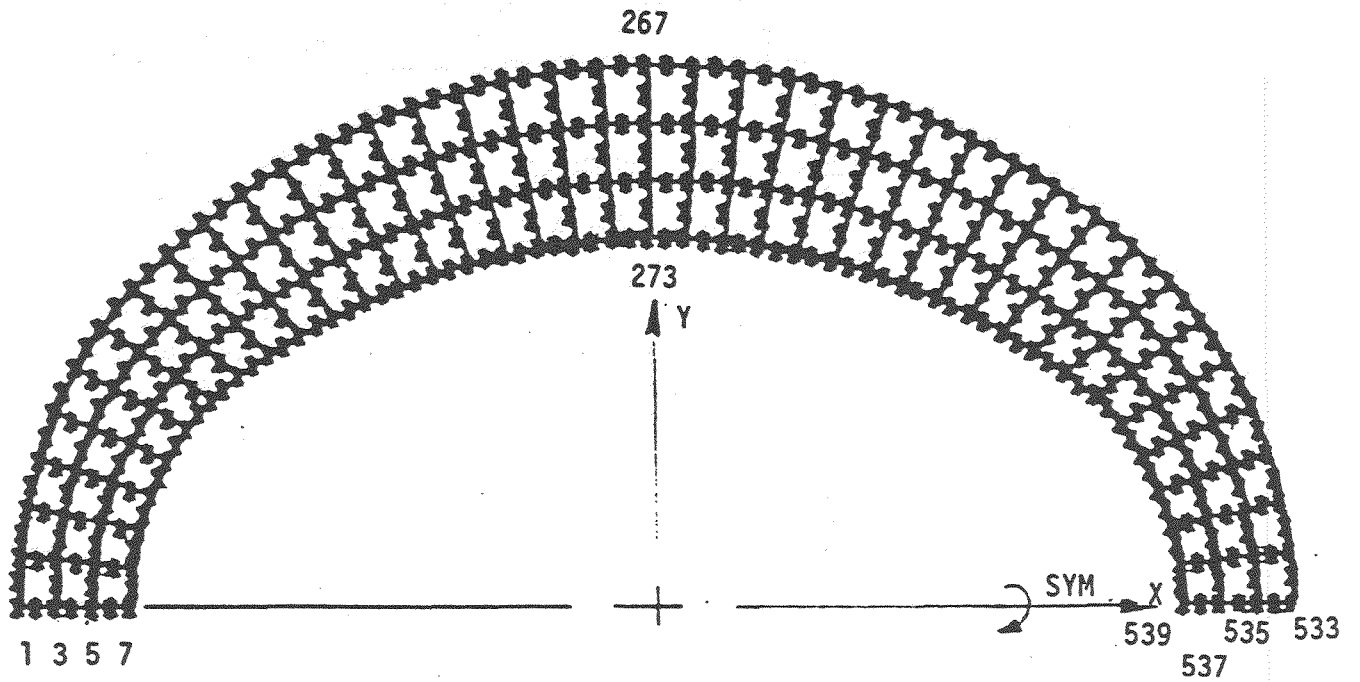


114 ELEMENTS
539 NODES

NASTRAN MODEL

CQUAD 8 ELEMENT - QUADRILATERAL SHELL ELEMENT
WITH EIGHT (8) GRID POINTS

Figure 2.2-13. Finite-Element Model of Elliptical Ring



Boundary condition at pin - symmetry across boundary - Fix X, Y, Z at two nodes of each pin location.

Figure 2.2-14. Node Identification on Elliptical Ring Model

Stress results for the titanium support ring illustrate relatively good stress values for the operating mode (σ - 62000 psi). The fracture mechanics aspect of failure would have to be addressed for further optimization. The developed stresses for transportation loading, however, exceed the allowable condition. The width of the structure (at the connection to the cold mass) will have to be increased from 3 inches to 3.5 inches. High discontinuity stresses are also indicated at the pins. However, a rotational fixity was assumed which is recognized as conservative.

Double Ring Support. A double-ring configuration was also considered and is illustrated in Figure 2.2-15. The inner ring is fastened to the cold mass and, in turn, to the outer ring which is pinned to the vacuum vessel. The design was intended to develop the longest heat path from the cold mass to the RT support point. Minimal effort was expended on this configuration because of the complex geometry, both in the load distribution and in providing for thermal radiation shields.

Titanium "J" Support. The J-support geometry and its relationship to the cold mass/vacuum vessel is illustrated in Figure 2.2-16. The "J" shape was developed in trying to establish the longest heat path from the cold-mass connection to the RT support location. The section width varies along the length in order to handle the developed moment.

Loading imposed on the "J" support structure is listed in Table 2.2-8.

A finite-element computer model of the J-support configuration was also generated. The J-support computer model is illustrated in Figure 2.2-17.

A summary of stress results for the J-support are presented in Table 2.2-9. Stress results indicate that the maximum stress developed for the Thermal + Seismic + Axial = .9" is 68 ksi. This is about the same stress level as the titanium elliptical ring configuration for the same operating condition. However, the transportation loading condition greatly exceeds the allowable without including any horizontal loading. The thickness used was 0.20" and would require a wider cross section in order to reduce the transportation loading effects. It was concluded, therefore, that the elliptical ring configuration was structurally a better approach and no further effort was made on the J-support configuration.

Table 2.2-8. J-Support Loading

CASE	CONDITION	LOADING PER SUPPORT*
①	<u>THERMAL</u>	
	Steady State	ΔT Grad. 4K/80K/4T
②	<u>MECHANICAL</u>	
	Dead Weight	$F_V = 2000$ lb/Support
③	Manufacturing (+2G /±1G) (-3G /±1G)	$F_V = 7380$ lb/ $F_H = 2000$ lb/Supt
④	Transportation (+4G /±1G) (-5G /±1G)	$F = 11380$ lb/ $F = 2000$ lb/Supt
⑤	Seismic (+ .7G /or .7G) (-1.7G /or .7G)	$F_V = 3400$ lb, $F_H = 0$ $F = 2960$ lb, $F_H = 0$
	<u>OPERATIONAL</u>	
	Steady State	Case ① + Case ② + $\Delta_{AXIAL} = +0.9$
	Low Prob. Event	Case ① + Case ⑤ + $\Delta_{AXIAL} = +0.9$

* Based on 5 supports per 55' cold mass length
(4000 lb/support location)

Table 2.2-9. J-Support Stress Summary

Node	Thermal (1)	DW+Seis+.9(2)	Summation (1) + (2)	Dead Weight (3)	Transportation (4)
5	-700/-1500	9000/-150	8300/-1650	5000/2000	2600/-500
7	1000/-1400	25000/500	3500/-900	14740/400	7500/1900
9	2200/-1000	4000/3200	6200/2200	24000/2000	120000/100000
11	3500/-900	55000/5300	58500/4200	32700/3340	163000/160000
13	1500/-800	62000/6100	63500/5300	35000/3700	184000/184000
15	5000/-800	63000/6200	68000/5400	38000/3600	188000/181000
17	5000/-850	61000/5600	66000/4750	36000/3400	182000/166000
19	5000/-850	57000/5000	62000/4250	34000/2900	168000/14500

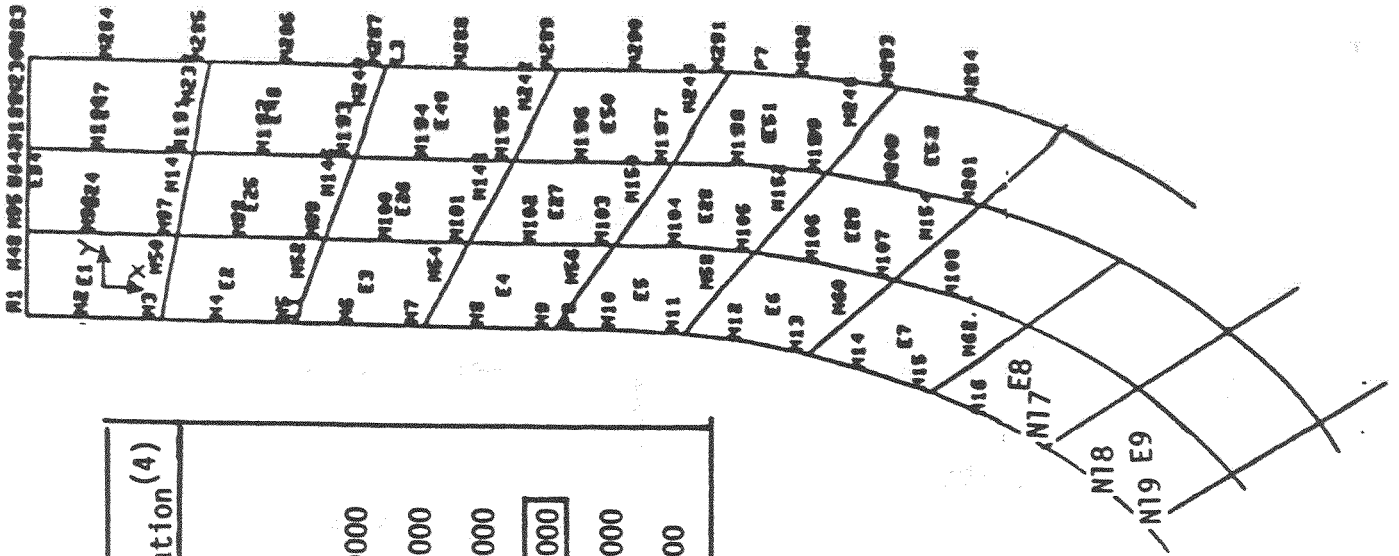
(1) INPUT DECK: NASTJIE, RUN 1 (-450°F to RT) (σ_x/σ_y)

(2) INPUT DECK: NASMJIA, RUN 7 ($F_{VERT} = 3400$)

(3) INPUT DECK: NASMJIA, RUN 4 ($F_V = 2000$ LB)

(4) INPUT DECK: NASMJIA, RUN 5 ($F_V = 10000$ LB - NO HORIZONTAL LOADING)

- MAXIMUM STRESS



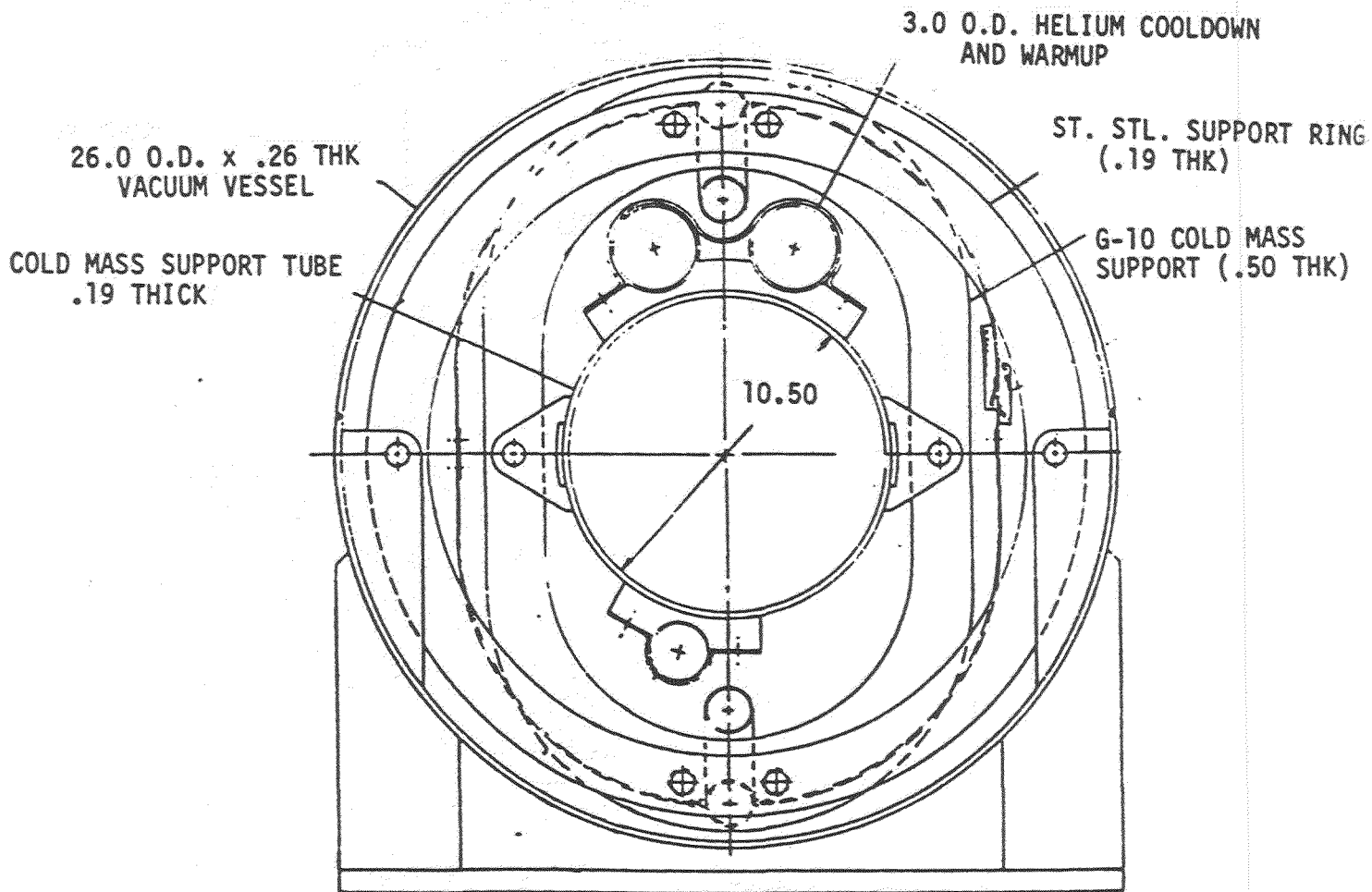


Figure 2.2-15. Double-Ring Support

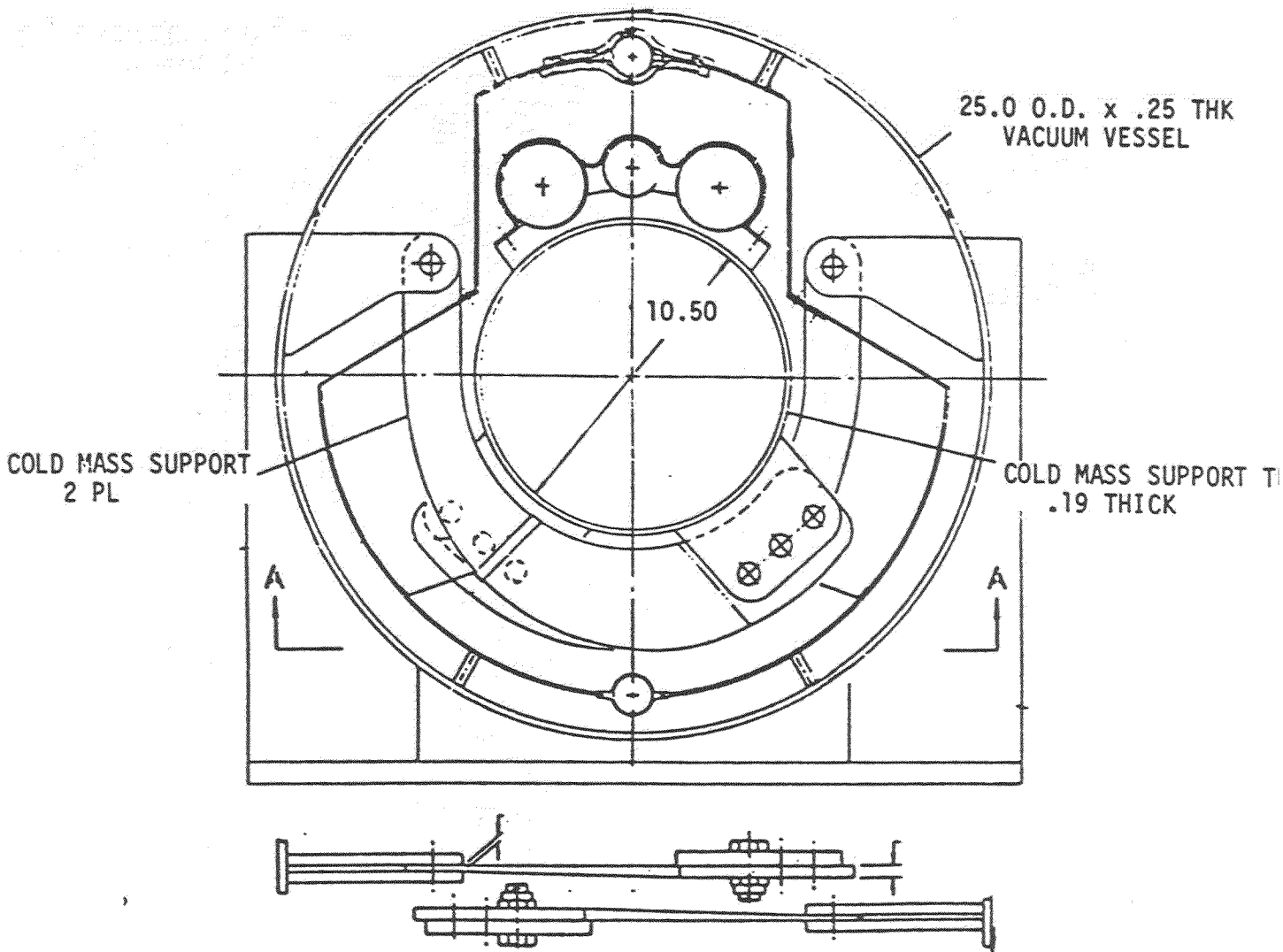
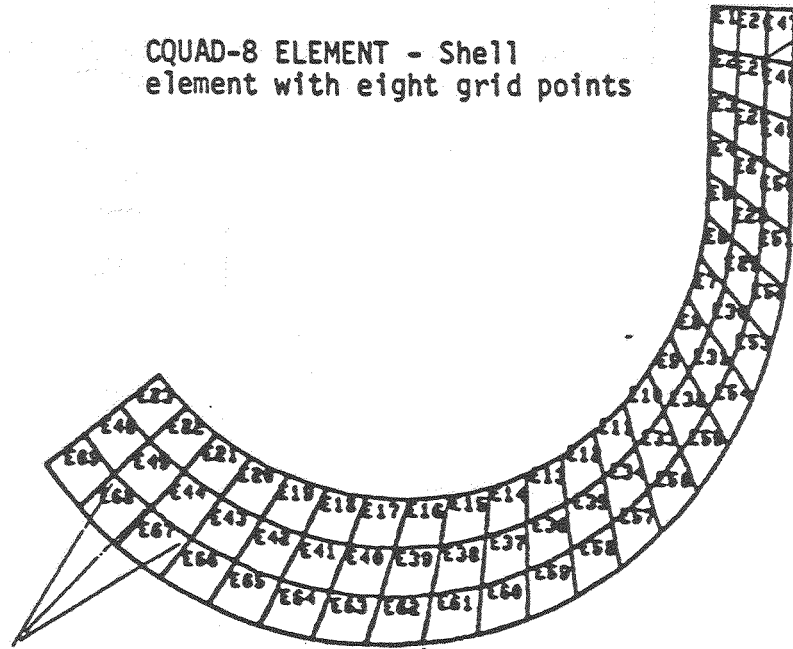


Figure 2.2-16. Section A-A J-Support Geometry Titanium

CQUAD-8 ELEMENT - Shell
element with eight grid points

NOTE 191
FIX X, Y, Z
(FREE TO ROTATE)



NODES 229, 231, 233
FIXED IN X DIRECTION

69 - ELEMENTS
329 - NODES

Figure 2.2-17. J-Support Model and Boundary Conditions

Strut Supports. Two strut geometries were considered for the vertical struts: (1) compression struts, and (2) tension strut arrangements. The side strut was positioned at the GG location of the cold mass to prevent additional loading of the vertical struts (couple effect). The attachment to the cold mass is by shear pins as shown in Figures 2.2-18 and 2.2-19. The length of the compression struts are 12 inches with the clevis inside the vacuum vessel support structure. The tension and side struts are 8.5 inches. The tension strut configuration requires an additional support ring around the vacuum vessel.

Loading conditions imposed on the tension and compression strut configuration are listed in Table 2.2-10.

Table 2.2-10. Rod Loading for the Compression* Configuration

	F _{Ver}	F _{Hor}
<u>Manufacturing/Handling</u>		
+2G /+ 1G	+4000	+4000
-3G /- 1G	-4000	-6000
<u>Transportation</u>		
+4G /+ 1G	+4000	+8000
-5G /- 1G	-4000	-10000
<u>Storage/Operation</u>		
+ .7G /+ .7G	+1400	+1400
-1.7G /- .7G	-1400	-3400

- * Horizontal load at center of cold mass.
- Reverse signs for tension configuration.
- Based on 5 supports per 55' cold mass length (4000 lb/support location)

The HP hand calculator program was used in sizing the struts for column buckling. The program computes the axial compressive working for columns (Ref. 2.2-6, HP-41 Handbook).

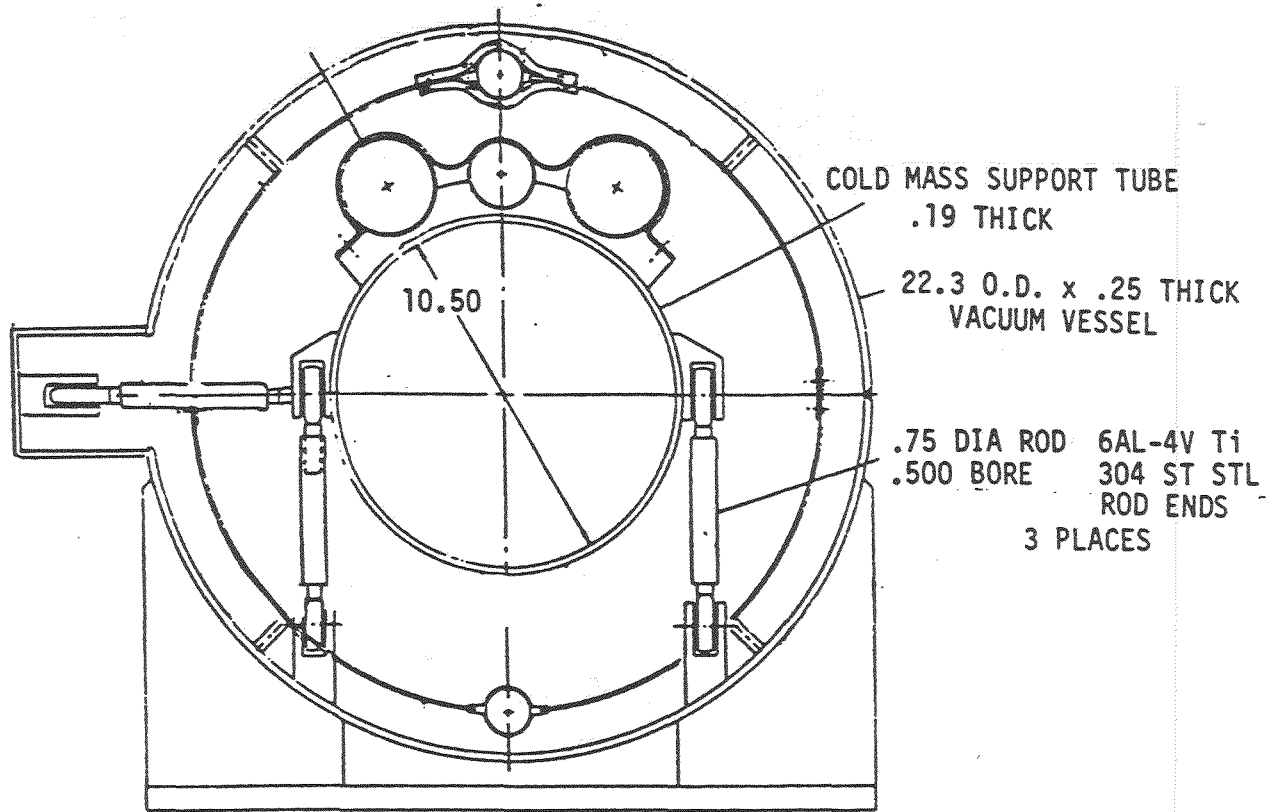


Figure 2.2-18. Compression Strut Supports for the Cold Mass

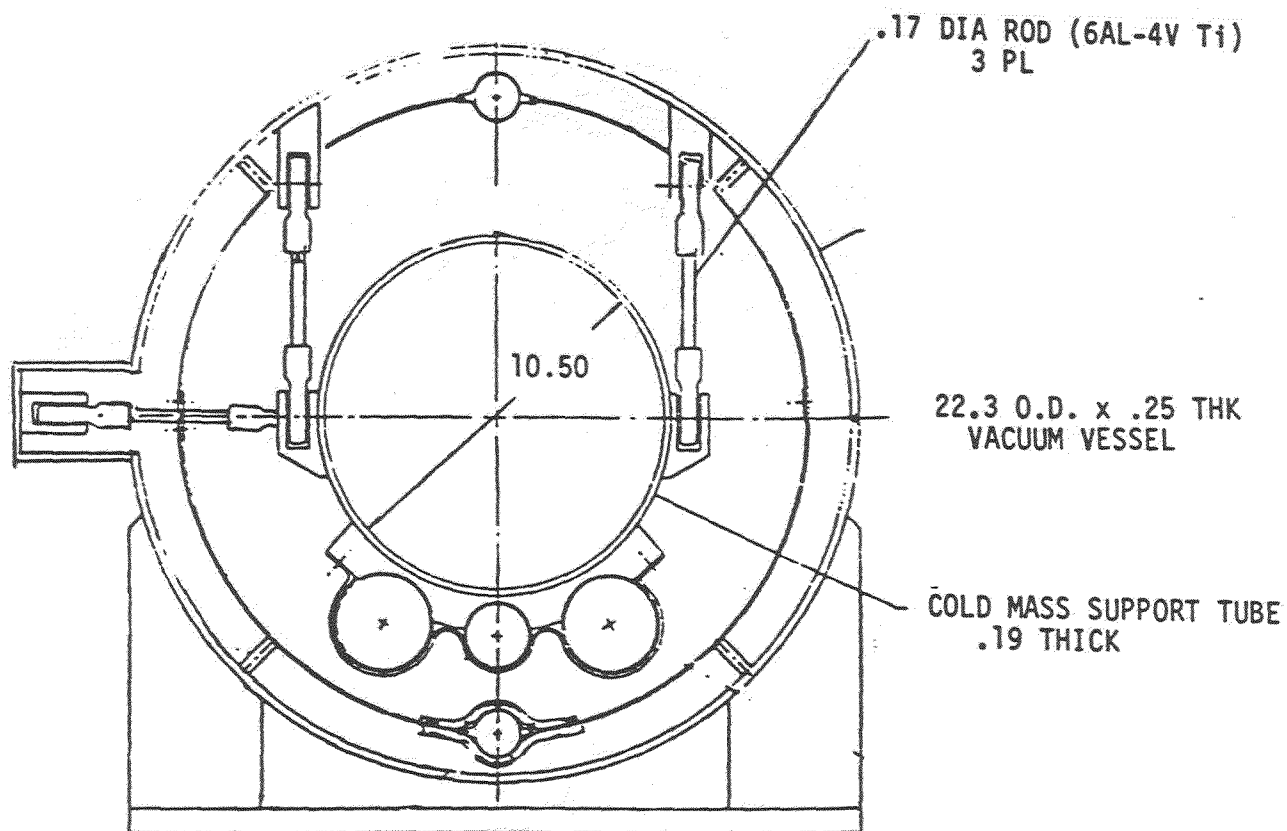


Figure 2.2-19. Tension Strut Supports for the Cold Mass

Both G-10CR and titanium were considered as support members. The following mechanical properties were used:

	G-10CR	Titanium	Fiberglass
Syp	-60,000 psi	+120,000	: 100,000 psi
E	4×10^6	15.5×10^6	4.9×10^6

Other factors considered included:

a = the initial crookedness of the column = 0.03

FS = factor of safety for the column = 2

K = effective length factor = 1

A stress-strain curve for the fiberglass material will be required in order to establish that the elastic modulus can be used at the given stress level.

Three modes of strut failure were investigated:

1) Tensile capacity based on $2/3 F_{ty}$, 2) column buckling (EULER), and 3) cylindrical axial buckling. The column buckling load is controlling in all geometries investigated as listed in Table 2.2-11. The length listed (Table 2.2-11) is based on pin-to-pin length.

A four-support configuration was considered using the strut support system. Two materials were considered, titanium and fiberglass. The results are listed in Table 2.2-12 a and b.

References

- 2.2-1 -- PMS II Final Design Review, GDC report dated 15 November 1984
- 2.2-2 -- Laminates for Superconducting Magnets, Engineering Digest, Oct. 1982, J. Benzinger
- 2.2-3 -- Analysis and Design of Flight Vehicle Structures, E. F. Bruhn
- 2.2-4 -- Fatigue Crack Growth and J-Integral Fracture Parameters of Ti-6AL-4V, Ambient and Cryogenic Temperatures, STP-601, 1976, R. L. Tabler.
- 2.2-5 -- Hewlett Packard (HP-41) Handbook

Table 2.2-11. Summary of Loading Conditions - Titanium Tube - 5 Supports

	HOR. STRUT L = 8.5"	VERTICAL STRUT	
		L = 12" COMPRESS. CONF.	L = 8.5" TENSION CONF.
TRANSPORTATION (+4G / ±1G)	±4000 lb	+ 8000 lb -10000 lb	- 8000 lb +10000 lb
Strut	Dia = 1", $t_w = 0.035$ Area = 0.1061 *(1) = 9200 (2) = 5242 (3) = 6366	Dia = 1-1/4", $t_w = .065$ Area = 0.242 *(1) = 20980 (2) = 10373 (3) = 14500	Dia = 1", $t_w = 0.058$ Area = 0.1716 *(1) = 14880 (2) = 8372 (3) = 10296
MANUFACTURING (+2G / ±1G)	±4000 lb	+4000 lb -6000 lb	-4000 lb +6000 lb
Strut	Dia 1", $t_w = 0.035$ Area = 0.1061 *(1) = 9200 (2) = 5242 (3) = 6363	Dia = 1", $t_w = .058$ Area = 0.1716 *(1) = 14800 (2) = 7105 (3) = 10296	Dia = 1", $t_w = .035$ (1) = 9200 (2) = 5242 (3) = 7373

* (1) = $P/A \leq \sigma_{ALL} = 2/3 F_{TY} = 86700$ PSI; (2) = Column Buckling (Euler) @ FS = 2.0; (3) Cylindrical Buckling - Axial, FS = 2.0

Table 2.2-12a. Summary of Loading Conditions - Titanium - Fiberglass - 4 Supports

TRANSPORTATION (+4G / ±1G) (-5G / ±1G)	HORIZONTAL STRUT L = 8.5 in	VERTICAL STRUT L = 12"
		±5000 lb
TITANIUM o $F_{ty} = 120$ ksi o Operating Stress (Vert. Strut) $\sigma = 10.5$ ksi	Dia = 1", $t_{wall} = 0.035$ Area = 0.106 in^2 (1) = 9200 lb (2) = 5242 lb (3) = 6366 lb	Dia = 1-3/8, $t_{wall} = 0.058$ Area = 0.24 in^2 (1) = 20808 lb (2) = 12300 lb Initial sizing OK (3) = 28800 lb
FIBERGLASS - Ohio Brass - o $F_{ty} = 100$ ksi o Operating Stress (Vert. Strut) $\sigma = 5$ ksi	(Using standard size) OD = 0.875 Solid Area = 0.6013 in^2 (1) = 19843 lb (2) = 8583 lb (3) = N/A	Dia = 1.25 $t_{wall} = 0.15$ Area = 0.5184 in^2 (1) = 17100 lb (2) = 12000 lb Initial sizing OK (3) need σ/ϵ curve

- (1) Tensile Capacity based on $2/3 F_{ty}$ for Titanium and $1/3 F_{ty}$ for Fiberglass
- (2) Euler Column Buckling (@ F.S. = 2.0)
- (3) Cylindrical Axial Buckling (@ F.S. = 2.0)

Table 2.2-12b. Summary of Loading Conditions - Titanium ;
 - Fiberglass - 4 Supports (Continued)

MANUFACTURING (+2G / ±1G) (-3G / ±1G)	HORIZONTAL STRUT	VERTICAL STRUT
	±5000 lb	+5000 lb -7500 lb
TITANIUM	See Table 2.2-12a	Dia = 1-1/8, $t_{wall} = .049$ Area = 0.1565 in ² (1) = 14361 lb (2) = 7515 lb (3) = 19880 lb
FIBERGLASS - Ohio Brass -	(Non-Standard Size) Dia = 1", $t_{wall} = .15$ Area = 0.4006 (1) = 13220 lb (2) = 5426 lb (3) need σ/ϵ curve	(Non-Standard Size) Dia = 1-1/8, $t_{wall} = .15$ Area = 0.4595 (1) = 15160 lb (2) = 8009 lb (3) need σ/ϵ curve

2.2.3 THERMODYNAMICS ANALYSIS

2.2.3.1 Scope/Ground Rules. The scope of the thermodynamics input to the trade study was primarily to determine the heat leak of the candidate support designs. Here "heat leak" means the total (room temperature) compressor power required to remove the heat intercepted at the 80K and 10K thermal shields as well as the heat conducted into the 4.5K cold mass. The total compressor power is the sum of the heat loads at the various temperatures weighted by the inverse of the corresponding refrigerator coefficient of performance (COP). Details of the algorithm are presented in Section 3.3.1. This cost function can be arbitrarily biased by the placement of the thermal intercepts on the support. To avoid doing this, the intercepts are located on all design candidates such that the total compressor requirement is minimized for the particular design.

Given the number of options to be analyzed, the heat leak calculations were made using very simple models. Only one-dimensional conduction along the length was treated. Thermal radiation and two-dimensional effects were ignored. In all cases it was assumed that the centers of the pins at the warm and cold ends were at 300K and 4.5K, regardless of the clevis structures. It was also assumed that the intercepts were 100 percent effective. The resulting calculated heat leaks are not especially accurate, but the errors should be systematic and not bias the comparisons between options. The analysis procedure was essentially the same as that for the final baseline design analysis which is documented in Section 3.3.4.

Calculations of heat leak were made using conductivity integrals. Pertinent values were taken from the FNAL Reference D Design Criteria (Reference 1.0-1). In those instances where a support was composed of two materials in thermal series, an interface temperature was calculated and the heat leak determined on that basis. In this way all options are compared on their "pin-to-pin" performance.

In addition to the objective evaluation of the conduction heat leaks, the candidate designs were subjectively evaluated in terms of the potential for effectively intercepting the conduction heat leak, the ability to accurately place the intercepts, and how well the support system lends itself to an effective, simple thermal shield system.

2.2.3.2 Heat Leaks. The results of the calculations are shown in Table 2.2-13. The 4.5K, 10K, and 80K heat leaks are shown, as well as the total compressor power and the associated lifetime refrigerator operating cost. The operating cost is the present value of the life cycle annual electric bills required to run the refrigerator. The derivation of this cost is presented in Section 3.3.1. The Reference D design criteria support heat leak budget from Reference 1.0-1 is also shown for comparison. All proposed concepts exceed the heat leak budget by a significant amount. This is a result of searching for support concepts that have very high mechanical and positional integrity, and that will be relatively inexpensive to produce and assemble into the cryostat. The operating cost provides a straightforward way of evaluating these benefits against the high heat leak penalty.

It turns out that there is not a lot to choose between candidates in terms of heat leak. The two elliptical beam concepts both have 4.5K heat leaks of .18 watts per magnet, while at the higher temperatures the titanium ring does a little better than the G-10 material. The strut concepts both have a 4.5K heat leak of .12 watts per magnet. They are the same because the 4.5K heat leak is dominated by the geometry of the rod end, which is the same for either a tension or compression strut. At the warmer temperatures, tension or compression yields about the same results, and both have 80K loads 20 percent higher than the elliptical beam concepts. Although the compression struts are 50 percent longer than the tension struts, the potential for buckling requires a proportionate increase in the cross-section, so the length advantage in terms of heat leak is lost. Heat leak calculations for the "J" support and the double ring concept were not made. It was judged that the "J" would yield approximately the same heat leak as the elliptical ring, since the cross-sectional area of the "J" had to increase to offset the higher bending moment of the longer support arm. This was judged to be equivalent in terms of length of area ratio relative to the elliptical beam. The double-ring concept is estimated to have the lowest heat leak of all the candidates, perhaps approaching the design criteria budget values. This was not pursued because of the impracticalities inherent in the design. In terms of operating cost only, of the viable alternatives, the titanium elliptical beam is the clear winner, followed by the G-10 elliptical beam and titanium compression struts in a virtual tie, with the titanium tension rods being the worst candidate.

Table 2.2-13. Potential Heat Leak Reduction for Design Evolution Options

Option	Q _{4.5}	Q ₁₀	Q ₈₀	W _c (kW/Magnet)	Op. Cost (\$/Magnet)
Baseline - All Titanium Compression Struts (4 Stations, 12" Pin-to-Pin Length)	.164	2.09	19.1	.66	2289
Titanium Vertical Supports Glass/Epoxy Horizontal and Anchor	.179	1.71	15.6	.55	1939
All Glass/Epoxy	.137	.605	5.51	.23	796
All Titanium, Sized for 3G Transportation Loads	.12	1.53	14.0	.48	1677
Ref. "D" Design Criteria Budget	.047	.268	4.19	.116	406

2.2.3.3 Discussion. In addition to refrigeration operating cost, the design concepts were evaluated in terms of their thermal impact on the rest of the cryostat design. The first point to be made is that the intercepts on a titanium support will be more efficient than those on a G-10 support. This is because the thermal resistance between the intercept and the heat flow path inside the support is much smaller for a thin metal section than for a thicker low conductivity section.

The second point is that it will be much easier to integrate struts with thermal shields than elliptical rings with shields. Struts penetrate the shields at one point only, whereas the rings will gradually pass through the shields due to different radii. Indeed, the most serious argument against the double ring concept is that it will be very difficult, if not impossible, to properly intercept and keep cold sections inside cold shields and warm sections outside warm shields. The problem is worse for a double-shield design.

For these reasons, the best candidate from a thermal point of view is the titanium compression strut concept. There is another attractive feature of this concept, which is the potential for reduction of heat leak. The primary reason for a titanium support is that creep will not be a problem. Creep should only be a concern for the vertical supports, thus the horizontal and axial supports could be made of G-10. The only reason they were not included in the baseline design is because it was not clear how the composite strut would be attached to a metallic rod end. This problem should not present a serious obstacle with further design work. Indeed, if a test program can show that creep is not a problem, all of the struts could be made of a glass/epoxy composite for further improvement in heat leak. One other potential means of reducing the heat leak of the baseline design is to reduce the worst case loading criteria from 5g transportation loads to 3g's with the use of special shipping fixtures.

The potential heat leak and refrigeration cost reduction of these options is shown in Table 2.2-14. Potential cost savings are: \$350/magnet to go to glass/epoxy horizontal and anchor supports, \$1500/magnet with all composite supports, and \$610/magnet relative to the baseline to reduce the shipping loads to 3g's. These cost reductions can be compared to the cost to achieve the improvements to evaluate the merits of these design options.

Table 2.2-14. Heat Leak Comparison of Support Concept Candidates

Concept	$Q_{4.5}$ (W/Magnet)	Q_{10} (W/Magnet)	Q_{80} (W/Magnet)	W_c (kW/Magnet)	Operating Cost (\$/Magnet)
Titanium Elliptical Beam (5 .090" Thick Rings)	.18	2.2	21	.70	2447
G-10 Elliptical Beam (10 0.5" Thick Rings)	.18	2.6	22	.78	2726
Titanium Tension Rods (5 Stations, 8.5" Pin-Pin)	.12	2.6	28	.83	2901
Titanium Compression Struts (5 Stations, 12" Pin-Pin)	.12	2.3	27	.77	2691
"J" Beam	--	--	--	--	--
Double Ring	--	--	--	--	--
Ref "D" Design Criteria Budget	.047	.268	4.19	.116	406

Note that the baseline design evolved to a configuration with struts at four stations along the length of the magnet, compared to a five-station concept evaluated in the trade study. The trade study results showed that five titanium elliptical beams had a lower overall heat leak than the five-station strut concept. The four-station strut concept has an even lower overall heat leak. Thus the only negative argument against the titanium compression strut concept is removed.

2.2.4 PRODUCIBILITY CONSIDERATION. Six alternative support concepts were considered from a manufacturing and fabrication standpoint, including the relative cost of material. These alternatives are summarized below:

2.2.4.1 Compression Struts. This concept, which was ultimately selected as the baseline, has the advantage of relatively low recurring fabrication and assembly costs through utilization of more sophisticated (nonrecurring) tooling. Assembly of the struts themselves can be accomplished using high-production techniques. Although some welding is required at final assembly, the amount is modest and operations can be accomplished in parallel. Precise positioning of the cold mass within the vacuum vessel can be achieved with the aforementioned tooling and by line drilling three holes at each support station. This concept is discussed further in Section 3.6.

2.2.4.2 Tension Struts. Tension struts offer many of the same advantages as the compression struts, however they have at least two disadvantages: assembly of the cryostat becomes considerably more difficult, and the reinforcing ring requires additional detailed parts and subassembly welding. Of the two strut concepts, these differences lead to the selection of the compression struts over the tension struts.

2.2.4.3 Double Ring. From a producibility standpoint, after being compared with the elliptical beam concepts described below, this concept was rated very low. There are roughly twice as many parts along with associated tooling, and assembly is about twice as complex. This, combined with the poor material utilization associated with any G-10 beam or ring, caused us to turn our attention to other support concepts.

2.2.4.4 Titanium Elliptical Beam. From a fabrication and assembly viewpoint, this concept is quite straightforward. If the beam is in one piece, material usage is very inefficient, however, if the beam is made in two pieces, the material utilization can be considerably improved by nesting for blanking. A two-piece beam would also somewhat simplify assembly, but would probably carry the penalty of a heavier beam section. Tooling complexity would be comparable with other nonadjustable support concepts. If structural requirements can be met with a two-piece beam, from a producibility standpoint, this would be one of the more attractive concepts.

2.2.4.5 G-10CR Elliptical Beam. A G-10CR beam would involve more costly fabrication techniques than titanium since blanking is not considered a viable method for the thickness involved. Again, material utilization for this configuration would be poor, and the two-piece option using G-10CR is not as attractive as it is in a titanium beam. For these reasons, as far as producibility is concerned, the titanium material would be preferred if a beam concept were selected.

2.2.4.6 Titanium J's. This concept is similar to the titanium elliptical beam from a producibility viewpoint. Fabrication costs are relatively low and the assembly task straightforward and fairly simple. The tooling would be similar to that required for a beam, except that sub-assembly of the J's to the cold mass would necessitate an additional set of fixtures.

2.3 SUMMARY OF THE SELECTED SUPPORT CONCEPT. The compression strut concept was selected for development of the cryostat preliminary design. A single generic approach had to be selected in order to proceed with the remainder of the design since the chosen configuration has a strong influence on the design arrangement of the other components within the cryostat. Selection of the compression strut approach was a joint LBL/GDC decision. The primary attributes of this approach are:

- o Lowest overall heat leak requiring .66 kW/magnet at the compressor.
- o Easy to correctly place thermal intercepts and shields.
- o Low fabrication and assembly costs.
- o Easy to assemble.
- o Lower material costs.

The baseline strut material selected by GDC was titanium. This material was selected as the baseline over fiberglass/epoxy due to concern that fiberglass epoxy may creep excessively relative to the long-term alignment requirements of the beam line. However, alternative strut materials can be evaluated and substituted when proven by verification testing. For example, fiberglass/epoxy struts would reduce the support heat load to 35 percent of titanium strut heat load. An estimate of the operational cost saving for this alternative is over \$1,500 per dipole magnet as described in Section 3.3 of this report.

In addition to material substitutions, alternative design criteria can also be readily evaluated. As an example, if special shipping and handling procedures were employed, such as the G-loads imposed on the struts were reduced, additional operating cost reductions could be realized. Reducing the vertical G-load design criteria for the titanium strut from 5Gs to 3Gs, the heat leak for support conduction would drop by 27 percent which corresponds to a reduction of \$1,120 in operating cost per magnet from the baseline design.

Additional design and analysis information for the selected approach is provided in Section 3.0 of this report.

3.0

SELECTED DESIGN CONCEPTS

3.1 DESIGN DESCRIPTION

3.1.1 INTRODUCTION. The cryostat of a dipole magnet contains the following items:

- o LN₂ and He radiation shields.
- o Multilayer insulation.
- o Fluid transport lines.
- o Cold-mass supports.
- o Vacuum vessel.

Each of the above cryostat items are described in the following pages. The cryostat (vacuum vessel) has an outside diameter of 22 inches and a length of 55 feet. There are 7,740 magnets required, each weighing approximately 20,000 pounds. The selected design uses compression struts of titanium alloy to support the cold mass. A cross section of the cryostat and the cold-mass supports are shown in Figure 3.1-1.

3.1.2 COLD MASS SUPPORT. The cold-mass supports are constructed of titanium tubing, with titanium end fittings welded to the tube. The strut material is an annealed titanium alloy, Ti-6Al-4V ELI. This titanium is a special low interstitial grade especially for use at low cryogenic temperatures. There are eight (8) compression struts, four (4) side struts, and one (1) axial load strut per magnet. The compression strut is 12 inches in length between bolt centers, and the tube is 1.38-inch O.D. x 0.058-inch wall. A cold-mass support is shown in Figure 3.1-2. The side-load strut is 8.50 inches long between bolt centers, with a 1.00-inch O.D. x 0.036-inch wall tube. The axial load strut is 12.00 inches between bolt centers and the tube is 1.38-inch O.D. x 0.083-inch wall.

Each strut has two thermal intercepts, one intercept at a temperature of 80K and the other at 20K. The titanium tube portion of the strut has attached collars, with braided copper straps connecting the collars to the radiation shields. A very low heat leak to the cold mass is provided by cooling the struts to 20K.

One bolt hole in each of the vertical struts and side struts will be left blank. During installation, the cold mass is aligned to the correct position, and a hole drilled in each strut, thus locking the cold mass permanently into its correct location.

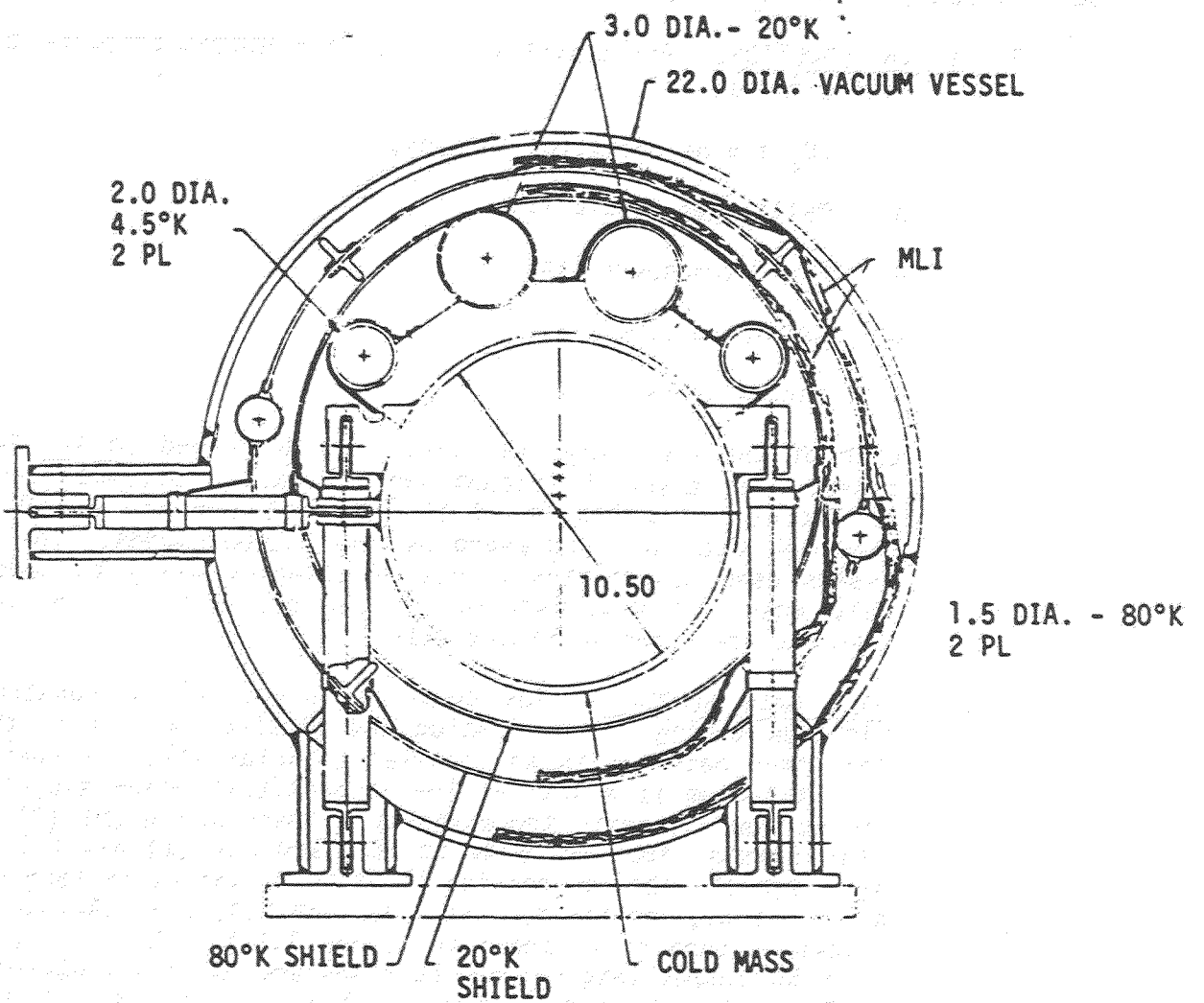


Figure 3.1-1. Cryostat Cross Section

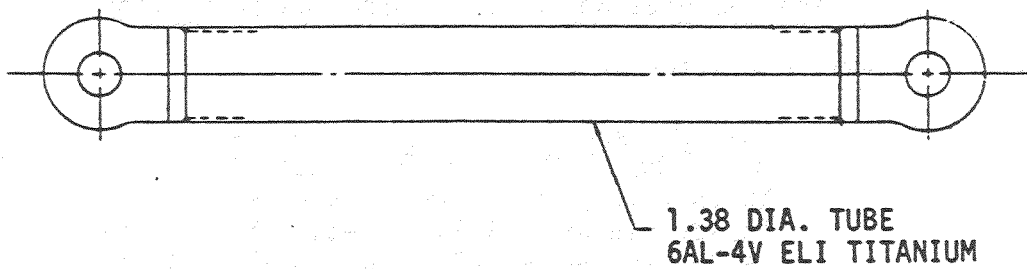


Figure 3.1-2. Cold-Mass Support Strut

Titanium compression struts were selected for the following reasons:

- o Titanium struts eliminate creep and maintain cold mass alignment for long-term gravity loading.
- o Titanium has low thermal conductivity when compared to other metals.
- o Tension and compression yield stresses are high at both room and cryogenic temperatures. This results in a strut with a small cross-sectional area and low heat leak.
- o Flaw growth problems and possible tension failures are minimized by having the struts in compression.
- o Thermal intercepts are easy to install on the tube portion of the strut.
- o Titanium does not require corrosion protection.

3.1.3 THERMAL RADIATION SHIELDS

3.1.3.1 80K LN₂ Radiation Shield. The 80K radiation shield is made from 0.100-inch thick 6061-T6 aluminum alloy. The 55-foot long shield is constructed in two halves, with an inside radius of 9.25 inches. The edge of each shield is welded to the 6061-T6 aluminum alloy tube that transports the LN₂. Figure 3.1-3 shows details of one-half of the shield, while Figure 3.1-1 shows the shield after it has been installed.

To minimize eddy current effects during a fast dump of the coil, slots are cut in the shield periodically along its length. These slots break up the eddy current paths and reduce the loads on the radiation shield.

Because of its good thermal conductivity, aluminum alloy was selected as the shield material. A highly conductive shield is required since the vacuum vessel is at approximately 300K, and the shield at 80K. Use of aluminum results in a thin and lightweight shield.

The shield is held in position by injection-molded fiberglass/epoxy stand-offs. These stand-offs are similar in appearance to an undriven rivet with a large head mounted on the radiation shield. The shank points toward the vacuum vessel or the 20K shield, but does not support the shield. The stand-offs are used for positioning only, and do not take any load. These are shown in the magnet cross section in Figure 3.1-1. They provide a small contact area and have low thermal conductivity, thus minimizing the heat load.

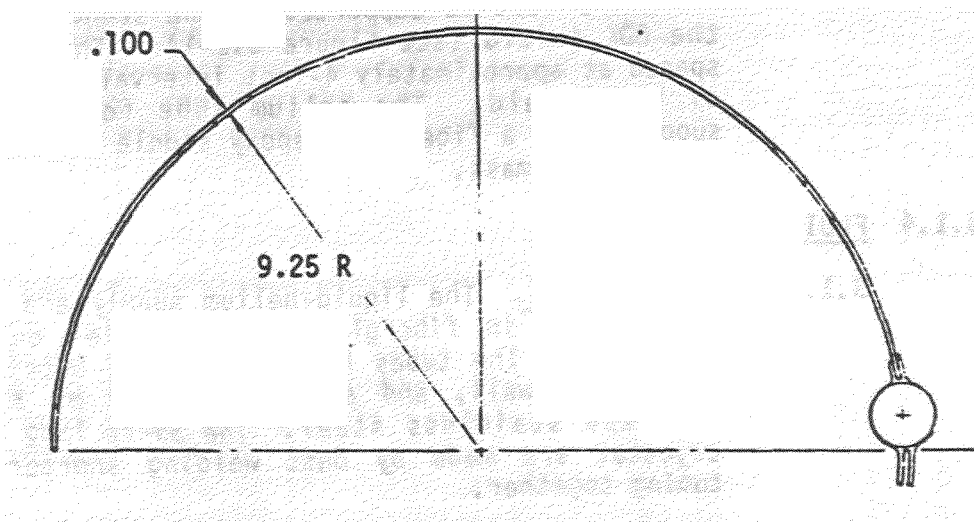


Figure 3.1-3. 80°K THERMAL SHIELD

An 80K aluminum radiation shield is the logical choice due to its good thermal conductivity, easily worked material, light weight, good strength, and low material cost.

- 3.1.3.2 20K He Radiation Shield. The 20K radiation shield (see Figure 3.1-4) is made of 0.060-inch thick 304L annealed steel, and is constructed in three (3) pieces: a lower half, and a two-piece upper shield. The two upper shields are welded to the helium transfer tube. The entire shield has an inside radius of 8.0 inches and is 55 feet long.

After the cold mass is installed in the cryostat, the upper shield is welded lengthwise to the lower shield. The 20K shield is supported by the stand-offs located on the 80K shield (see Figure 3.1-1). The stand-offs are spaced at approximately 4-foot intervals along the length of the shield. The helium tube for this shield is supported by a fiberglass/epoxy saddle located on the top of the cold mass.

3.1.4 FLUID TRANSPORT LINES

- 3.1.4.1 Helium Lines. The liquid-helium supply and return lines are located in fiberglass/epoxy saddles on top of the cold mass. The tubes have a 2.0-inch outside diameter, 0.065-inch wall, and are constructed of 304L annealed seamless stainless steel. The 55-ft long tubes in the cryostat are made by butt welding shorter lengths of tubing together.

The gaseous-helium supply and return lines are supported on top of the cold mass by fiberglass/epoxy saddles. These tubes are each 55 feet long, with a 3.0-inch outside diameter and a 0.065-inch wall, and are constructed of 304L annealed seamless stainless steel. The gaseous-helium supply tube is at 20K, and is welded to the stainless steel radiation shield along the length of the cryostat. This line supplies cooling for the radiation shield nearest the cold mass.

- 3.1.4.2 LN₂ Lines. The liquid-nitrogen supply and return lines are located near the horizontal centerline of the cryostat and adjacent to the vacuum vessel. Each line is welded to an LN₂ radiation shield running the length of the cryostat.² The shield provides support for the 55-long, 1.5-inch diameter, 0.065-inch wall, LN₂ line. This extruded 6061-T6 aluminum alloy line has² integral tabs which mate with the radiation shield. These lines supply the cooling for the LN₂ radiation shield.

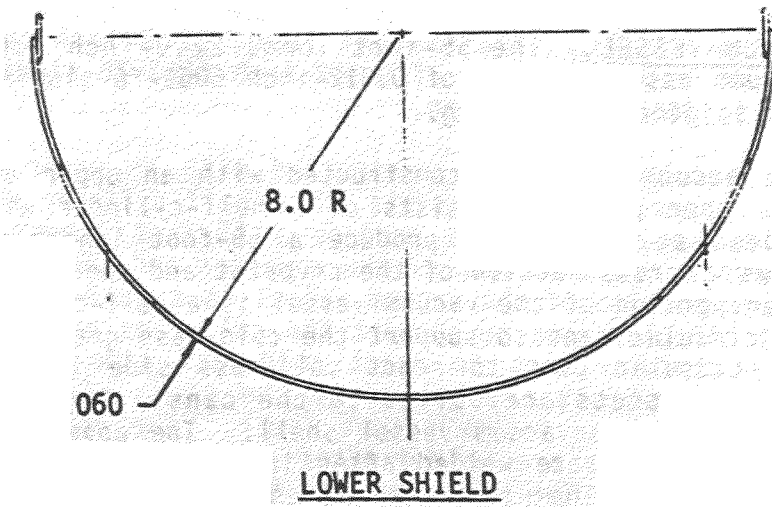
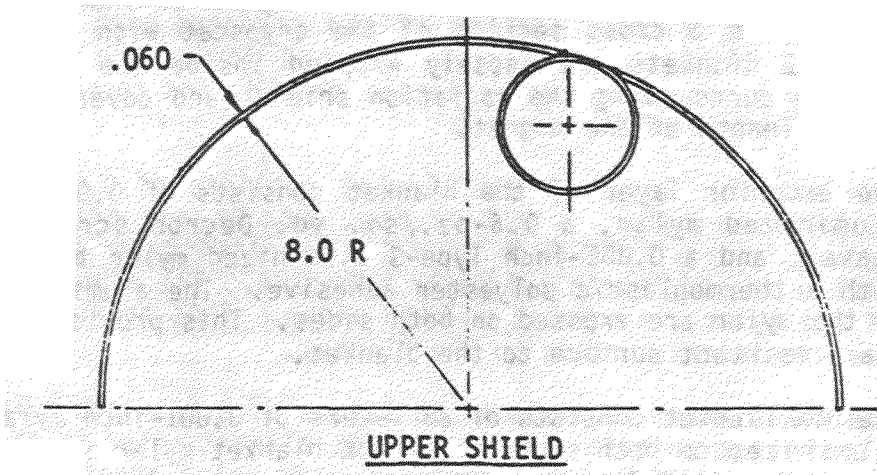


Figure 3.1-4. 20°K THERMAL SHIELD

3.1.5 MULTILAYER INSULATION. Aluminized mylar is used as a multilayer insulation between the vacuum-vessel wall and the liquid-nitrogen radiation shield, and between the liquid-nitrogen radiation shield and the helium radiation shield. The multilayer insulation is supplied in rectangular blankets, with the 20K shield having 20 layers and the 80K shield having 30 layers of insulation. Figure 3.1-1 shows a cross section of the cryostat with MLI installed. The MLI blankets are loosely wrapped inside the cryostat, completely surrounding the radiation shields and covering the entire inside length of the magnet.

The exterior layer of the blanket consists of 0.001-inch Type-S aluminized mylar, a 0.6-oz./sq. yd. Dacron scrim (12x6 leno weave), and a 0.001-inch Type-S aluminized mylar bonded together with a thermoplastic polyester adhesive. The aluminized surfaces of the mylar are exposed on both sides. This provides a tough and tear-resistant surface to the blanket.

The 80K blanket consists of 28 layers of 0.001-inch mylar, Type-S, aluminized on both sides. The 20K blanket mylar is the same, but consists of 18 layers. Between each mylar sheet is a 40-denier Dacron net made of nominal 53 mesh/square inch, 0.0066-inch thick, and 0.18 oz./sq. yd. The net is scoured with heat-set resinless finish. This type of insulation is an efficient radiation barrier and keeps the heat load on the magnet at a low level.

3.1.6 VACUUM VESSEL. The 55-foot long, 22.0-inch outside diameter vacuum vessel is made of 0.312-inch 6061-T6 aluminum alloy plate and is joined by welding.

The vacuum vessel is constructed with an upper and lower half. The upper portion consists of a half-cylinder with plates butt welded as required to produce a 55-foot length. Figure 3.1-1 shows a cross section of the cryostat and the vacuum vessel. The lower portion of the vacuum vessel is a half-cylinder, with eight (8) circular cans to support the cold-mass gravity loads and four (4) circular cans to react cold-mass side loads. The cold mass support struts are bolted to the cans. The support cans are welded to the vacuum vessel shell. The upper and lower vacuum vessel halves are welded after installation of all the cryostat components. The welds run the entire length on each side of the vacuum vessel.

An all-welded 6061-T6 aluminum alloy structure provides an excellent structure for the vacuum vessel. The structure is leak proof, readily welded, and has good corrosion resistance. Should a liquid-helium leak occur in the cold mass, or a leak appear in the radiation shields and/or plumbing, the aluminum selected has good cryogenic properties which would minimize possible damage. Due to ductile-to-brittle transition below 220K (-65°F), carbon steel was not selected for the vacuum vessel.

3.1.7 MAGNET INTERCONNECT REGION. The liquid-helium supply and return lines are made of 304L stainless-steel tubes employing bellows at the interconnect region between the magnets. These tubes have a 2.0-inch outside diameter and 3.0-inch outside diameter. To accommodate tube contraction, each tube has two bellows connected in line. The bellows have an internal liner with the downstream end of the liner free to slide. The liner provides smooth flow of the liquid or gaseous helium in the tube, reducing pump losses. The bellows will be made of stainless steel or inconel 625. Final material selection is dependent upon the bellows manufacturer, deflections, pressure, etc. The bellows material will be compatible for welding to the stainless steel tubing.

The shield's liquid-nitrogen supply and return lines are made of extruded 6061-T6 aluminum alloy. Two bellows in line at the inter-connect region are required to accommodate deflections between the shields. The tubes and bellows are constructed of different materials and require a transition joint. The transition joint is explosively formed from two plates, one of stainless steel and the other of aluminum alloy with tantalum as a binder. The joint is machined to match the tubes and bellows and welded in place.

The stainless steel bore tube has two bellows in line to accommodate thermal deflections at the interconnect region. The bellows are 1.375-inch in diameter and are made of 321 stainless steel. There is a bleed line from the bellows to the vacuum portion of the cryostat outside of the cold mass. This exhausts helium to the vacuum chamber in the event of a small leak.

The 10.5-inch inside diameter, 304L stainless-steel helium vessel has one 9.0-inch diameter bellows between magnets. The bellows are made from Inconel 625. Since the bellows diameter is smaller, two transition reducers are required between helium vessels. Because of cold-mass deflection between the supports, the helium vessel wall thickness has been increased from 0.188 inch thick to 0.250 inch thick.

The vacuum vessel joint in the interconnection region has a sleeve that slides over the vacuum vessels. The sleeve has a 22.06-inch inside diameter, a 0.25-inch wall, and a length of approximately 28.0 inches. It is made of 6061-T6 aluminum alloy and is joined to the vacuum vessel with a circumferential fillet weld at each end. Bellows are not required for this joint since deflections can be readily accommodated at fewer locations, such as the spool regions.

3.2 STRUCTURAL ANALYSIS

3.2.1 INTRODUCTION. This section presents the structural analysis of the SSC magnet components. These components include the cold mass, the vacuum vessel, the LHe tubing, the bellows around the expansion joint region, and the support struts. For the cold-mass vertical support design, various materials and configurations were analyzed in order to optimize the design. Titanium support struts, positioned at four stations along the magnet axis, were selected for further refinements. A detailed analysis of this support configuration is also provided in this section.

3.2.2 DESIGN CRITERIA. The preliminary design criteria for the LBL SSC magnet is shown in Tables 3.2-1 through 3.2-3. The loading factors used in this study are similar to those provided in Reference 3.2-1; however, the maximum loading factor (5g) is classified as a handling load in the reference document, while in this document it is applied to the transportation loads.

Table 3.2-1. Design Criteria for the LBL SSC Magnet Support System and Vacuum Vessel

●	LOADING	
	- Pressure (Vacuum Vessel)	
	Operating	See Table 3.2-2
	Faulted	
	- Temperature Gradients	
	Supports	4°K to RT
	- Support Loading	See Table 3.2-3
●	ENVIRONMENTAL CONDITIONS	
	- Radiation Requirements	None
	- Ambient Temperature Conditions	Up to 120°F
●	DEFLECTION LIMITS	
	- Vertical Deflection	
	Initial alignment of support panels	± TBD
	Cold mass deflection between supports	≤ .020"
	- Axial Deflection	

Due to cold mass temperature change (relative to midlocation fix point) 1.0"

3.2.3 MATERIALS PROPERTIES. The properties of the various materials used for the magnet components are listed in Table 3.2-4.

3.2.4 COLD MASS - HELIUM SUPPORT VESSEL AND SUPPORT ANALYSIS. The cross section of the cold mass geometry used in this study is illustrated in Figure 3-2-1. A solid iron laminate was assumed in developing the cold-mass deflection potential as a function of the number of supports. Figure 3.2-2 illustrates the deflection characteristics of the cold mass based on equalizing deflection in all spans (i.e., deflection of the cantilever ends equal to an intermediate midspan deflection). This support spacing, based on equalizing deflections, is considered to be optimum.

The wall thickness required for the helium vessel allowing for a 0.020-inch deflection relative to suspension points (again assuming equal deflection of the cantilever and midspan) is:

$$N = 4 \text{ supports}$$

$$L = \text{length of magnet} = 55 \text{ ft} = 660 \text{ in}$$

$$2 \ell_{\text{canti}} + (N-1) \ell_{\text{midspan}} = 660 \text{ in}$$

$$\text{with: } \ell_{\text{midspan}} = 2.632 \ell_{\text{canti}} \\ \text{(for equal deflection)}$$

$$L_{\text{canti}} = 66.67 \text{ in}$$

$$L_{\text{midspan}} = 175.54$$

$$\text{cold mass: } A_{\text{cross section}} = \pi(5.25 + t_{\text{wall}})^2$$

$$\text{weight: } w = \rho A_{\text{c-s}} = (.283 \text{ lb/in}^3) \pi(5.25 + t_{\text{wall}})^2$$

Table 3.2-2. Operating Pressure Conditions

Pressure Condition	Pressure, Atmospheres					
	1.375" ϕ Bore Tube	1.5" ϕ 80°K Shield	2.0" ϕ He Lines	3.0" ϕ He Lines	9.0" ϕ He Vessel	22.0" ϕ Vac. Vessel
Operating	-5	+5	+4	+3.7	-4	-1 (vac)
Back Press Operation	--	-5	-5	-5	-5	+5
Quench	-20	+20	+20	+20	+20	--

where: external pressure (+)
internal pressure (-)

Ref. 3.2-1, SSC Design "D" Cryostat Design Criteria Initial Release, FNAL
Memo dated 15 February 1985

Table 3.2-3. Cold-Mass Support Design Loading

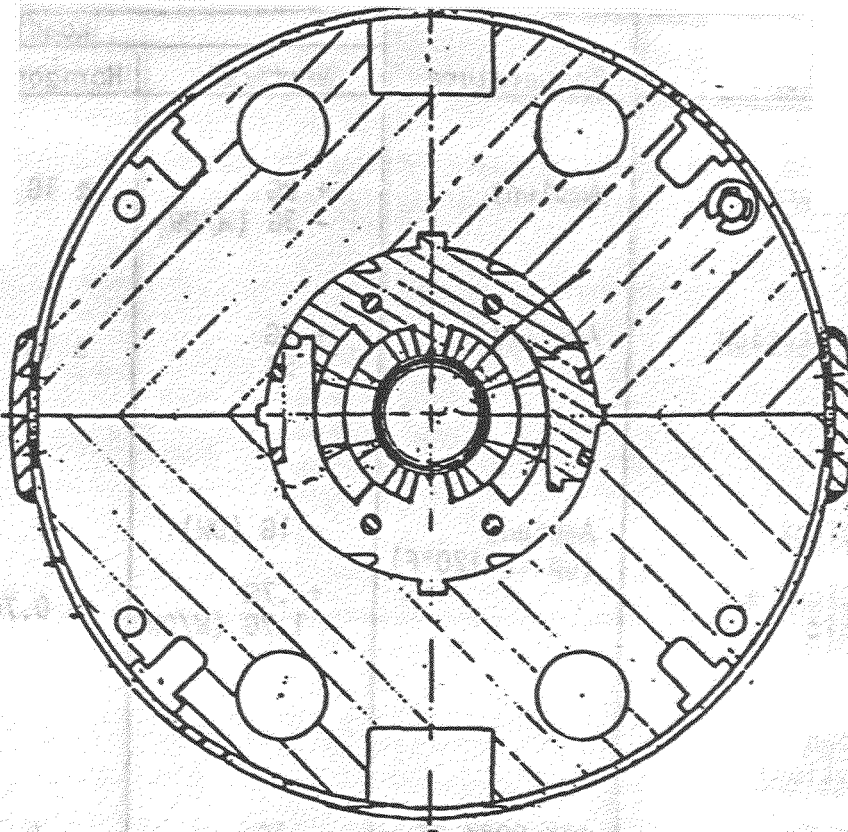
Load Condition	Temperature	Loading		
		Vertical	Horizontal	Axial ⁽¹⁾
(2) Manufacturing	Ambient	+ 2G - 3G (W/DW)	± 1G	± 1G
(3) Transportation	Ambient	+ 4G - 5G	± 1G	± 1G
Storage:				
Dead Weight	Ambient (up to 120°F)	- 1G (DW)	∅	∅
Dead Weight + Seismic		+ .7G - 1.7G (W/DW)	± 0.7G	± 0.7G
(4) Cooldown (Operation)				
DW + Temp	4°K-80°K-RT (w/Intercept)	- 1G	∅	Δ _{max} =0.9"
(3) DW+Temp+Seismic		+ .7G -1.7G (W/DW)	± 0.7G	± 0.7G Δ _{max} =0.9"

(1) Axial "G" loading effects will be taken by an axial restraint system (not by the cold-mass support).

(2) Transportation and handling loads shall not be considered with seismic.

(3) Seismic - single axis only.

(4) No additional load due to operation.



IRON LAMINATE; OD = 10.5 IN

STAINLESS-STEEL VESSEL

Assuming that a solid iron cross section
(conservative) the weight is:

26.29 lb/in

Figure 3.2-1. Cold-Mass Geometry

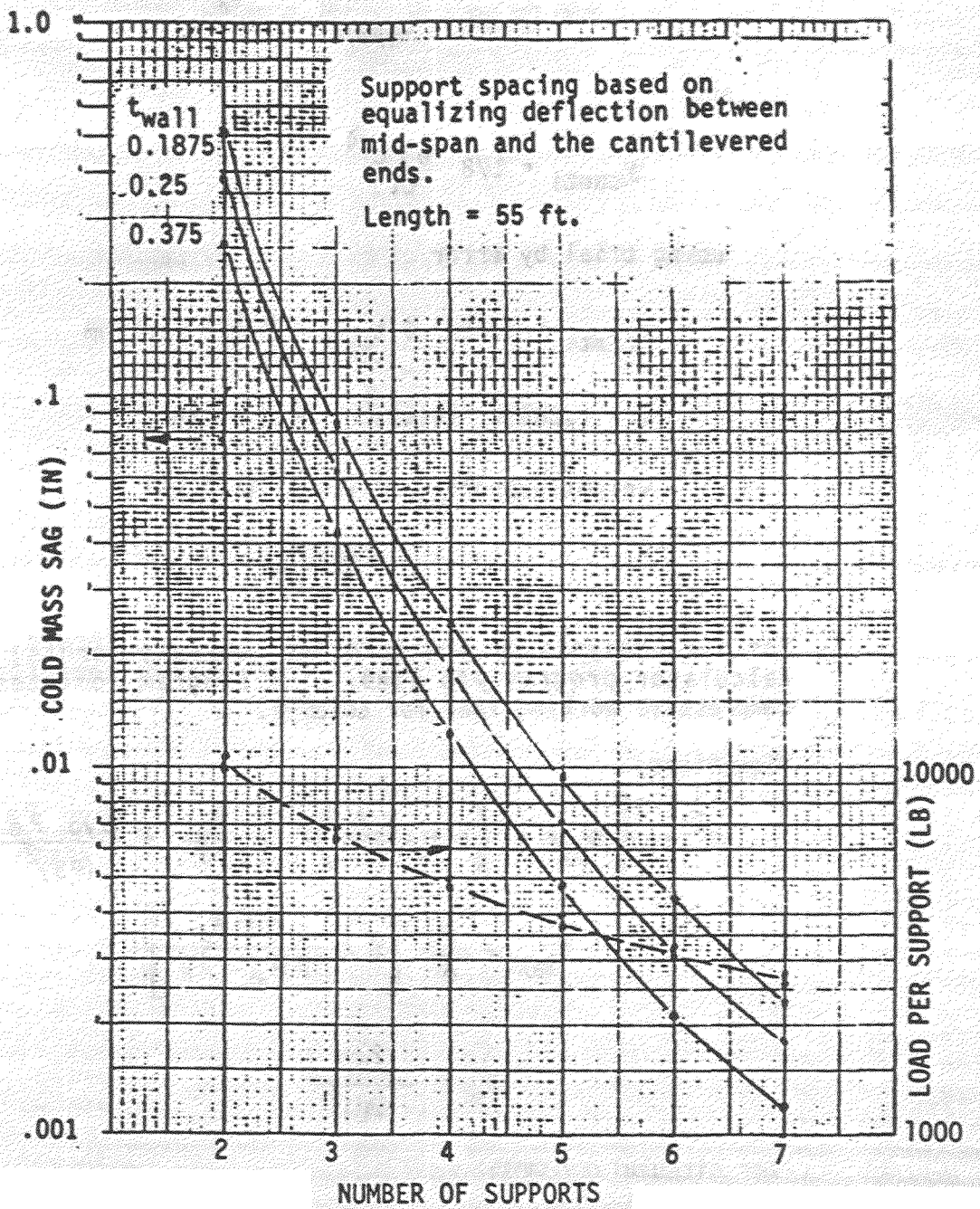


Figure 3.2-2. Cold-Mass Deflection Between Supports and Load at the Supports

Using the helium vessel wall only:

$$I = 1/4 [5.25 + t_{\text{wall}}]^4 - 5.25^4]$$

and

$$y_{\text{canti}} = 1/8 \frac{w l c^4}{EI}$$

using trial by error

$$y_{\text{canti}} = 0.020" @ t_{\text{wall}} = 0.22" \text{ minimum}$$

$$w = (.283)\pi (5.47)^2 = 26.6 \text{ lb/in}$$

$$\begin{aligned} \text{weight/support}_{\text{max}} &= (26.6) (175.54) \\ &= \underline{4670 \text{ lb}} \end{aligned}$$

For the analysis of the cold mass support struts, an HP hand calculator program was used. The program computes the axial compressive working load for columns.

*Equations:

$$p^2 - \left[S_{yp} A + \left(1 + \frac{acA}{I} \right) p_e \right] \frac{p}{FS} + \frac{S_{yp} p_e}{(FS)^2} = 0$$

$$S_{\text{max}} = \frac{p}{A} \left[1 + \frac{acA p_e}{I(p_e - p)} \right]$$

$$p_e = \frac{\pi^2 EI}{(KL)^2}$$

For circular columns:

$$A = \pi r^2$$

$$I = \frac{\pi r^4}{4}$$

$$c = r$$

where

- A is the section area.
- a is the initial crookedness of the column; assume $a = 0.03$.
- c is the distance from the minimum neutral axis to the edge of the cross section.
- S_{yp} is the yield point stress of the material.
- E is the modulus of elasticity of the material.
- FS is the factor of safety for the column; used $FS = 2$.
- K is the effective length factor for the column; for pinned connect at both ends $K = 1$.
- L is the length of the column.
- I is the minimum moment of inertia of the column.
- P is the column working load.
- S_{max} is the maximum stress in the column.
- P_e is the Euler load for the column.
- r is the radius of a circular column.

Three modes of strut failure were investigated in the analysis: (1) tensile capacity based on $2/3 F_{ty}$, (2) column buckling (Euler), and (3) cylindrical axial buckling. The column buckling load is controlling in all geometries investigated as shown in Table 3.2-4. The length listed is based on pin-to-pin length.

A four-support configuration using a compression strut support system as shown in Figure 3.2-3 was considered in this analysis. The results are given in Table 3.2-4.

If a special fixture is designed for supporting the cold mass during transport, the diameter of the struts can be decreased from 1-3/8 inches to 1-1/8 and the wall thickness can be decreased from .058 to .049 inches. This is a result of changing the design driver loading from transportation loads to manufacturing loads, as shown in Tables 3.2-5a and 3.2-5b.

Table 3.2-4. Material Properties

Material	E - MSI		CTE In/In/°F	YIELD - KSI		ULTIMATE - KSI	
	RT	4K		RT	4K	RT	4K
304L	28.2	30.0	5.7	25	65	70	170
6061-T6	10.0	11.1	9.8	35	45	42	63
A-286	29	--	5.5	85	--	130	--
Fiberglass	4.9-6	--	--	--	--	100	--
Titanium	15.5	--	4.6	120	--	130	--

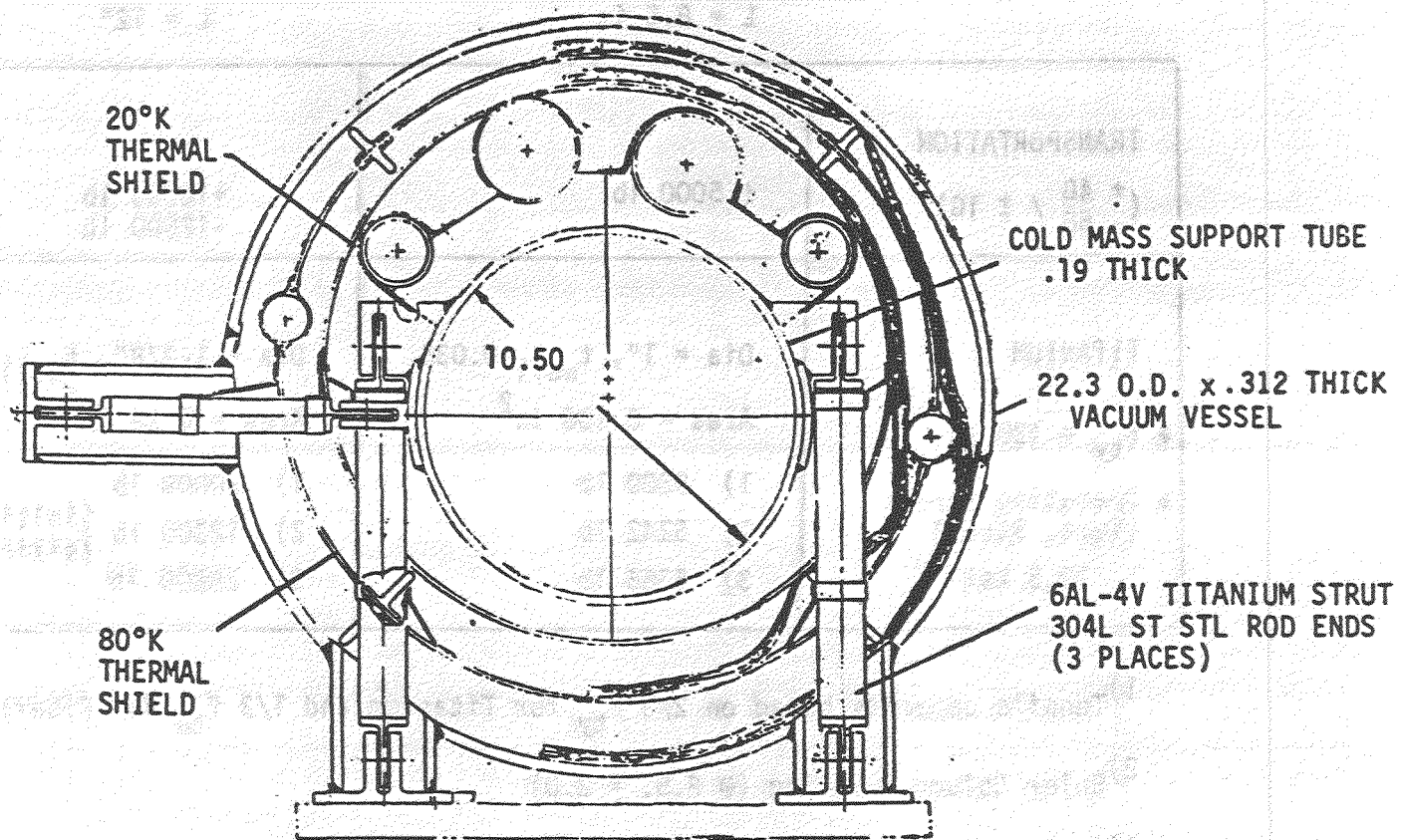


Figure 3.2-3. Compression Strut Supports for the Cold Mass

Table 3.2-5a. Summary of Loading Conditions - Titanium - 4 Supports

	Horizontal Strut L = 8.5 in	Vertical Strut L = 12"
TRANSPORTATION (+ 4G / ± 1G) - 5G	± 5000 lb	+10000 lb -12500 lb
TITANIUM ● $F_{ty} = 120$ ksi ● Operating Stress (Vert. Strut) 10.5 ksi	Dia = 1", $t_{wall} = 0.035$ Area = 0.106 in ² 1) 9200 lb 2) 5242 lb 3) 6366 lb	Dia = 1-3/8", $t_{wall} = 0.058$ " Area = 0.24 in ² 1) 20808 lb 2) 12300 lb {initial 3) 28800 lb {sizing - OK

- 1) Tensile capacity based on $2/3 F_{ty}$ for Titanium and $1/3 f_{tu}$ for Fiberglass
- 2) Euler Column Buckling (@ F.S. = 2.0)
- 3) Cylindrical Axial Buckling (@ F.S. = 2.0)

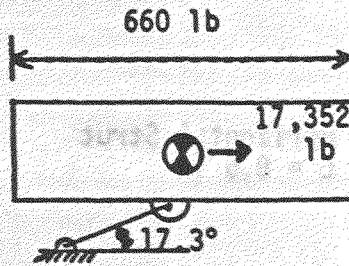
Table 3.2-5b. Summary of Loading Conditions

Horizontal Strut
L = 8.5 fn

Vertical Strut
L = 12"

<p>MANUFACTURING (+2G / ±1G) -3G</p>	<p>± 5000 lb</p>	<p>+5000 lb -7500 lb</p>
<p>TITANIUM</p>	<p>See Table 2.2-12a</p>	<p>Dia = 1-1/8, $t_{wall} = .049$ Area = 0.1656 in² 1) 14361 lb 2) 7515 lb 3) 19880 lb</p>

Calculations for sizing the axial support strut using titanium alloy are provided below:



$$26.29 \text{ lb/in (660 in)} = 17,352 \text{ lb.}$$

The strut is 12 inches long.

Axial Compression Load is

$$P_{\text{axial}} = 17,352 \text{ lb}/(\cos 17.3^\circ) = 18,174 \text{ lb}$$

Checking Euler Column Buckling using the HP-41 hand calculator program described previously:

$$P_{\text{cr}} = 20,085 \text{ lb for a tube having an}$$

$$\text{O.D.} = 1.375 \text{ in and a wall thickness} = .083 \text{ in.}$$

The Factor of Safety for the above calculation is 2.0. (see pg. 3-16, 17)

3.2.5 BELLOWS ANALYSIS. This study considers a cold-mass length of 55 feet with the axial restraint located at the cold-mass midspan. This geometry configuration produces a relatively large axial displacement at the junction between the two magnets during the cool-down/warm-up operation. The design cyclic life used in approximately 1000 cycles (240 design thermal cycles x 4). The pressure loads on the bellows are given in Table 3.2-2. The preliminary bellow sizing was performed for the following tubes:

- 1) 1.375" ϕ , stainless-steel bore tube.
- 2) 1.5" ϕ , aluminum - 80°K shield.
- 3) 2.0" ϕ , stainless-steel - He line.
- 4) 3.0" ϕ , stainless-steel - He line.
- 5) 9.0" ϕ , stainless-steel - He vessel.

The summary of results are listed in Table 3.2-6 and a discussion follows:

- 1.375" \emptyset bore tube - 2 bellows

The internal design pressure loading condition for this tube is a vacuum condition, therefore, a bellows with a low-stability pressure is adequate. The length of each bellows could be reduced from the 6 inches listed to 4 inches with a bellows material change to Inconel 625; however, this change would not reduce the length of the interconnect region.

- 1.5" \emptyset 80K shield - 2 bellows

It is believed that aluminum bellows would not be capable of handling the large axial displacements. Therefore, a steel bellows was used, requiring a bi-metallic weld or a flanged joint. Both types introduce problems and will effect costs significantly. The preferred structural method would be the bi-metallic weld. This could be performed with the use of a transition joint. The transition joint would be explosively formed from two plates, one of them stainless steel and the other aluminum (using tantalum as the binder), and the final assembly machined to the tube size. This is the only bellows that requires two plies in order to handle the high internal pressure (squirm).

- 22" \emptyset vacuum vessel

The low design pressure and thermal loading of the vacuum vessel would indicate a small relative motion between adjacent vessels. This would suggest that a welded sleeve be used for fabrication purposes instead of a bellows.

3.2.6 VACUUM VESSEL ANALYSIS. The vacuum vessel was sized per the requirements of Section VIII of the ASME Boiler and Pressure Vessel Code (Reference 3.2-6) for shells under external pressure. Results are provided in Table 3.2-7.

Aluminum was considered for the vacuum vessel primarily because of the loss-of-coolant faulted event. Under this event it is postulated that there could be a cryogen leak onto the vessel. The aluminum alloys do not exhibit a marked transition in fracture resistance as do the carbon steels, thereby reducing the risk of catastrophic failure.

Table 3.2-6. Summary of Bellows Configurations

	1.375" ϕ Bore Tube	1.5" ϕ 80K Shield	2.0" ϕ He Lines	3.0" ϕ He Lines	9.0" ϕ He Vessel	22" ϕ Vac. Vesse
Tube Matl.	Stainless Steel (SS)	Aluminum	SS	SS	SS	Aluminum
Axial Thermal Movement (Cooldown/Warmup)	(55')(12") (5.9×10^{-6}) [-452-(70)] = 2.03"	(55')(12") (9.8×10^{-6}) [-315-(70)] = 2.49"	2.03	2.03	2.03	Small
No. of Bellows	2 (2)	2 (4) 2 Plies	2 (4)	2 (4)	1 (4)	1 (3)
Wall (1) Thickness	0.010	2x.012"	0.014	0.018	0.031	--
Length of Convolutions	6"	4"	3"	4"	8"	--
Maximum Pressure (Not incl. squirm)	390	940	348	368	393	--
Stability Pressure (PSI) -Squirm	49	310	295	370	523	--
Axial Spring Rate (lb/in)	141	592	423	706	2000	--

(1) Reference 3.2-5, EJMA Standards, 5th Edition.

(2) Type 321 stainless-steel bellows.

(3) Will require vendor information on aluminum bellows (if bellows is required).

(4) Inconel 625 bellows.

Table 3.2-7. Vacuum Vessel Wall Thickness Required

Material	T _{reqd} (in)
Al 6061-T6 (Welded condition)	0.313
Al 5083	0.313
304L Stainless Steel	0.25
Carbon or Low-Alloy Steel (YS = 33 ksi to 60 ksi)	0.25

- Design driver is the vacuum load.
- Code F.S. = 3.0.
- I.D. of Vessel = 22 in, Length 55 ft.

Backup sample calculations for the vacuum vessel wall thicknesses required are given below. Thicknesses given in Table 3.2-7 are for standard gage sizes.

Al 6061-T6 Vacuum Vessel

Vessel Dimensions: Di = 22 in
t = 0.313 in
L = 660 in (55-ft)

$$Do/t = 22.626/.313 = 72.288$$

$$L/Do = 660/22.626 = 29.17$$

from Figure 2-AG θ , 28.0 in Appendix 2, ASME Boiler and Pressure Vessel Code, Section VIII.

$$\text{Factor A} = .00022$$

from Figure 2, ANF - 28.3 for welded Al 6061-T6.

$$\text{Factor B} = 1080 \text{ (up to } 200^{\circ}\text{F)}$$

$$P_{\text{allow}} = \frac{4B}{3 (Do/t)} = 19.9 \text{ psi}$$

The modulus of 5083 is about the same as that for 6061-T6, therefore, the required wall thickness using 5083 Al is the same.

304 Stainless-Steel Vessel

Vessel Dimensions: $D_i = 22$ in
 $t = 0.2$ in
 $L = 660$ in (55-ft)

$$D_o/t = 22.4/.2 = 112$$

$$L/D_o = 660/22.4 = 29.46$$

Factor A = .00009 (from Figure 2, AHA - 283)

$$P_{allow} = \frac{4B}{3(D_o/t)} = \frac{2(.00009)(28 \times 10^6)}{3(112)} = 15 \text{ psi}$$

Again, the modulus of the carbon steel is the same as that for 304L Stainless-Steel, therefore, the required wall thickness is the same.

3.2.7 VACUUM VESSEL/CLEVIS ANALYSIS. The vacuum vessel and cold-mass support configuration uses the three-strut/location support system as previously illustrated in Figure 3.2-3. The vacuum vessel has three penetrations at each cold-mass support location allowing the support struts a pass-through. The clevises are made from 304L stainless steel. The clevis pins are to be made of A-286 because of the low-temperature application and to avoid galling.

The ground rules used for the clevis attachment relate to safety factors. The service load for each load type is calculated and the component sized to carry this load times its appropriate safety factor. The following safety factors will be used.

OPERATING LOADS include dead weight
YIELD, SF = 1.5; ULTIMATE, SF = 3.0

DESIGN LOADS are operating loads plus seismic
YIELD, SF = 1.25; ULTIMATE, SF = 2.5

ABNORMAL LOADS include dead weight and transportation or manufacturing loading
YIELD, SF = 1.0; ULTIMATE, SF = 1.67

The developed loading is listed in Table 3.2-8.

A preliminary clevis and pin sizing was performed and a summary of the results are listed in Table 3.2-9. The margin for the pin could be increased by changing the clevis material. That is, if a higher strength material is used for the clevis the wall thickness could be reduced, thus shortening the moment arm on the pin.

Table 3.2-8. Summary of Developed Clevis Loading - Four Support Locations/Magnet

LOADING	DIRECTION	LOADING, LB			
		HORIZONTAL		VERTICAL	
		YIELD	ULTIMATE	YIELD	ULTIMATE
OPERATIONAL LOADING (& Storage)	Tension	ϕ	ϕ	ϕ	ϕ
	Comp.			$(2500)(1.5) = 3750$	$(2500)(3) = 7500$
DESIGN LOADS (DW + Seismic)	Tension	$(.7)(5000)(1.25) = 4375$	$(.7)(5000)(2.5) = 8750$	$(.7)(2500)(1.25) = 2188$	$(.7)(2500)(2.5) = 4375$
	Comp.	$= 4375$	$= 8750$	$(1.7)(2500)(1.25) = 5313$	$(1.7)(2500)(2.5) = 10625$
ABNORMAL LOADING (TRANSPORTATION)	Tension	$(1)(5000)(1.0) = 5000$	$(1)(5000)(2) = 10000$	$(2500)(4)(1.0) = 10000$	$(2500)(4)(2) = 20000$
	Comp	$= 5000$	$= 10000$	$(2500)(5)(1.0) = 12500$	$(2500)(5)(2.0) = 25000$

Table 3.2-9. Summary of Margin-of-Safety Values on the Strut Clevis and Pin

MARGINS OF SAFETY		
	CLEVIS SIDE	ROD END SIDE
MATERIAL	304L @ RT $F_{ty} = 25 \text{ ksi}$ $F_{tu} = 70 \text{ ksi}$	Titanium @ RT $F_{ty} = 120$ $F_{tu} = 130$
GEOMETRY	$t = 0.375$, width = 2	$t = 0.25$, width = 1.625
CLEVIS BEARING		
- Ultimate	+0.66	+0.057
- Yield	+0.24	+0.876
CLEVIS TENSION		
- Ultimate	+0.27	+0.04
- Yield	+0.78	+0.92
CLEVIS WELD		
- Tension, Ult.	+0.12	N/A
- Bending, Ult.	+3.14	N/A
PIN	MATL. 286 $F_{ty} = 130 \text{ ksi @ RT}$ $F_{bend} = 186 \text{ ksi (x1.7 bending section factor)}$	
- Shear	+ 0.915	
- Bending (peak)	+ 0.0	

For the 3-Inch Tubing

$$* \rho = \rho_{\text{tube}} + \rho_{\text{LHe}} = .289 \text{ lb/in}^3 + 0.005 \text{ lb/in}^3 = .03 \text{ lb/in}^3$$

$$A = \pi/4 (D^2 - d^2) = \pi/4 (3.0^2 - 2.834^2) = 0.76 \text{ in}^2$$

$$W = \rho A = .3 \text{ lb/in}^3 (.76 \text{ in}^2) = .23 \text{ lb/in}$$

$$I = \pi/64 (D^4 - d^4) = 0.81$$

*(ρ = density (lb/in³))

Assuming tubing is simply supported

$$\Delta_{\text{max}} = .02 \frac{5wL^4}{384 EI} (5 \text{ G's})^*$$

*5G handling load

$$.02 = \frac{5(.23)L^4 (5)}{384 (28 \times 10^6) (.81)}$$

Solving for L,

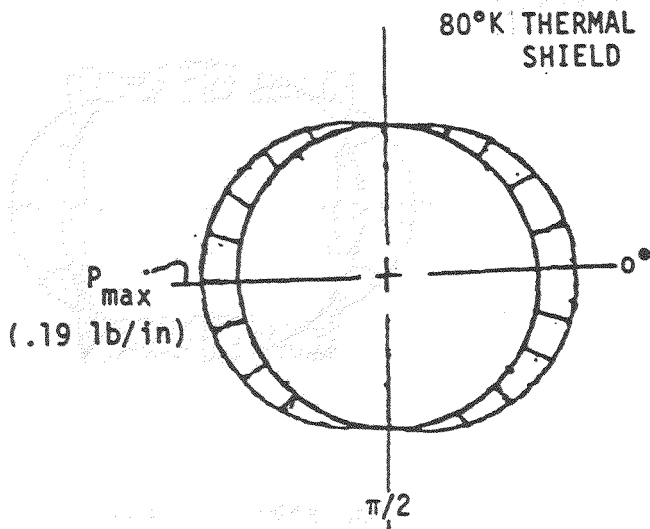
$$L = 6.18 \text{ ft}$$

For the 2-Inch Tubing:

$$L = 5.018 \text{ ft}$$

- 3.2.9 THERMAL SHIELDS ANALYSIS. There are two thermal shields shown in Figure 3.2-3, a 20°K stainless-steel inner shield and an 80°K aluminum outer shield. Both shields have a wall thickness of 0.10 inches. Between the shields, and also between the outer shield and the vacuum vessel, spacers are provided to hold the various surfaces in place and prevent contact. As such, the thermal shields are not structural components, they are self-supporting with respect to dead weight and seismic load. One area of structural concern, however, is the moment imposed on the 80°K shield resulting from the electromagnetic eddy currents. The magnitude of the eddy current load was substantially reduced by slotting the shield circumferentially every 16 inches.

The following is the analysis of the bending stresses imposed on the 80°K shield due to the eddy current.



$$O.D. \text{ shield} = 22.0''$$

Assume:

- o Free-standing shield
- o Eddy current loading is a cosine function
- o $P_{max} = 0.19 \text{ lb/in.}$

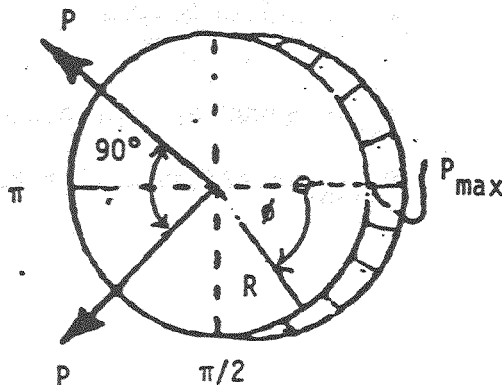
Ref. 3.2-7 Convair Report AZS-27-276, Rev. A, "Rigid Ring Frames - Load and Deflection Summary."

The analysis uses Case 24 of Ref. 3.2-7 and applies superposition to arrive at an equivalent loading.

$$P_{max} = 0.19 = \frac{4 \sin \theta / 4}{\pi R} P = 0.0818 P$$

$$P = 2.32 \text{ lb}$$

Case 24:

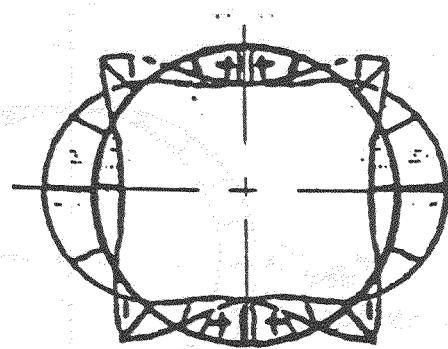
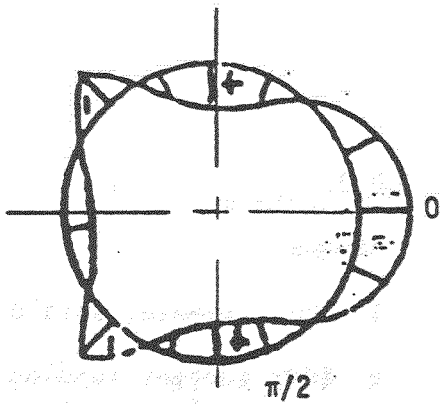


$$M = K_M PR$$

$$P = P_{max} \cos \theta$$

$$P_{max} = \frac{4 \sin \theta / 4}{\pi R} P$$

Factor	Location	Formula
K_M	$0 - \pi/2$	$\sin \pi/4 \left[\frac{2 \theta \sin \theta}{\pi} + (3/2 + 1/4) \cos \theta - 4/\pi^2 \right] - 1/\pi$
	$\pi/2 - 3/4$	$\sin \pi/4 \left[\sin \theta + (1/4 - 1/2\pi) \cos \theta - 4/\pi^2 \right] - 1/\pi$
	$3\pi/4 - \pi$	$\sin \pi/4 \left[-(3/4 + 1/2\pi) \cos \theta - 4/\pi^2 \right] - 1/\pi$



ϕ	K_M Moment Factor
0	-0.09050
$\pi/8$	+0.06200
$\pi/4$	+0.00884
$3\pi/8$	+0.09193
$\pi/2$	+0.10222
$5\pi/8$	+0.02382
$3\pi/4$	-0.15030
$7\pi/8$	-0.01095
π	+0.03799

- applying superposition as shown above, the max. moment factor will be
 $0.10222 + 0.10222 = 0.20444 @ \pi/2$

$$M = .20444 (2.32 \text{ lb})(22.5 \text{ in}) = 10.7 \text{ in-lb}$$

$$\sigma = MC/I$$

$$I = \frac{bh^3}{12} = \frac{(.1)^3}{12} = 8.33 \times 10^{-5} \text{ in}^4$$

$$\sigma = \frac{(10.7)(0.05)}{8.33 \times 10^{-5}} = 6420 \text{ psi}$$

$$F_{ty} = 35000 \text{ psi for Al6061-T6 at RT}$$

$$\sigma_{allow} = 2/3(35 \text{ ksi}) = 23.3 \text{ ksi}$$

3.2.10 REFERENCES

- 3.2-1 SSC Design "D" Cryostat Design Criteria Initial Release, FNAL Memo dated 15 February 1985
- 3.2-2 MIL-HDBK-5C, dated 15 December 1978
- 3.2-3 Analysis and Design of Flight Vehicle Structures, E. F. Bruhn
- 3.2-4 HP-41 Hand Calculator Handbook
- 3.2-5 Expansion Joint Manufacturers Association Standards, 5th Edition, 1980
- 3.2-6 ASME Boiler and Pressure Vessel Code, Section VIII
- 3.2-7 Convair Report AZS-27-276, Rev. A, "Rigid Ring Frames - Load and Deflection Summary"

3.3 THERMODYNAMICS ANALYSIS. This section is a summary of the thermal analysis calculations. The objectives of the analysis are two-fold: first, to establish a rational criteria for determining certain significant thermal design parameters; and second, to estimate the heat loads of the design to the point that they may be compared with alternate cryostat designs and to provide a preliminary capacity requirement for the cryogenic plant.

The criteria to determine the thermal design parameters is cost; specifically, the cost of refrigeration associated with a given element of the design. The first part of this section shows how the total lifetime cost of refrigeration required to remove a watt of heat from the cryostat is determined.

There are two primarily thermal design parameters that are addressed in this study: the location of the thermal intercepts on the cold-mass supports, and the thickness of the MLI blankets. In each case, a certain choice will produce a minimum cost. These analyses are reported in the second and third parts of this section.

Finally, the details of the calculations made to determine the cold-mass support heat leak, the heat leak through the MLI blankets, and the thermal shield support heat leak are documented. In addition, analyses to determine the thermal shield thickness and intercept effectiveness are presented. A summary table of heat leaks for the LBL SSC cryostat design concludes the section.

3.3.1 LIFE CYCLE COST OF REFRIGERATION. The cost of refrigeration impacts the choice of the support concept for the SSC, the location of the thermal intercepts on the supports, and the number of layers of MLI used to insulate the thermal shields. In order to properly evaluate the relative costs of an option, when part of the costs are distributed over a period of years, the time value of money must be accounted for. In the following analyses, the present value of the cost of refrigeration of an option is determined so that it may be compared on an equal basis to the material and manufacturing costs of that option. What is meant here by the present value of the cost of refrigeration is that amount of money which, when placed in a bank account at a given interest rate, will buy the necessary refrigeration equipment and pay the annual electric bill for the lifetime of the accelerator, leaving nothing left at the end of the lifetime. The cost includes both operating cost and capital cost of the refrigerator.

3.3.1.1 Operating Costs. There are two components to the cost of refrigeration: the operating cost, which is the cost of electricity required to run the refrigerator compressors; and the capital cost, which is the price of the refrigeration plant. The operating cost is directly proportional to the amount of work required at the compressor which in turn is directly related to the refrigeration heat load. For the SSC, it is anticipated there will be three levels

of refrigeration, occurring at 4.5K, 10-20K, and at 80K. It is assumed that, from the point of view of the refrigerator, the capacities at these three temperature levels are independent. This is true for the 80K load, since this will be handled by a separate refrigerator. The low-temperature and 4.5K capacities are not truly independent. The assumption of independence is based on the assumption that the low temperature (10-20K range) will be chosen to optimize the overall efficiency of the refrigerator, and that small excursions from the optimum load distribution will not affect the performance significantly.

Given that the refrigeration capacities are independent at various temperatures, the total compressor work (room-temperature work input) can be determined by summing the loads at each temperature divided by the refrigerator coefficient of performance at that temperature:

$$\dot{W}_c = \sum_i \frac{\dot{Q}(T_i)}{\text{COP}(T_i)}$$

The value of coefficient of performance (COP) at a given temperature is based on accumulated operating experience with cryogenic refrigerators. Sources of data include References 3.3-1 and 3.3-2, which are surveys of refrigerator performance, and Reference 3.3-3, which is a computer analysis of a particular refrigeration cycle. Representative values are listed in Table 3.3-1 for temperatures of 4.5K, 10K, 20K, and 80K. Two low-temperature values are carried because it is unclear at this time what the final cold-shield temperature will be. The COP values actually used in the following analyses are taken from the first reference: 1/430 w/w @ 4.5K, 1/170 w/w @ 10K, 1/85 w/w @ 20K, and 1/12 w/w @ 80K. These values were chosen since they weight the 4.5K heat load the most.

Once the required compressor power is known, it is easily converted into an annual electric bill:

$$A = 8760 d c \dot{W}_c, \$$$

Here d is the average duty cycle of the load, c is the cost of electricity in \$/kw-hr, and 8760 is the number of hours in one year. In the refrigeration cost studies reported in the following sections, the cost of electricity has been assumed to be \$0.06/kw-hr. An optimistic 100 percent duty cycle has also been assumed.

Table 3.3-1. Representative Values of Cryogenic Refrigerator Coefficients of Performance (COP)

Temperature	Ref. 3.3-1*	Ref. 3.3-2	Ref. 3.3-3
4.5K	.0023 (430 W/W)	.0028 (360 W/W)	.0029 (345 W/W)
10K	.0059 (170 W/W)	.0069 (145 W/W)	N/A
20K	.012 (85 W/W)	.014 (70 W/W)	.0081 (123 W/W)
80K	.083 (12 W/W)	.069 (14 W/W)	.047 (21 W/W)

*Chosen design values.

The life cycle refrigeration operating cost for a particular component has been taken to be the present value of the annual electric bills paid over the lifetime of the SSC. It is determined from the formula:

$$PV = A \left[\frac{(1+i)^n - 1}{i(1+i)^n} \right], \$$$

where i is the prevailing annual interest rate, and n is the lifetime of the machine in years. For these studies i has been taken as the current T-bill rate of 8.2 percent. The refrigeration load has been assumed to have a 10-year life. (Note that the analyses need to be updated to reflect the true situation of a 50 percent duty cycle over a 20-year economic life.

When the above calculations are carried out for unit heat loads at the various design temperatures, the results are: \$1500/watt at 4.5K, \$594/watt at 10K, \$297/watt at 20K, and \$42/watt at 80K.

3.3.1.2 Capital Costs. The capital cost of the refrigeration system can also be estimated for SSC. Reference 3.3-2 yields a correlation between refrigeration cost and installed compressor capacity:

$$C = 6000 (\dot{W}_i)^{0.7}$$

Note that installed compressor capacity, \dot{W}_i (in kW) is a little different than the required compressor power computed above, it includes the margin m , or excess capacity, incorporated into the cryogenic plant:

$$\dot{W}_i = (1+m) \dot{W}_c$$

When computing the capital cost of refrigeration attributable to one relatively small element of a large refrigeration load, the incremental cost should be used. This is defined as:

$$\Delta C_{cap} = \frac{dC}{d\dot{Q}} \Delta \dot{Q}$$

which, when combined with the above correlation, becomes

$$\Delta C_{\text{cap}} = 4200 (1+m)(W_i)^{-0.3} \frac{\Delta \dot{Q}}{1000 \text{ COP}}$$

where W_i is in kW and the incremental heat load $\Delta \dot{Q}$ is in watts. From Reference 3.3-3, the nominal baseline capacity required for the 1-in-1 reference design "D" is 12 x 928 kW at 80K, which includes a margin of 140 percent, and 12 x 2100 kW for combined 4K and 20K (or 10K) refrigeration, including a 50 percent margin. Using these values, at 80K

$$\begin{aligned} \frac{\Delta C}{\Delta Q} &= (4200)(2.4)(928)^{-0.3} (.012) \\ &= \$15.6/\text{watt} \end{aligned}$$

while at 10K,

$$\begin{aligned} \frac{\Delta C}{\Delta Q} &= (4200)(1.5)(2100)^{-0.3} (.170) \\ &= \$108/\text{watt} \end{aligned}$$

and at 4.5K

$$\begin{aligned} \frac{\Delta C}{\Delta Q} &= (4200)(1.5)(2100)^{-0.3} (.430) \\ &= \$274/\text{watt} \end{aligned}$$

The total combined refrigeration costs are \$57.6/watt at 80K, \$702/watt at 10K, and \$1774/watt at 4K. With this relation the impact of a change in heat leak of a component on the capital cost of the refrigerator can be fairly assessed.

Likewise, the total life-cycle cost (capital plus present value of operating) of a change in heat leak of a component can be fairly assessed against the material and/or manufacturing cost of making the associated design change.

3.3.2 THERMAL INTERCEPT LOCATIONS. There is an optimum location for a thermal intercept on a cold-mass support strut. For example, a 4.5K heat leak can be made to essentially vanish if a 20K intercept is placed "far enough" away from the cold end. This is done at the expense of increasing the heat load into the 20K intercept. The object of this analysis is to find the locations of the intercepts that minimize the total room temperature compressor work input.

The cost function in this case is the total compressor work,

$$\dot{W}_c = \frac{\dot{Q}(4.5)}{\text{COP}(4.5)} + \frac{\dot{Q}(10)}{\text{COP}(10)} + \frac{\dot{Q}(80)}{\text{COP}(80)}$$

To get a general result, a general support must be analyzed. Such a support, together with the pertinent nomenclature, is defined in Figure 3.3-1. The key assumption is that the inverse area integral is linear in x , i.e., constant area. The following analysis will be valid for supports that have essentially a constant cross section. If an 80K intercept is located at x_1 , and a 10K intercept at x_2 , the 4.5K, 10K, and 80K heat leaks are

$$\dot{Q}_{4.5} = \frac{\theta(10) - \theta(4.5)}{\left(1 - \frac{x_1}{l}\right) \int \frac{dx}{A}}$$

$$\dot{Q}_{10} = \frac{\theta(80) - \theta(10)}{\left(\frac{x_2}{l} - \frac{x_1}{l}\right) \int \frac{dx}{A}} - \dot{Q}_{4.5}$$

$$\dot{Q}_{80} = \frac{\theta(300) - \theta(80)}{\frac{x_1}{l} \int \frac{dx}{A}} - (\dot{Q}_{10} + \dot{Q}_{4.5})$$

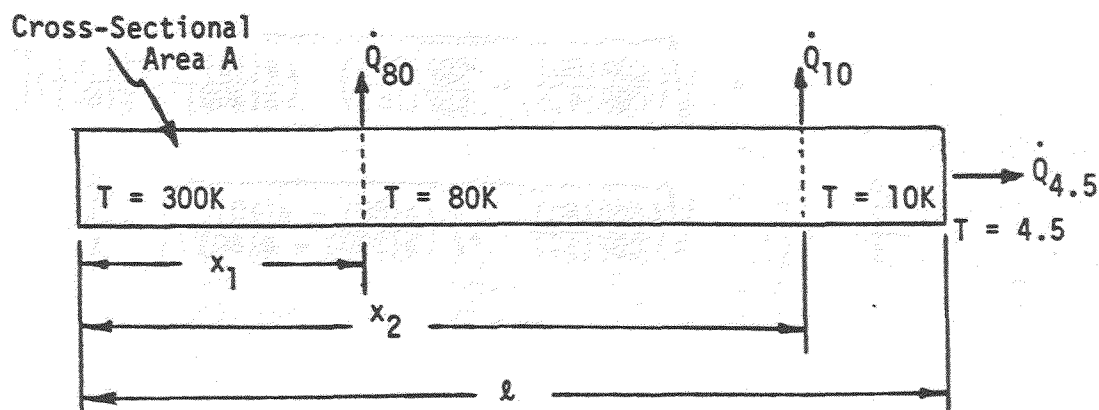


Figure 3.3-1. Generalized Support for Intercept Location Analysis

respectively, where $\theta(T)$ is the thermal conductivity integral of the support material. These can be incorporated into the cost function, rearranged, and the result generalized to yield

$$\begin{aligned} \dot{W}_c \int \frac{dx}{A} &= \left[\frac{1}{\text{COP}(4.5)} - \frac{1}{\text{COP}(10)} \right] \left[\frac{\theta(10) - \theta(4.5)}{1 - x_2/l} \right] \\ &+ \left[\frac{1}{\text{COP}(10)} - \frac{1}{\text{COP}(80)} \right] \left[\frac{\theta(80) - \theta(10)}{x_2/l - x_1/l} \right] \\ &+ \left[\frac{1}{\text{COP}(80)} \right] \left[\frac{\theta(300) - \theta(80)}{x_1/l} \right] \end{aligned}$$

The cost for any support with a given length-to-area ratio will depend on the thermal conductivity integral of the support material, the refrigerator COP at the intercept temperatures, and the location of the intercepts relative to the total length. Given that the intercept locations are the only free design variables, the cost can be minimized by finding the values of x_1 and x_2 that simultaneously satisfy

$$\frac{\partial}{\partial x_1} \left[\dot{W}_c \int \frac{dx}{A} \right] = 0$$

$$\frac{\partial}{\partial x_2} \left[\dot{W}_c \int \frac{dx}{A} \right] = 0$$

The solution of this system of two equations is

$$\begin{aligned} \frac{x_1^0}{l} &= \left[1 + \sqrt{\left(\frac{\text{COP}(80)}{\text{COP}(10)} - 1 \right) \left(\frac{\theta(80) - \theta(10)}{\theta(300) - \theta(80)} \right)} \right. \\ &\quad \left. + \sqrt{\left(\frac{\text{COP}(80)}{\text{COP}(4.5)} - \frac{\text{COP}(80)}{\text{COP}(10)} \right) \left(\frac{\theta(10) - \theta(4.5)}{\theta(300) - \theta(80)} \right)} \right]^{-1} \end{aligned}$$

$$\frac{x_2^0}{l} = \left[1 + \sqrt{\left(\frac{\text{COP}(80)}{\text{COP}(10)} - 1 \right) \left(\frac{\theta(80) - \theta(10)}{\theta(300) - \theta(80)} \right)} \right] \frac{x_1^0}{l}$$

For this study, the COP for refrigeration at 4.5K has been taken to be 1/430 w/w, at 10K 1/170 w/w, and at 80K 1/12 w/w. Two materials were considered, 6Al-4V-Ti and G-10CR. The appropriate thermal conductivity integrals for these materials are listed in Table 3.3-2. When these values are inserted into the above equations for x_1 and x_2 , the results are, for titanium supports:

$$\frac{x_1^0}{\ell} = .40$$

$$\frac{x_2^0}{\ell} = .92$$

and for G-10CR:

$$\frac{x_1^0}{\ell} = .37$$

$$\frac{x_2^0}{\ell} = .88$$

These values were used on all support concepts analyzed in the trade study described in Section 2.0, and for the baseline design analyzed in Section 3.3.4.

3.3.3 MLI TRADE STUDY. In this section the thermal design details of the proposed MLI system is described and the method of computing the heat leak through a blanket is defined. A basic trade-off between the cost of refrigeration and the capital cost of a blanket is established as a function of the number of layers in the blanket. The results are plotted to determine the optimum number of layers in the SSC MLI blankets, and to establish recommendations for further work during detailed design.

3.3.3.1 DAM/Dacron Scrim. The multilayer superinsulation blankets are made of double-aluminized Mylar film reflectors, with Dacron scrim cloth separators. The aluminum coating on the one-mil thick Mylar film is vacuum deposited to a thickness of roughly 200-300 angstroms. This yields a surface total hemispherical emittance of less than 0.035 for the virgin surface. The "installed" emittance may be as high as 0.07 after handling, aging, etc. The nominal design for the scrim cloth is a loose leno weave, which creates a lockstitch in the weave. The result is a flimsy, lightweight, open cloth that does not tend to unravel and hence is sturdy and easy to work with. The reflectors and scrim layers are held together with full

Table 3.3-2. Thermal Conductivity Integrals for Titanium and G-10

Temperature	$\phi(T)$ (W/cm)	
	6Al-4V-Ti	G-10CR
4.5	0	0
10	.0236	.00615
20	.0990	.0228
80	1.63	.195
300	13.9	1.54

penetration fasteners, typically made of nylon. The fasteners degrade the insulating performance of the blanket, but offer structural integrity primarily for ease of handling during manufacturing. Added strength is provided by the reinforcing threads glued to the two outer sheets. The adhesive is rated for cryogenic service. This type of system has been used on numerous space flights to insulate cryogenic fuel tanks.

3.3.3.2 Effective Conductivity. Several studies have experimentally evaluated the effective conductivity of MLI blankets of this type. Two extensive investigations are reported in References 3.3-4 and 3.3-5. The typical approach is to divide the effective "k" into a conduction component and a radiation component. The radiation component depends on the number of reflectors in the blanket and on the emissivity of the surfaces, and can be calculated with standard radiation heat transfer techniques. The conduction component depends on the contact resistance between the various elements in the blanket, and is determined empirically. The significant parameter is the layer density of the blanket: layers compressed together yield a much higher heat leak. In the following heat transfer calculations, the MLI effective "k" is computed from (Reference 3.3-4):

$$k = 3.007 \times 10^{-25} n^{8.6} \frac{T_h + T_c}{2} + \frac{N}{N-1} \frac{\sigma}{12n(2/\epsilon-1)} (T_h^2 + T_c^2)(T_h + T_c)$$

where k = effective conductivity, BTU/hr-ft²-R

N = number of reflector layers in the blanket

n = layer density of the blanket, layer/inch

ε = emissivity of reflector

σ = Stefan-Boltzmann constant, BTU/hr-ft²-R⁴

T_h = hot side boundary temperature, R

T_c = cold side boundary temperature, R

GDC standard practice is to multiply the resulting value by a factor of four to account for degradations due to seams, penetrations, etc. in the blanket. For an application such as SSC, where the surface-to-volume ratio of the "tank" is very large, the degradation is probably not this serious. However, the factor has been used to provide conservatism in the calculations.

For an unconstrained thickness blanket, i.e., one that is not compressed except by its own weight, the layer density is a parameter of the blanket itself. The only design variable affecting the heat leak of the blanket is the number of layers. A basic trade-off exists between the cost of refrigeration, which is reduced by adding more layers, and the cost of the blanket, which increases with more layers. The object of this study is to determine the optimum of layers, and therefore the minimum total cost, of the MLI blankets for the SSC. The analysis is done for a unit area of blanket.

The first step is to determine the cost of the refrigeration attributable to the heat leak through the blankets. In the following, "warm" blanket will refer to the blanket insulating the 80K shield from the vacuum vessel (i.e., the blanket boundary temperatures are 300K and 80K), and "cold" blanket will refer to the MLI between the 80K and low-temperature shields. Note that in the actual analysis done, the low-temperature shield was assumed to be at 4.5K. The layer density in either blanket is nominally 75 layers per inch. The effective conductivity for the warm blanket is, then:

$$\begin{aligned}
 k_w &= 4 \left[(3.007 \times 10^{-25}) (75)^{8.6} \left(\frac{540+144}{2} \right) \right. \\
 &\quad \left. + \frac{(1.714 \times 10^{-9}) (540^2 + 144^2) (540+144) N}{(12)(2/.03-1)(75) N-1} \right] \\
 &= 5.49 \times 10^{-6} + 2.32 \times 10^{-5} \frac{N}{N-1}, \text{ BTU/hr-ft-R}
 \end{aligned}$$

while for the cold blanket is

$$\begin{aligned}
 k_c &= 4 \left[(3.007 \times 10^{-25}) (75)^{8.6} \left(\frac{144+8}{2} \right) \right. \\
 &\quad \left. + \frac{(1.714 \times 10^{-9}) (144^2 + 8^2) (144 + 8) N}{(12)(2/.03-1)(75) N-1} \right]
 \end{aligned}$$

$$= 1.22 \times 10^{-6} + 4.04 \times 10^{-7} \frac{N}{N-1}, \text{ BTU/hr-ft-R}$$

The blanket heat leak, per square foot, is

$$\frac{\dot{Q}}{A} = \frac{k\Delta T}{t}$$

where now t is the thickness in feet through the blanket, equal to $N/12n$. The heat leak through each blanket can now be expressed in terms of the number of layers in the blanket:

$$\begin{aligned} \frac{\dot{Q}}{A} &= \frac{k_w}{N} (12)(75)(540-144) \\ &= \frac{1.96}{N} + \frac{9.73}{N-1}, \text{ BTU/hr-ft}^2 \end{aligned}$$

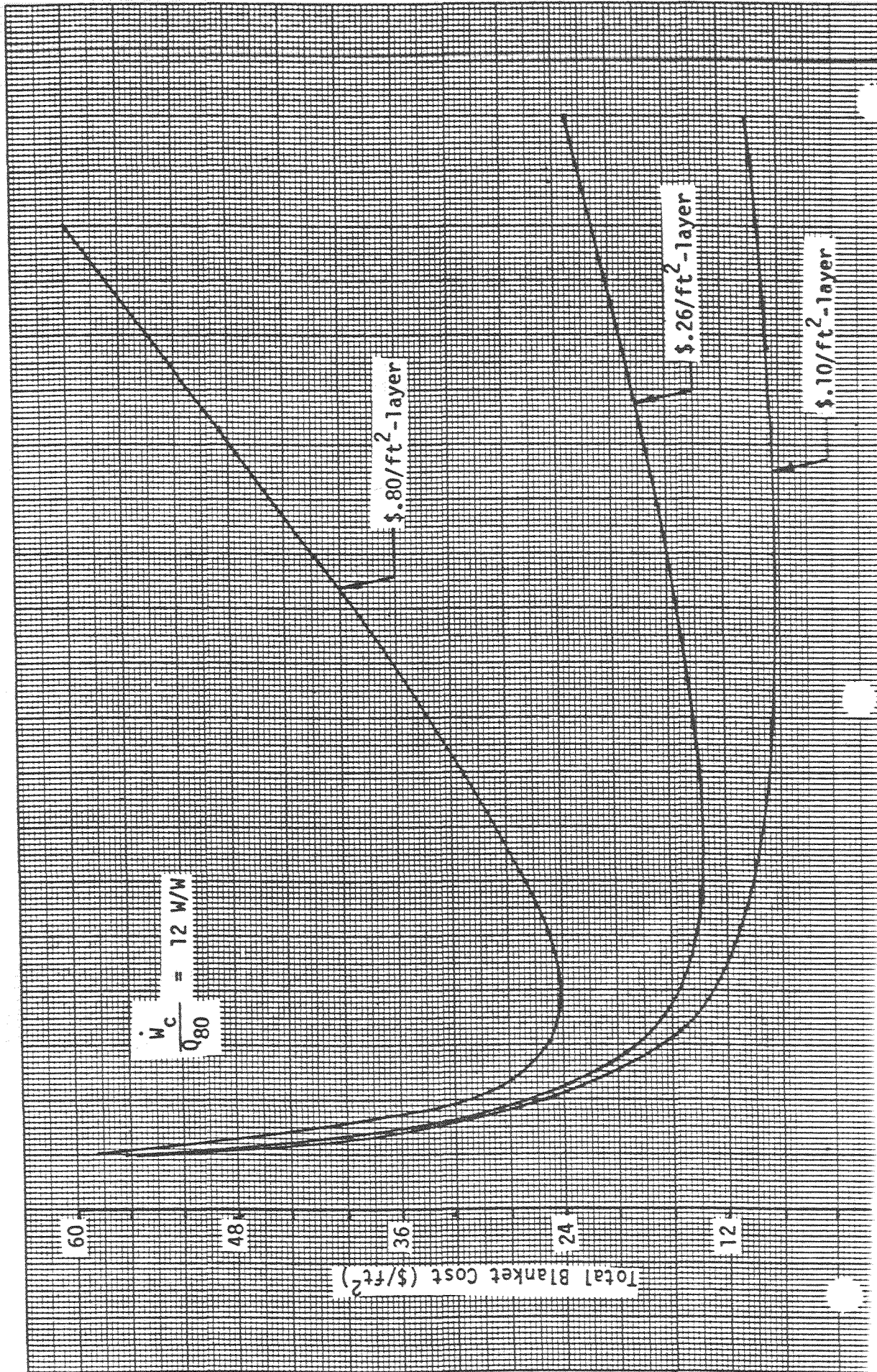
for the warm blanket, and

$$\begin{aligned} \frac{\dot{Q}}{A} &= \frac{k_c}{N} (12)(75)(144-8) \\ &= \frac{.149}{N} + \frac{0.496}{N-1}, \text{ BTU/hr-ft}^2 \end{aligned}$$

for the cold blanket.

This heat leak is converted to an operating life cycle cost as outlined in Section 3.3.1. For 80K refrigeration, the operating life-cycle cost is \$42/watt, and for 4.5K refrigeration is \$1500/watt. Therefore, the refrigeration costs attributable to the blankets, per square foot, are

$$C_{\text{ref}_w} = \frac{29.1}{N} + \frac{144}{N-1}, \text{ \$/ft}^2$$



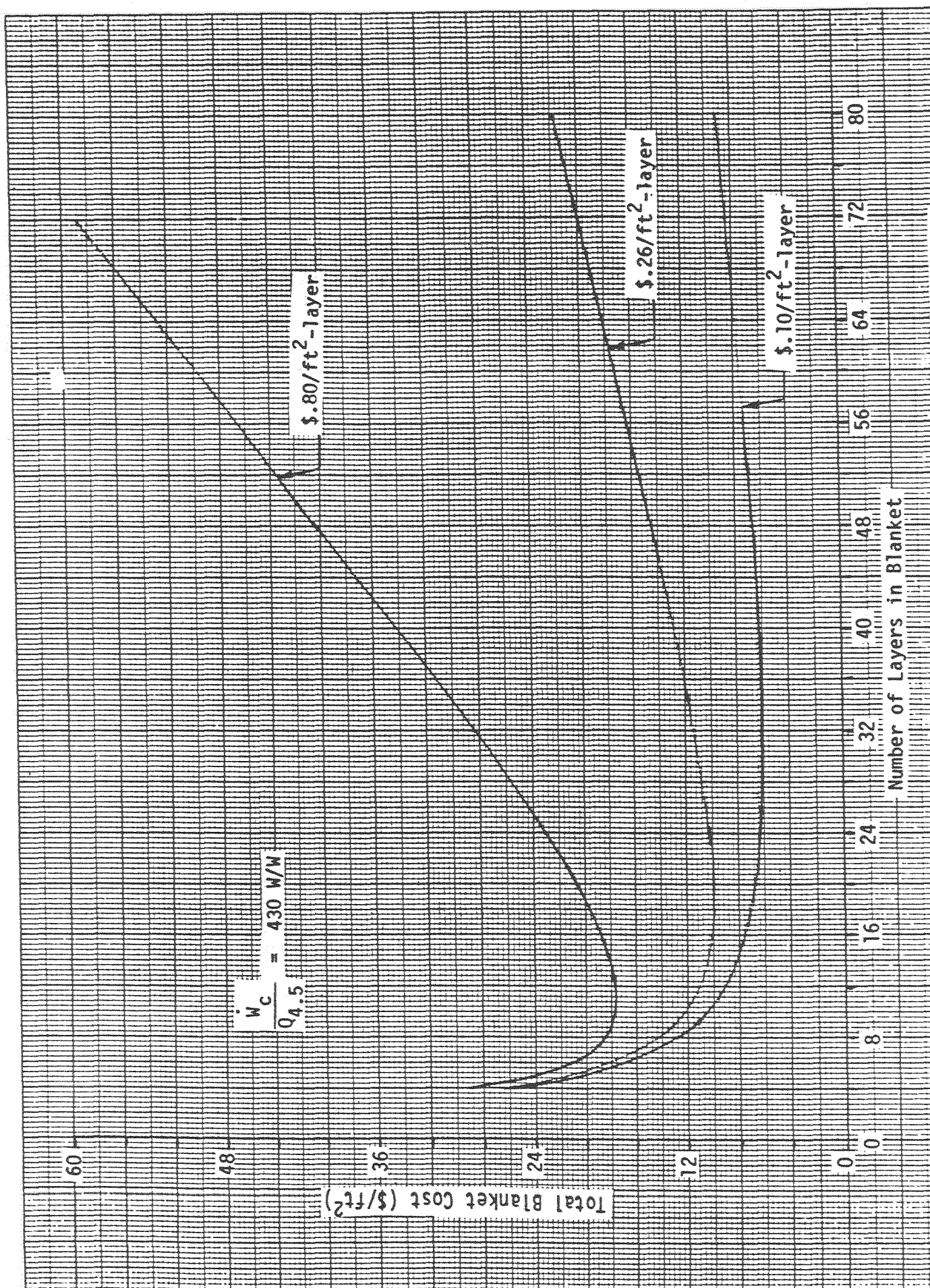


Figure 2-2-3 Combined Material and Refrigeration Costs for an 80K-5K Blanket

longer the pump-down time due to increasing outgassing and a higher flow impedance through the blanket. Thus there is a cost penalty associated with a large number of layers in the blanket. This tends to shift the optimum layer number to the left. At present, GDC has no data to quantify this effect; it may or may not be significant.

With this study, the pertinent parameters that influence the optimum number of blanket layers have been identified. Estimates of the appropriate values have been made to determine a preliminary optimum (minimum cost) design. To advance to a detailed design level, the real unit cost of the blanket must be better defined. Refrigerator operating efficiencies for SSC should be better defined, as well as the cost associated with pump-down time. With these inputs, a minimum-cost MLI system can be established.

3.3.4 BASELINE DESIGN THERMAL ANALYSIS

3.3.4.1 Support Heat Leak. The chosen baseline design for the cold mass supports is a set of three titanium struts (two vertical and one horizontal) located at four stations along the magnet length. The struts are anchored at each end with a pin through a bushing in a "rod-end." As in the heat leak analysis for the support trade study, the heat leak analysis for the baseline design assumes 1) one-dimensional heat conduction only; 2) the warm and cold boundaries of the support are located at the pin centerlines and are 300K and 4.5K, respectively; 3) the struts are heat sunk to 80K and 10K shields which are located to minimize the total required compressor work; and 4) required compressor work is 430 w/w @ 4.5K; 170 w/w @ 10K, and 12 w/w @ 80K.

The significant geometry parameters of the struts are shown in Figure 3.3-4. The pin-to-pin length of the vertical struts is 30.5 cm, the OD is 3.51 cm, and the wall of the tube is .147 cm thick. The rod ends are not completely defined at the time of this analysis, but are assumed to be made of titanium, penetrate the end of the tube to a depth of 1.27 cm, and have a .635-cm thick tongue. The end of the tube is assumed to be 1.27 cm away from the pin centerline. For the horizontal struts, the only differences are a 21.6-cm pin-to-pin length, 2.54 cm OD, and a .0889-cm thick wall.

and

$$C_{ref_c} = \frac{70.6}{N} + \frac{23.4}{N-1}, \text{ \$/ft}^2$$

respectively.

The capital cost of the blanket is less well defined. Logically, the cost should be composed of the material costs, which should be directly proportional to the number of layers, and a fixed cost of assembly. The available data is sketchy and does not provide this information. What was done was to take three estimates of blanket costs and divide by the blanket area and number of layers to get an approximate unit cost. The resulting costs are \$.10/layer-ft² (judged to be a realistic minimum), \$.26/layer-ft² (ROM estimate for accelerator state of the art) and \$.80/layer-ft² (judged to be a reasonable upper limit, based on other GDC magnet experience).

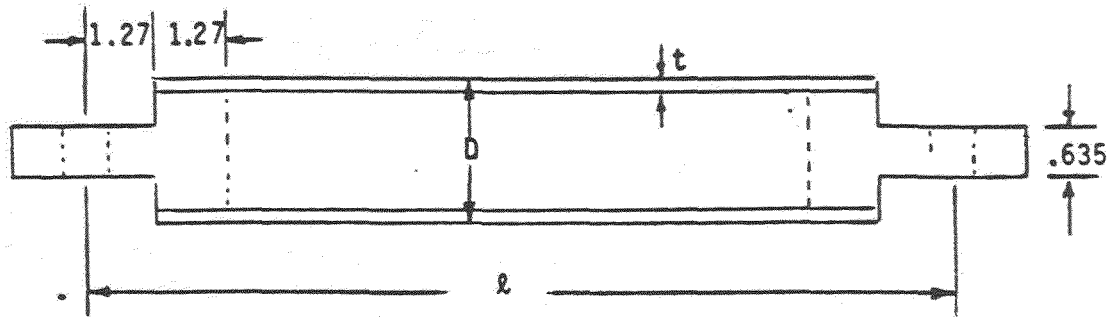
3.3.3.4 Results. The results are plotted in Figure 3.3-2 for the warm blanket and in Figure 3.3-3 for the cold blanket. The most significant result is that for the unit blanket capital costs of less than \$.25/layer-ft², the cost curve has a shallow minimum and the number of layers in the blanket has little impact on the total cost. At higher unit costs, getting the right number of layers has more significance.

Although it cannot be seen from the plots, a comparison of total costs was made assuming different refrigerator COP's. At 23W/W for 80K refrigeration, the curves of Figure 3.3-2 shift upward and to the right by roughly 30 percent on each scale. The shape is the same.

The cost curves for the cold blanket are qualitatively the same as for the warm blanket, but due to the higher cost of refrigeration at the lower temperature, the optimum number of layers shifts to the left. This means it is cost effective to save a little money on the capital cost of the cold blankets and use it to pay the electric bill for refrigeration over the life of the magnet. Note that the total cost of the warm blanket is roughly half again the cost of the cold blanket.

There is one factor that will influence the results of a study of this nature which has been ignored. There is an operating cost associated with the effort required to pump down the vacuum space. This is dominated by the outgassing rate of the MLI. The more layers of MLI, the

All dimensions in centimeters



	<u>Vertical</u>	<u>Horizontal</u>
D	3.51	2.54
t	.147	.0889
	30.5	21.6

Figure 3.3-4. Thermal Parameters for Baseline Support Analysis

The inverse area integrals for the struts are computed assuming heat is only conducted parallel to the strut axis.

For the vertical strut:

$$\int \frac{dx}{A} = \frac{1.27}{(3.51)(.635)} + \frac{1.27}{(\pi/4)(3.51)^2} + \frac{25.4}{(\pi/4)(3.51^2 - 3.20^2)} + \frac{1.27}{(\pi/4)(3.51)^2} + \frac{1.27}{(3.51)(.635)} = 16.9 \text{ cm}^{-1}$$

For the horizontal strut:

$$\int \frac{dx}{A} = \frac{1.27}{(2.54)(.635)} + \frac{1.27}{(\pi/4)(2.54)^2} + \frac{16.5}{(\pi/4)(2.54^2 - 2.36^2)} + \frac{1.27}{(\pi/4)(2.54)^2} + \frac{1.27}{(2.54)(.635)} = 16.9 \text{ cm}^{-1}$$

The optimum location for the 10K shield is at 90 percent of the total inverse area integral, measured from the warm end. This requires the intercept to be located 4.19 cm from the cold pin centerline. The rod end dominates the thermal resistance between the 10K shield and the cold mass, therefore the 4.5K heat leak is really only known as well as the rod end is defined. Given that the thermal conductivity integral for titanium between 4.5K and 10K is .0236 w/cm and the 4.5K heat leak is conducted over 10 percent of the total inverse area integral, the vertical and horizontal titanium strut heat leaks are:

$$Q_{4.5_v} = \frac{.0236}{(.10)(16.9)} = .0140 \text{ W/vertical strut}$$

$$Q_{4.5_h} = \frac{.0236}{(.10)(25.9)} = .00911 \text{ W/horizontal strut}$$

The optimum 80K shield location is at 40 percent of the total inverse area integral as measured from the warm end. This puts the 80K intercept at 12.4 cm from the warm pin centerline. The design of the rod ends does not contribute significantly to the location of the 80K intercepts. For a titanium thermal conductivity integral of 1.62 w/cm from 10K to 80K, the vertical and horizontal strut 10K heat leaks (conduction over 50 percent of the total inverse area integral less the 4.5K heat leak) are:

$$Q_{4.5_v} = \frac{1.62}{(.5)(16.9)} - .0140 = .178 \text{ W/vertical strut}$$

$$Q_{4.5_h} = \frac{1.62}{(.5)(25.9)} - .00911 = .116 \text{ W/horizontal strut}$$

Finally, the 80K heat leak is determined for a conductivity integral of 12.3 w/cm and conduction over 40 percent of the inverse area integral, less the combined 4.5K and 10K heat leaks.

$$Q_{80_v} = \frac{12.3}{(.4)(16.9)} - (.178 + .0140) = 1.63 \text{ W/vertical strut}$$

$$Q_{80_h} = \frac{12.3}{(.4)(25.9)} - (.116 + .00911) = 1.06 \text{ W/horizontal strut}$$

The totals per magnet, given eight vertical and four horizontal supports, are:

$$Q_{4.5} = (8)(.0140) + (4)(.00911) = .148 \text{ W/magnet}$$

$$Q_{10} = (8)(.178) + (4)(.116) = 1.89 \text{ W/magnet}$$

$$Q_{80} = (8)(1.63) + (4)(1.06) = 17.3 \text{ W/magnet}$$

These heat loads can be translated back to an equivalent room temperature compressor work requirement. At 430 w/w for 4.5K refrigeration, 170 w/w for 10K refrigeration, and 12 w/w for 80K refrigeration, the total compressor power required is:

$$\dot{W}_c = (430)(.148) + (170)(1.89) + (12)(17.3) = 593 \text{ W}$$

For 8,760 hours in a year and at an electric rate of \$.06/kw-hr, the annual electric bill to refrigerate one magnet is \$306. The operating cost of refrigeration attributable to the titanium strut support concept, i.e., the present value of 10-year series of annual payments of \$306, is \$2,038 per magnet, given an interest rate of 8.2 percent.

3.3.4.2 MLI Blankets. The heat loads and associated life-cycle costs for the two MLI blankets are determined using the methods and results outlined in Section 3.3.3. A unit cost of \$.26/layer-ft² is selected as being most representative of true blanket costs. The optimum number of layers for the warm blanket is taken from Figure 3.3-2 to be 30 layers. For the cold blanket, from Figure 3.3-3, the optimum number is nominally 20 layers. The warm blanket has an estimated thermal conductivity, including the factor-of-four degradation, of 5.82×10^{-7} watts/cm-K. At a thickness of .953 cm, the heat flux through the blanket is

$$\begin{aligned} \frac{\dot{Q}}{A} &= \frac{k\Delta T}{t} = \frac{(5.82 \times 10^{-7})(300-80)}{.953} \\ &= 1.34 \times 10^{-4} \text{ W/cm}^2 \end{aligned}$$

The cross-sectional area of the warm blanket is approximately $2.78 \times 10^5 \text{ cm}^2$, given an average blanket diameter of 52 cm and a length of 17m. Therefore the total heat leak through the MLI to the 80K shield is

$$\begin{aligned} \dot{Q}_{80} &= (1.34 \times 10^{-4})(2.78 \times 10^5) \\ &= 37.3 \text{ watts/magnet} \end{aligned}$$

Likewise for the cold blanket, the effective conductivity, including the factor-of-four degradation, is 2.85×10^{-8} watts/cm-K for a 20-layer blanket between 80K and 4.5K. Assuming a 20K cold shield temperature, the heat flux is

$$\begin{aligned} \frac{\dot{Q}}{A} &= \frac{(1.85 \times 10^{-8})(80-20)}{.635} \\ &= 2.69 \times 10^{-6} \text{ W/cm}^2 \end{aligned}$$

through the .635 cm thickness. The inner blanket average diameter is 45.7 cm, so the total area per magnet is $2.44 \times 10^5 \text{ cm}^2$. The 20K heat leak through the cold blanket is, then,

$$\begin{aligned} \dot{Q}_{20} &= (2.69 \times 10^{-6})(2.44 \times 10^5) \\ &= .657 \text{ watts/magnet} \end{aligned}$$

From Section 3.3.1, the life-cycle cost associated with a watt of refrigeration at 80K is \$42, and with a watt of refrigeration at 20K is \$297. Therefore the life-cycle refrigeration cost of the warm MLI blanket is \$1567, and for the cold blanket is \$195.

3.3.4.3 Shield Analysis. It has been implicitly assumed that the thermal shields have no circumferential temperature gradient. In fact, there will be a finite temperature difference between the cryogenic fluid which cools the shield, and the point on the shield most remote from the coolant line. The necessary shield thickness required to keep the temperature rise within an allowable range can be determined by treating the shield as a fin subject to a uniform heat flux. The concept is illustrated in Figure 3.3-5. Along the shield circumference, the temperature is described by the differential equation

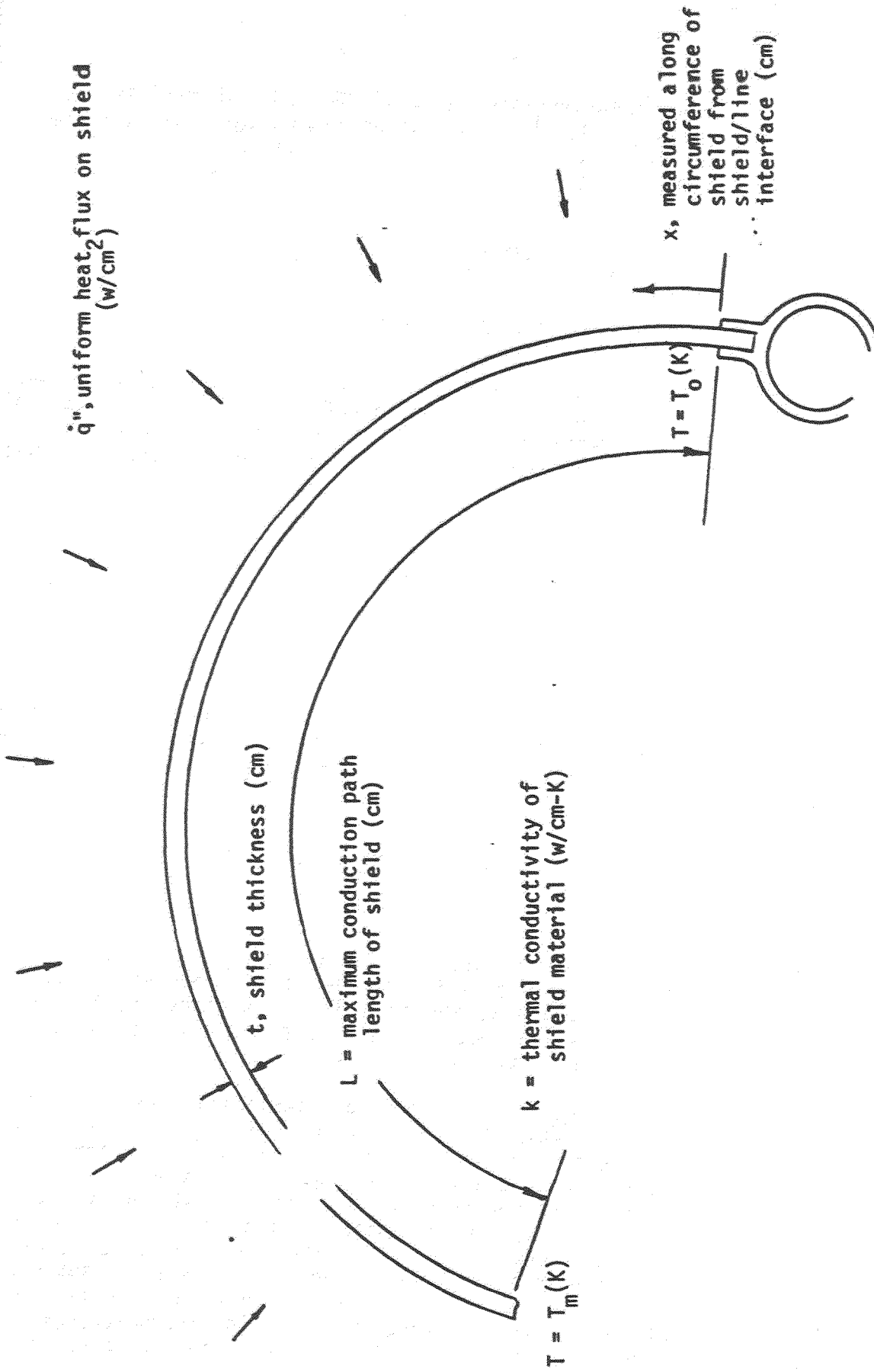


Figure 3.3-5. Geometry and Nomenclature of Shield Thickness Analysis.

$$\frac{d}{dx} \left[kt \frac{dT}{dx} \right] + q'' = 0$$

$$\frac{dT}{dx} \Big|_L = 0$$

$$T(0) = T_0$$

(Variables are defined in Figure 3.3-4.) For temperature ranges small enough that the thermal conductivity is constant, the solution of the above predicts the shield maximum temperature as

$$T_m = T_0 + \frac{q''L^2}{2kt}$$

The desired relation between the thickness of the shield and the allowable circumferential temperature rise is thus obtained.

The 80K shield is made from 6063 aluminum, for which the thermal conductivity at 80K is 2.3 w/cm-K. To keep the temperature rise to less than 2K over the 75 cm half-circumference, the required thickness is

$$t = \frac{(1.35 \times 10^{-4})(75)^2}{(2)(2.3)(2)}$$

$$= .0834 \text{ cm } (.033 \text{ in})$$

given an average heat flux of 1.35×10^{-4} w/cm² (from the blanket analysis above).

The 20K shield, for manufacturing reasons, is made from 304 stainless steel. At 20K, the thermal conductivity is .0173 w/cm-K. The thermal constraint on minimum thickness is, then

$$t = \frac{(2.69 \times 10^{-6})(64.4)^2}{(2)(.0173)(2)}$$

$$= .161 \text{ cm } (.063 \text{ in})$$

for an average heat flux of 2.69×10^{-6} w/cm² (blanket analysis) and a maximum temperature rise of 2K.

These thicknesses are thermal requirements only. Stress analysis may show a thicker section is required for structural integrity.

3.3.4.4 Shield Supports. At the time of the analysis the shield supports are only conceptually defined. Only a rough estimate of the heat leak can be made. The area is estimated by scaling the required G-10 cold mass support area by the ratio of the weight of the shields to the weight of the cold mass. From Section 2.0, the total G-10 support area is 42.2 cm², which supports the 17000 lbm cold mass. The 80K shield weighs approximately 400 lbm and the 10K shield weighs about 1000 lbm. The shield supports must be capable of supporting both shields at once, so the total required area is

$$A = \left(\frac{400 + 1000}{17000} \right) (42.2) = 3.5 \text{ cm}^2$$

The average gap between shields is estimated at 3.8 cm. The conduction heat leak to the 80K shield is

$$Q_{80} = \frac{\Delta \theta_{80} A}{l} = \frac{(1.35 \text{ W/cm})(3.5 \text{ cm}^2)}{3.8 \text{ cm}} = 1.24 \text{ W}$$

Similarly, the heat leak to the 10K shield through the standoffs is

$$Q_{10} = \frac{\Delta \theta_{10} A}{l} = \frac{(.195)(3.5)}{3.8} = .180 \text{ W}$$

3.3.4.5 Thermal Intercepts. It was also implicitly assumed that the thermal intercepts on the support struts were 100 percent effective, which is not the case in reality. There will be some contact resistance between the strut and the intercept, and between the intercept and the cryogen thermal sink on the shield. The net effect is that the support is subjected to a higher intercept temperature and will have higher heat load as a result. The locations of the intercepts can be adjusted somewhat to account for the added resistance, and the design of the intercept can be adjusted to improve the efficiency. The analysis approach is to treat the finite length of the support in contact with the intercept as a fin with boundary conditions at each end relating the end temperature to the end heat fluxes. This is an analysis task which is straightforward but tedious and must be addressed during a detailed design phase.

Table 3.3-3. Baseline Design Heat Leak Summary

Source	$Q_{4.5}$ (W/mag)	Q_{10} (W/mag)	Q_{80} (W/mag)	W_c (kW/mag)	Op. Cost (\$/mag)
MLI	.0025	.657	37.3	.560	1960
Supports	.146	1.86	17.0	.583	2040
Anchor	.018	.229	2.1	.072	252
Shield Supports	N/A	.18	1.2	.045	158
Voltage Taps	.01	.01	0.1	.007	24
Splices	TBD	N/A	N/A		
Ends	.001	.037	1.8	.028	98
Total	.178	3.00	56.0	1.33	4530
Ref. "D" Design Criteria Budget	.25	1.50	15.0	.543	1900

3.3.5 SUMMARY. The cost of refrigeration at various temperatures has been developed for the SSC to support the various trade studies that have been done for this preliminary design study, and to provide a rational means of choosing among alternatives. Nominal costs are \$1774/watt of heat leak to 4.5K, \$351/watt of heat leak to 20K, and \$58 of heat leak to 80K.

These costs were used to evaluate the thermal performance of several cold-mass support concepts. They were also used to optimize the location of the thermal intercepts on the supports, and to determine the optimum number of layers of reflectors for use in the MLI blankets.

The heat leak for the cold-mass supports, the MLI, and the shield supports were computed for the baseline design. The results have been summarized in Table 3.3-3. The totals are .178 W/magnet at 4.5K, 3 W/magnet at 10K, and 56.0 W/magnet at 80K. The format of the table has been taken from the FNAL Reference D Design Criteria Document (Reference 1.0-1). Life-cycle refrigeration costs are included to provide a basis for comparison with alternative designs. For this baseline design, the refrigeration costs are higher than what is established by the heat leak budget, but this must be weighed against the manufacturing costs of any alternative designs.

3.4 EDDY CURRENTS ANALYSIS. Eddy currents are induced in conducting components due to magnet fast discharge following a quench. Components which are primarily affected by the eddy currents are the thermal radiation shields. Eddy currents are calculated in this report for design purposes using two different analytical models. First, the case of having a shield of a given width and infinite length is considered to determine eddy currents upper limit. A computer program has also been developed to determine eddy currents for a two-dimensional surface subject to applied field given as $B(x,y,a)$.

3.4.1 INFINITELY LONG CONDUCTING PLATE. For a shield of a width as shown in Figure 3.4-1 and subject to magnetic B we have

$$E = \int \frac{\dot{B}_x}{2\rho} \quad (3.4-1)$$

where E is the electric field and \dot{B} is the rate of field change with respect to time.

Equation 3.4-1 gives the current distribution as

$$J = \int \frac{\dot{B}_x}{2\rho} \quad (3.4-2)$$

The above analysis is valid as long as the field produced by the eddy current is small compared to the applied field.

Assuming that the field component normal to the shield is given by

$$B_x = B_c \cos a x \quad (3.4-3)$$

gives the current density J as

$$J = - \frac{\dot{B}_c}{\rho a} \sin a x \quad (3.4-4)$$

Note that $a = \frac{2}{D}$, where D is the diameter and thus J is given by

$$J = \frac{\dot{B}_c D}{2\rho} \sin \left(\frac{2x}{D} \right) \quad (3.4-5)$$

Radial and tangential forces can be calculated as

$$F_r = B \sin \theta t j = - \frac{\dot{B}_0 B_0 t}{2\rho} \sin^2 \frac{2x}{D} \quad (3.4-6)$$

where t is the shield thickness and

$$F_\theta = B \cos \theta t j = - \frac{\dot{B}_0 B_0 t \cos (2x/D)}{2\rho} \sin^2 \frac{2x}{D} \quad (3.4-7)$$

Note that the radial forces are acting inward as the magnet is being discharged. The tangential forces are pulling away from the centerline. The maximum radial force on the two thermal shields is given in Table 3.4-1:

Table 3.4-1. Maximum Possible Radial Pressure on Thermal Shields

Shield	Material	Resistivity $\mu\Omega/m$	Maximum Pressure (N/m^2)	
			$B = 1.0 \text{ T/s},$ $B = 0.1 \text{ T}$	$B = 0.1 \text{ T/s}$ $B = 0.05 \text{ T}$
10-20K	St. Stl.	0.5	1064	55.2
80K	Al	0.03	17733	886.6

High pressures will thus be induced in the 80K shield (≈ 3.8 psi) if fast discharges occur. For the present design the discharge rate is given in the last column and the calculated magnetic pressure is negligible.

3.4.2 EDDY CURRENT IN TWO-DIMENSIONAL SURFACES. For a two-dimensional surface subject to applied field we have

$$\frac{1}{\rho} \nabla \times j = \frac{dB}{dt} \quad (3.4-8)$$

Again assuming that the field produced by the surface current is negligible (dB/dt) can be taken as the applied field rate of change with time. The above equation is used for the numerical calculation, where Kirchoff's Law is used. The surface is divided into a grid as shown in Figure 3.4-2 and thus we have

$$\begin{aligned}
J(i,J) = & [B \Delta x \Delta Y + J(i-1,J) R_{i-1,J} \\
& + J(i+1,J) R_{i+1,J} + J(i,J-1) R_{i,J-1} \\
& + J(i,J+1) R_{i,J+1}] / 4 [R_{i+1,J} + R_{i-1,J} \\
& + R_{i,J-1} + R_{i,J+1}] \quad (3.4-9)
\end{aligned}$$

An IBM computer program was used to calculate the current distribution in the shield using the above equation. Using the program for the case of having shield slots 15 inches apart, the maximum pressure given in Table 3.4-1 for the different shields:

Table 3.4-2. Maximum Radial Pressure on Thermal Shields (with Radial Slots)

Shield	Material	Resistivity $\mu\Omega/m$	Maximum Pressure (N/m^2)	
			B = 1.0 T/s, B = 0.1 T	B = 0.1 T/s B = 0.05 T
10-20K	St. Stl.	0.5	2500	125
80K	Al	0.03	41667	2083

It can also be shown that the maximum pressure is proportional to the square of spacing and lower pressure can be obtained by further reducing the spacing.

3.4.3 DISCUSSION. The magnet discharge rate of 0.1 T/s and external field of 0.05T result in magnetic pressure which can be easily tolerated in the thermal shields design. Higher dB/dt and B may require having slots in the shields. The slots, however, cannot be made along the entire circumference of the shield. As long as the length of the part connecting the shield segments, which is left after slotting, is small as compared to the slot spacing, the current will be the same as predicted for a finite rectangle. If the connecting parts are equal to the spacing, the infinite length analysis can be used to determine the effect of the width. Shorter spacing will not be as effective in this case.

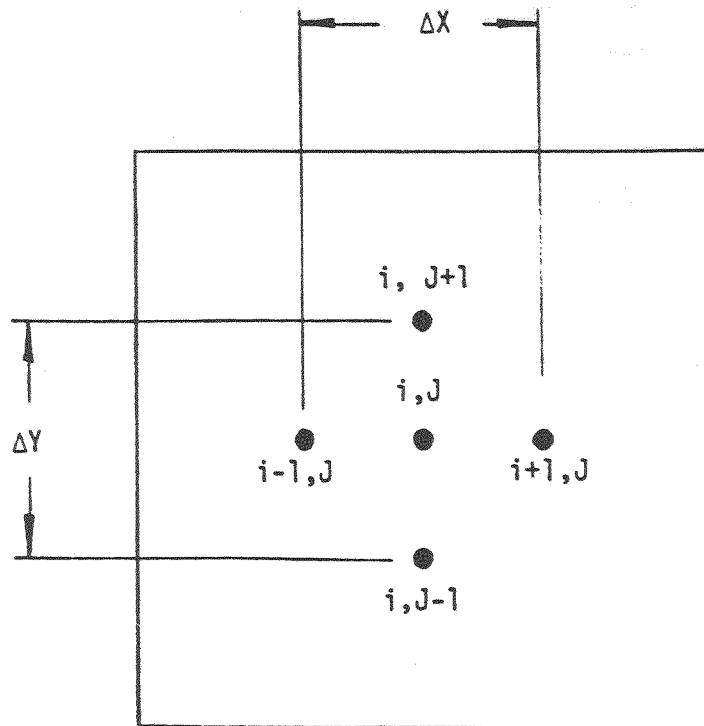


Figure 3.4-2. Two-Dimensional Surface for Eddy Current Calculations

Radial and tangential forces can be calculated as

$$-F_r = B \sin \theta t j = - \frac{\dot{B}_0 B_0 t}{2\rho} \sin^2 \frac{2x}{D} \quad (3.4-6)$$

where t is the shield thickness and

$$F_\theta = B \cos \theta t j = - \frac{\dot{B}_0 B_0 t \cos (2x/D)}{2\rho} \sin^2 \frac{2x}{D} \quad (3.4-7)$$

Note that the radial forces are acting inward as the magnet is being discharged. The tangential forces are pulling away from the centerline. The maximum radial force on the two thermal shields is given in Table 3.4-1:

Table 3.4-1. Maximum Possible Radial Pressure on Thermal Shields

Shield	Material	Resistivity $\mu\Omega/m$	Maximum Pressure (N/m^2)	
			$B = 1.0 \text{ T/s},$ $B = 0.1 \text{ T}$	$B = 0.1 \text{ T/s}$ $B = 0.05 \text{ T}$
10-20K	St. Stl.	0.5	1064	55.2
80K	Al	0.03	17733	886.6

High pressures will thus be induced in the 80K shield (≈ 3.8 psi) if fast discharges occur. For the present design the discharge rate is given in the last column and the calculated magnetic pressure is negligible.

3.4.2 EDDY CURRENT IN TWO-DIMENSIONAL SURFACES. For a two-dimensional surface subject to applied field we have

$$\frac{1}{\rho} \nabla \times j = \frac{dB}{dt} \quad (3.4-8)$$

Again assuming that the field produced by the surface current is negligible (dB/dt) can be taken as the applied field rate of change with time. The above equation is used for the numerical calculation, where Kirchoff's Law is used. The surface is divided into a grid as shown in Figure 3.4-2 and thus we have

suitable for cryogenic service include solid-solution-strengthened 5000-series alloys and the precipitation-hardened 6000-series and 2000-series alloys. Preferred alloys are: (i) Al-4.5 Mg (5083), a weldable alloy generally used in the annealed condition; (ii) Al-1.0 Mg-0.61 Si (6061), a versatile alloy available in a variety of product forms and heat-treatments; and (iii) Al-6 Cu (2219), a high strength alloy used in the precipitation-hardened condition.

3.5.1.3 Ferritic Fe-Ni Steels. The nickel steels have a predominantly body-centered-cubic crystal structure and consequently undergo a ductile to brittle transition as the temperature is reduced. The transition temperature decreases with increasing nickel content and may be further reduced by special heat treatments. Of the commercially available steels suitable for cryogenic service (minimum service temperature 77K), are alloys with 5.5 Ni and 9 Ni. A 12 percent Ni family and a 13 percent Ni family of experimental alloys have been developed for service below 4K. This has been achieved by reducing the grain size by special thermal cyclings. High purity components have been used to reduce the interstitial content and, in addition, Nb, Ti, or V are added to serve as a getter for interstitials as well as a grain refiner. These alloys are not available in commercial quantities. The welding of nickel steels is complicated by the fact that the low-temperature toughness of the base material is achieved, in a large part, by thermal treatments. Nickel-based austenitic weld filler metal is used to ensure satisfactory toughness in the as-deposited weld. The tensile properties of the nickel base weld metals are generally lower than the base-metal properties. The fracture toughness of the heat-affected zone (HAZ) tends to be lower than that of base metal or the weld metal. Ferritic Fe-Ni steels are magnetic and need protective coatings for corrosion protection.

3.5.1.4 Titanium Alloys. Titanium alloys are not generally preferred for cryogenic applications. Their use is limited to applications where the strength/weight ratio is of primary concern. Two alloys of titanium, Ti-5Al-2.5 Sn (an alpha alloy) and Ti-6Al-4V (an alpha-beta alloy) have been used. To improve ductility and toughness at low temperatures, extra-low interstitial (ELI) grades are specified and the alloys are used in the annealed condition. Even with these improvements, they are not considered candidates for applications where satisfactory performance can be obtained with austenitic stainless steels, nickel steels, or aluminum alloys. They are considerably more expensive than the previous materials.

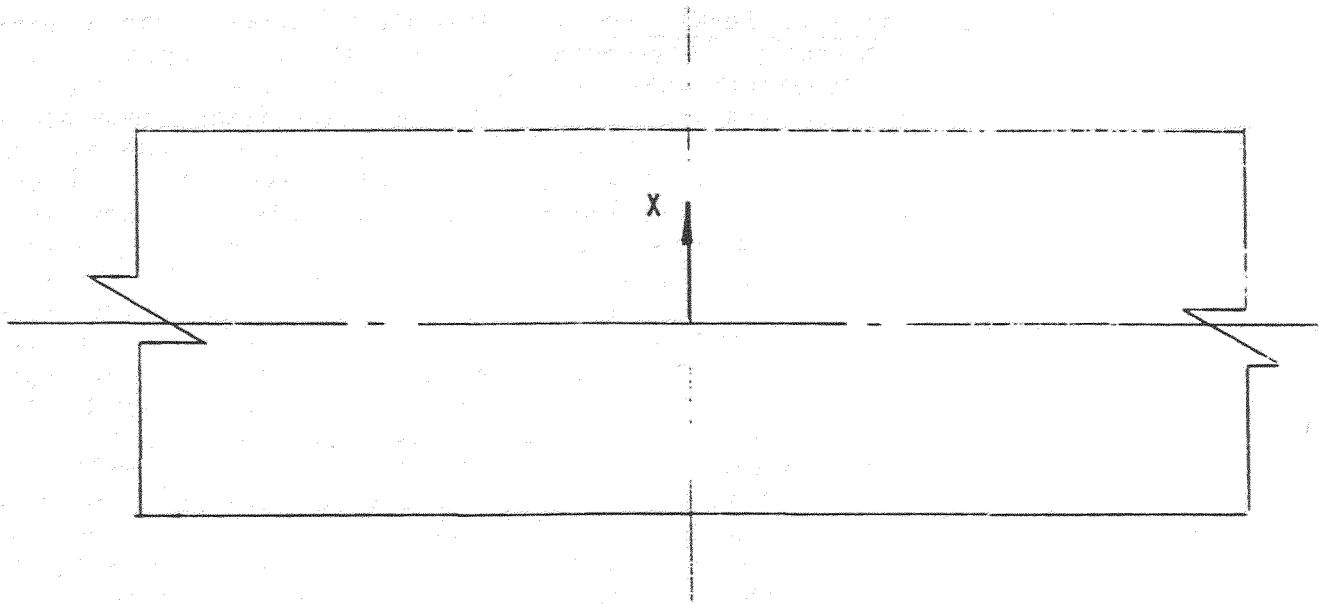


Figure 3.4-1. Infinitely Long Shield

Table 5.3-1. Structural Material Selection for LBL Cryostat

Component	Material	Specification
1. Vacuum Vessel	Al 6061-T6	QQ-A250/11E
2. 80K Radiation Shield	Al 6061-T6	QQ-A250/11E
3. LN ₂ Tubes for 80K Shield	Al 6061-T6	QQ-A200/16A
4. 20K Radiation Shield	Steel Type 304L-CRES	ASTM A240-84a
5. LHe Tubes	Steel Type 304L-CRES	ASTM A269-84c
6. Side and Vertical Struts	Titanium-6 Al-4V ELI	MIL-T-81556 A
7. Fittings for Struts		
a) Cold Mass Side	Steel Type 304L-CRES	ASTM A276-84
b) Vacuum Vessel Side	Al 6061-T6	QQ-A200/16A
8. Bolts and nuts	Steel A-286	NAS 6308 & 6310
9. Insulation Standoffs and Supporting Blocks for LHe Tubes	Fiberglass-Epoxy G-10CR	ASTM D709-82

3.5 MATERIALS AND PROCESSES

3.5.1 INTRODUCTION. One of the major considerations and an important guiding factor in the selection of structural materials for the LBL cryostat, has been to identify the materials with the lowest cost consistent with the materials properties requirements for the application. We have considered and evaluated the major structural alloys that have been used in commercial quantities for cryogenic applications. As a class or group, these alloys fall into the following categories:

- o Austenitic stainless steels
- o Aluminum alloys
- o Ferritic Fe-Ni steels
- o Titanium alloys

Before going into the specific criteria used in the final selection of materials, characteristics pertinent to this application are briefly described for each of the alloy groups.

3.5.1.1 Austenitic Stainless Steels. Austenitic stainless steels are Fe-Cr alloys with sufficient (8 to 24 percent) nickel and manganese and sometimes nitrogen to stabilize the austenitic (face-centered-cubic f.c.c.) phase. Chromium (16 to 20 percent) provides corrosion resistance. The most typical austenitic steels are variations of 18 Cr-9 Ni alloys. Some of these alloys (type 304L/316L) have been widely used in a variety of cryogenic applications. Low-carbon grade alloys have better weldability. Austenitic stainless steels have excellent fracture toughness down to 4K, a nonmagnetic behavior, are readily available, have ease of fabrication, weldments that are as strong and tough as base metal, good service experience, and design code coverage. They are more expensive and have lower yield strength than ferritic Fe-Ni steels and aluminum alloys. Their machinability is poorer than that for aluminum alloys. However, precipitation-hardened austenitic grade steels (like A-286) are high-strength alloys and have been considered as the material choice for nuts and bolts.

3.5.1.2 Aluminum Alloys. Aluminum alloys have a face-centered-cubic crystal structure. They retain their strength, ductility, and toughness at cryogenic temperatures. They have low density, nonmagnetic properties, excellent machining, forming and forging characteristics. Disadvantages are low strength in weldments, low elastic modulus, and high thermal expansion. Aluminum alloys

The shield supports/standoffs can be economically manufactured by more than one method. The predesign concept shows an epoxy/fiberglass shape from a pultrusion or extrusion, subsequently router profiled to develop the standoffs. Depending on final spacing, individual injection moldings might be more economical. The standoffs are installed at the shield subassembly level, thereby reducing labor at the final assembly station.

- 3.6.3 FLUID LINES. Subassembly of the cryogenic fluid transport lines can be accomplished using state-of-the-art techniques. Tubing can be joined into the required lengths using automatic orbital arc welding equipment, followed by thermal shocking and leak testing. The grouping of the helium lines within the cryostat has been developed in such a way that the four lines, with their common support blocks, can be subassembled and then attached to the cold mass either before or after it is located in the lower vacuum vessel.
- 3.6.4 MULTILAYER INSULATION. The multilayer insulation (MLI) is a very producible material that will undoubtedly be produced by a specialty house and delivered in "ready-to-install" blankets. Our experience on other magnet programs has provided a number of options for low heat leak and economical joining and fastening methods. The cryostat assembly sequence has been established so that there will be one longitudinal splice in each blanket, near the top of the magnet. Circumferential splices will be located based on handling considerations and other economic factors.
- 3.6.5 VACUUM VESSEL AND FINAL ASSEMBLY. The vacuum vessel, from a producibility point of view, is one of the most straightforward fabrication tasks on the cryostat assembly. Cost studies, as summarized in Table 3.6-1, have been made with respect to the vessel material, comparing structural steel, stainless steel, and aluminum, and the basic material cost is indeed a significant cost driver. However, the basic fabrication processes are the same regardless of the choice, and the fabrication costs are not expected to vary widely due to material. The vessel halves are roll-formed and weld back-up bars are tack welded in place. The cylindrical extensions for the support struts are welded to the lower half of the vacuum vessel at the subassembly level.

At the final-assembly station, the half of the vacuum vessel, together with precision tooling at the four support locations, becomes the assembly jig. The vertical support strut clevises are precisely located, with the struts pinned to them, and are welded to the tubular extensions. The MLI, lower thermal-shield halves, and the cold-mass assembly are sequentially lowered into position. The tooling accurately establishes the location of the cold mass with respect to the base, and the cold ends of the struts are drilled and pinned in place. With the cryogenic plumbing installed, the upper thermal shields and MLI are installed. Finally, the upper half of the vacuum vessel is positioned and welded in place with automatic GMAW welding.

3.5.2 SPECIFIC CRITERIA USED IN SELECTION OF MATERIALS. Having described the cryogenic characteristics of the four classes of alloys, we decided to leave the ferritic Fe-Ni steels for further consideration. The reasons are the following: The less-expensive commercially available, low Ni alloys undergo a ductile-to-brittle transition as the temperature is reduced. Even if these alloys are used in the outer vacuum vessel structure, which in normal service is not exposed to cryogenic temperatures, there will always be a potential risk of a brittle fracture in the event of a cryogen spill from inside of the vacuum vessel. The high nickel and specially processed experimental alloys having ductile-to-brittle transition temperature below 4K will cost more and this would offset the cost advantage the low nickel alloys have over austenitic stainless steels or the aluminum alloys. The additional cost of protecting their surface from corrosion also works against the selection of ferritic nickel steels for this application.

The following specific criteria were used in the selection of structural materials for the LBL cryostat:

- o Excellent mechanical and physical properties at room and cryogenic temperatures.
- o Large data base and ASME specification coverage.
- o Reliability established by service history.
- o Proven fabrication methods and processes.
- o Availability in required shapes and sizes.
- o Previous team member design and fabrication experience.
- o And, finally, the cost.

Based on these considerations, the list of structural materials chosen for the major components of the LBL cryostat and their specifications are shown in Table 5.3-1.

As can be seen from an examination of this table, the structure material selected are either austenitic stainless steel type 304L or Aluminum 6061-T6. Both of these materials meet the requirements of the criteria mentioned above. The bottom line has been the cost. Selection of Ti-6Al-4V ELI for the vertical support struts is a very special case. This choice has been influenced largely by the superior creep properties combined with low thermal conductivity and higher yield strength of the titanium alloy. The design allowables for all these alloys are given in MIL-HDBK-V.

CONCLUSIONS AND RECOMMENDATIONS

- 4.1 STRUCTURAL ANALYSIS. The beneficial aspects of the SSC structural design include: (1) In order to minimize the required bellows length, the material used in the bellows is specified to be Inconel 625 instead of 304 stainless steel. (2) The use of Al 6061-T6 to fabricate the vacuum vessel. In case of the loss-of-coolant faulted event, the aluminum alloys do not exhibit a marked transition in fracture resistance as does carbon steel. (3) The use of titanium struts which exhibit high strength and relatively low conductivity.

A development program for testing an alternate low heat leak support should be implemented. Fiberglass/epoxy composite struts should be considered and tested to investigate the creep characteristics of the fiberglass. Compression and tension tests should also be run to provide the mechanical properties.

- 4.2 THERMODYNAMIC ANALYSIS. An algorithm to determine cost of refrigeration has been developed for the SSC to support the various trade studies that have been done for this preliminary design study. Refrigeration costs were developed to evaluate the thermal performance of several cold-mass support concepts. The locations of the thermal intercepts on the supports were optimized with respect to refrigeration costs, as were the number of layers of reflectors in the MLI blankets. The heat leak of the cold-mass supports and the MLI was computed for the baseline design. The refrigeration costs are higher than what is established by the heat leak budget, but this must be weighed against the manufacturing costs of any alternative designs.

One area of fruitful development work is MLI performance and cost improvement. MLI blanket designs developed for spaceflight applications accommodate a weight penalty that does not exist for the SSC. It is probable that heat leak and/or cost reductions can be realized by investigating heavier designs.

- 4.3 MANUFACTURING/PRODUCIBILITY. All elements of the cryostat assembly have been examined for producibility. As the conceptual design evolved, each part and assembly was considered from a cost effectiveness standpoint, both in fabrication of the detail parts and in the related effects on the overall assembly sequence. Many changes resulted from these considerations and are reflected in the preliminary design shown in this report. Many more producibility refinements can, and should, be made as the design is solidified. One development project that would be most beneficial in improving producibility would be the construction of two full-size mock-ups, one of the cold-mass support area, and one of the magnet interconnect region. This would give early visibility to the effect of spatial constraints of design of the parts in these areas.

3.6 PRODUCIBILITY ANALYSIS

A key consideration in the selection of a design concept is its analysis from a producibility standpoint. This is especially true when the number of units to be produced is relatively large, as is the case with the cryostat assembly. Our objective was, once all design parameters were set, to examine alternate fabrication and assembly methods in order to arrive at the most cost-effective and straightforward approach. One aspect of the objective, due to the relatively high production rates dictated by the schedule, is to incorporate features into detailed parts and subassemblies that will minimize tasks in the final assembly of the cryostat.

3.6.1. COLD-MASS SUPPORTS. Some of the producibility considerations contributing to the selection of the baseline support system are discussed in Section 2.0 of this report. Once the baseline support concept of titanium compression struts was selected, additional efforts were made to optimize the design from a producibility standpoint.

The struts were originally conceived with adjustable rod-end bearings. It was quickly recognized that more sophisticated tooling to control cold-mass location could eliminate the high recurring cost of the adjustable rod ends. Efforts were then made to reduce the amount of machining required for the fixed rod ends. Castings appear attractive, but consideration has been deferred until fracture toughness data at this temperature can be fully evaluated. The most cost-effective approach at this time appears to be a simple blade welded into the slotted titanium tube.

The clevis fittings into which the rod ends are pinned were also studied from a fabricability standpoint. Again, casting will be considered, at least for the room-temperature aluminum fittings on the vacuum vessel.

3.6.2 THERMAL RADIATION SHIELDS. Both of the radiation shields are fairly straightforward from a producibility standpoint. The CRES 20K shield and the aluminum 80K shield are both made in halves using the same basic processes: slots are punched in the flat, semicylinders which are formed and welded circumferentially to the required lengths.

Longitudinal welding of the 20K shield is accomplished with automatic Gas Metal-Arc Welding (GMAW) and is facilitated by a back-up bar tack welded to one of the shield halves. The longitudinal joint in the 80K shield is simplified by an extruded shape incorporating the LN₂ line. The shape is welded to each half of the shield as a subassembly; only tack welding is required at the final assembly station.

APPENDIX A
SUPERCONDUCTING SUPER COLLIDER MAGNET
DRAWINGS FOR PRODUCTION DIPOLE MAGNET CRYOSTAT
Report Number SSC-LBL-306-RWB
1 May 1985

Table 3.6-1. Vacuum-Vessel Material Cost Comparison

	Lbs/In ³	T	\$/Lb (R.O.M.)	Lbs/Unit	\$/Unit
304L CRES	.290	.250"	1.05	3021	3172
6061-T6 Alum	.098	.313"	1.87	1278	2390
Mild Steel	.283	.250"	0.22	2948	649

Savings on 7,740 Units:

Alum. vs. CRES -- \$ 6.1M

Steel vs. CRES -- \$19.5M

Forming - Comparable

Welding - Comparable

Finishing - Comparable

PARTS LIST

0.70916 REQUIRED FOR ABBREVIATION, CODE AND SYMBOL INTERPRETATION

CONVAIR DIVISION OF GENERAL DYNAMICS
SAN DIEGO, CALIFORNIA

PDA

PL SSC 850320

REV LTR

TITLE *CRYOSTAT ASSY - SSC MAGNET*

PADR

RELEASE DATE

CODE IDENT NO

SH 1 OF

DOC TYPE

DOC OPT

DOC CONT

GROUP *673-2*

REPRO CODE

CONTRACT NO

UNDIM DWG

14170

1 SHS

DRAFTSMAN

DESIGNER *AS 95*

GR ENGR

STRESS

PROD. ENGR *1/1*

MATERIAL *1/1*

CHECKER

DISTRIBUTION CODE

PACKAGE NO

NOTE SYMBOL: *

D - DOCUMENT NO.
E - END ITEM

G - GENERAL NOTE
L - LIMIT

M - MATERIAL
N - NOMENCLATURE

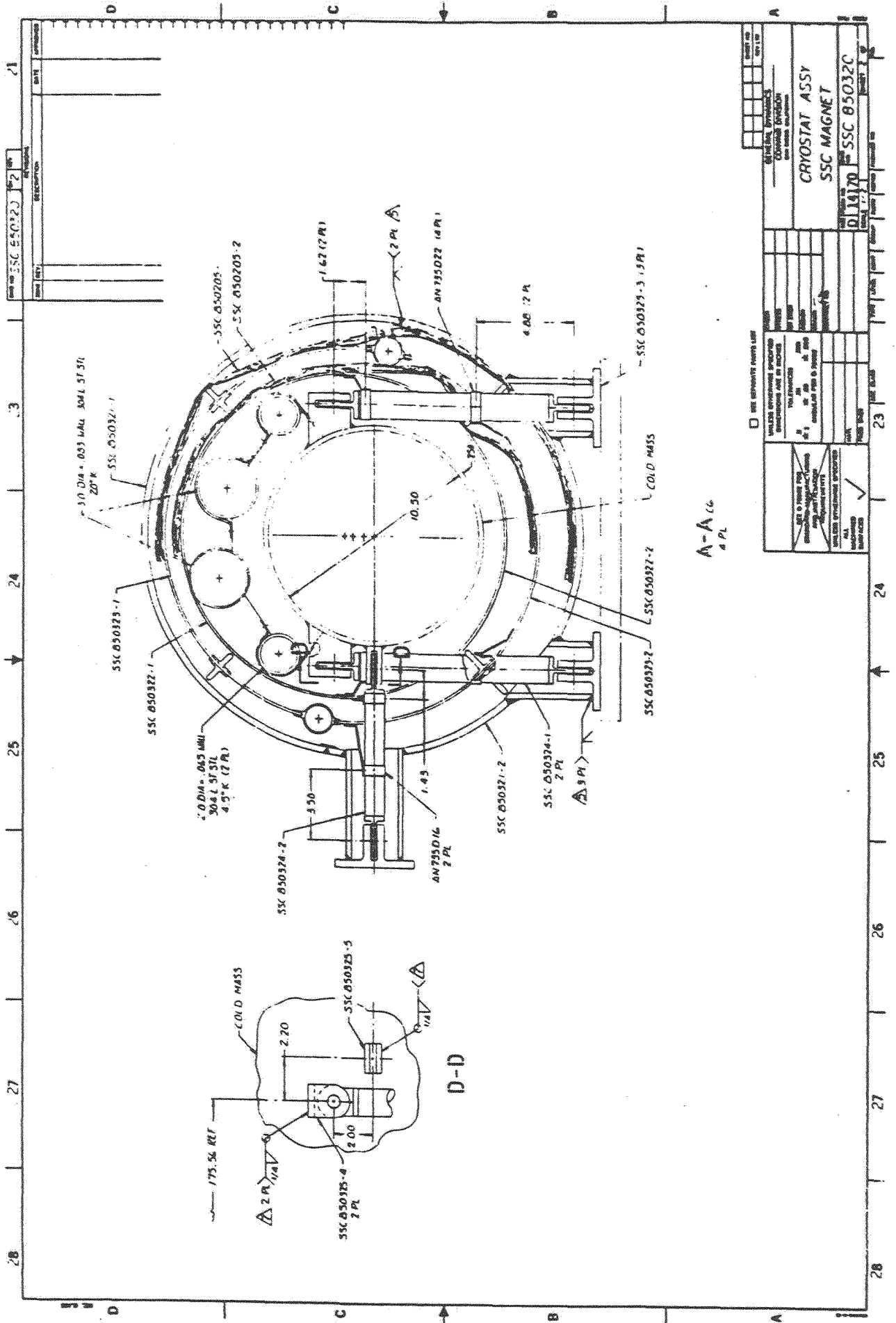
R - REF DESIG
T - TYPE DESIG VALUE

U - USAGE DATA
V - VENDOR ITEM

REQ	REQUIREMENTS PER ASSY/INSTR	UNIT OF MEAS	FIND NO	CODE IDENT NO	PART OR IDENTIFYING NUMBER	NOMENCLATURE OR DESCRIPTION	ZONE		NOTE SYM *	NOTES
							L	R		
	-1				-1	CRYOSTAT ASSY				
	1				SSC 850321-1	UPPER VAC VESSEL				
	1				850321-2	LOWER VAC VESSEL				
	1				850322-1	UPPER SHIELD-20K				
	1				850322-2	LOWER SHIELD-20K				
	1				850323-1	UPPER SHIELD-80K				
	1				850323-2	LOWER SHIELD-80K				
	8				850324-1	SUPPORT-VERTICAL				
	4				850324-2	SUPPORT-SIDE				
	1				850324-3	SUPPORT-AXIAL				
	1				850325-2	FITTING				
	12				850325-3	FITTING				
	8				850325-4	FITTING				
	4				850325-5	FITTING				
	2				850304-1	BELLOWS				
	2				850304-2	BELLOWS				
	2				850304-3	BELLOWS				
	2				850304-4	BELLOWS				
	2				850304-5	BELLOWS				
	1				850205-1	MLI				
	1				SSC 850205-2	MLI				
	2				REDUCER					
	2				TRANSITION JOINT					
	AR				5356	FILLER WIRE				
	AR				EE 316L	FILLER WIRE				
	AR				RN-82	FILLER WIRE				
	DOC				MIL-STD-248	SPEC				
	DOC				ASME CODE	SPEC				

APPENDIX A

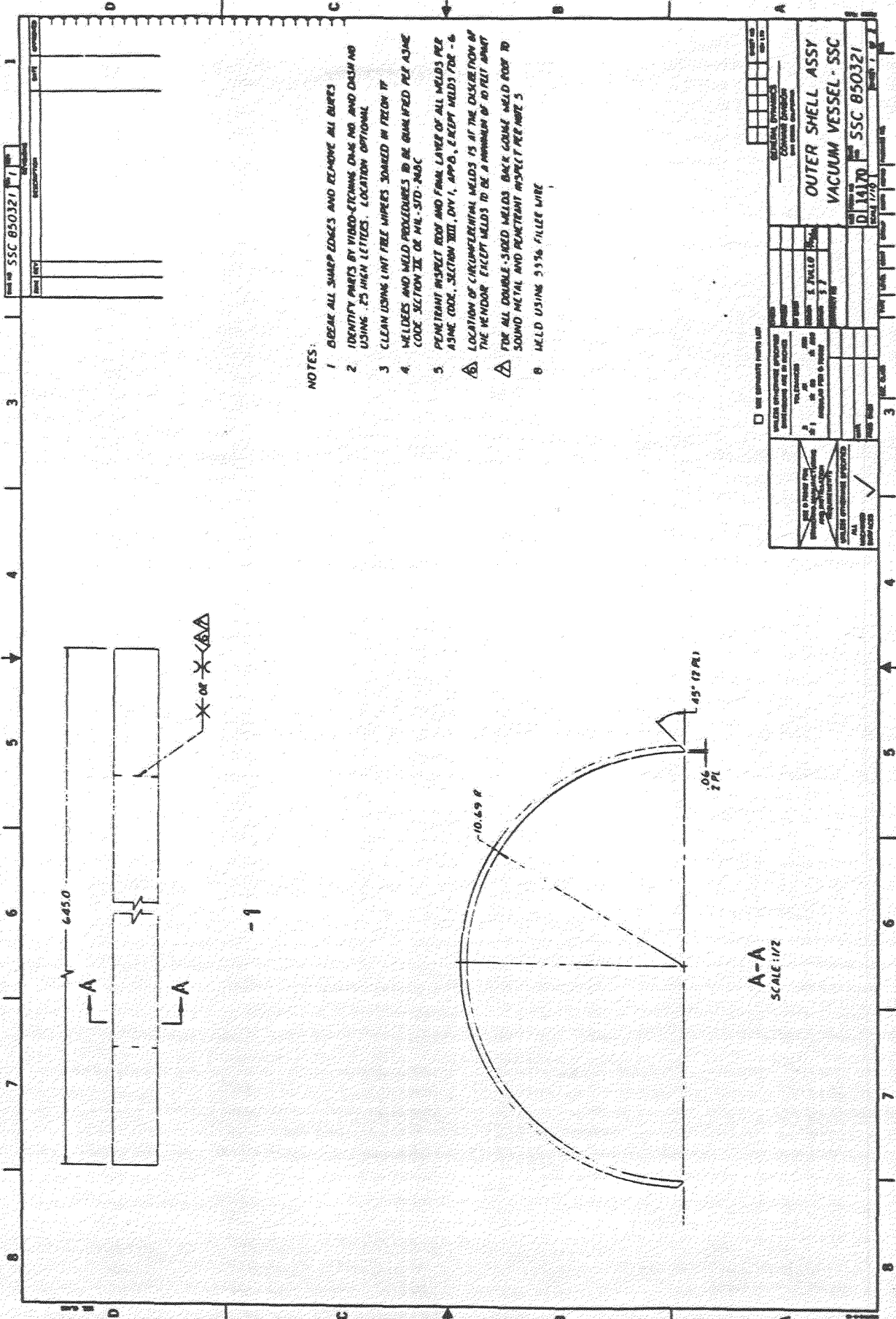
<u>Drawing Number</u>	<u>Title</u>	<u>Page</u>
PL SSC 850320	Parts List	A-3
SSC 850320	Cryostat Assy	A-4
PL SSC 850321	Parts List	A-9
SSC 850321	Vacuum Vessel Outer Shell Assy	A-10
PL SSC 850322	Parts List	A-12
SSC 850322	20K Thermal Shield Assy	
PL SSC 850323	Parts List	A-15
SSC 850323	80K Thermal Shield Assy	A-16
PL SSC 850324	Parts List	A-18
SSC 850324	Cold Mass Supports	
PL SSC 850325	Parts List	A-20
SSC 850325	Cold Mass Support Fittings	A-21
SSC 850326	LN ₂ Tube Assy	A-22
SSC 850327	LN ₂ Tube - Extruded Shape	A-23
SSC 850304	LN ₂ and He Formed Bellows	A-24
PL SSC 850205	Parts List	A-25
SSC 850205	MLI Blankets	A-26



REV	DATE	DESCRIPTION

<input type="checkbox"/> SEE SUPPLEMENTARY PARTS LIST PARTS LIST PREPARED BY: [] PARTS LIST CHECKED BY: [] PARTS LIST APPROVED BY: []		FEDERAL BUREAU OF INVESTIGATION COMMERCIAL DIVISION 400 ANDREWS AVENUE WASHINGTON, D.C. 20535
GET TO KNOW THE FEDERAL BUREAU OF INVESTIGATION COMMERCIAL DIVISION THE COMMERCIAL DIVISION OF THE FBI IS THE SOURCE OF ALL INFORMATION RELATING TO THE COMMERCIAL DIVISION OF THE FBI.		CRYOSTAT ASSY SSC MAGNET
DRAWING NO. SSC 050320	REV. 2	DATE 10/17/70

A-A
6
4 PL



SSC 850321

REV	DESCRIPTION	DATE

NOTES:

1. BREAK ALL SHARP EDGES AND REMOVE ALL BURRS
2. IDENTIFY PARTS BY VIDEO-ETCHING, CHAM. NO. AND DASH NO. USING .25 HIGH LETTERS. LOCATION OPTIONAL
3. CLEAN USING LINT FREE WIPERS SOAKED IN TOLUOLITE
4. WELDERS AND WELD PROCEDURES TO BE QUALIFIED PER ASME CODE SECTION III OR MIL-STD-240C
5. PENETRANT INSPECT BODY AND FINAL LAYER OF ALL WELDS PER ASME CODE, SECTION VIII, DIV 1, APP'D, (EXCEPT WELDS FOR -6)
6. LOCATION OF CIRCUMFERENTIAL WELDS IS AT THE DISCRETION OF THE VENDOR EXCEPT WELDS TO BE A MINIMUM OF 10 FEET APART
7. FOR ALL DOUBLE-SIZED WELDS, BACK-GRADE WELD TOOFT TO SOUND METAL AND PENETRANT INSPECT PER NOTE 5
8. WELD USING 55% FILLER WIRE

USE DIMENSIONED PARTS LIST

WELDS TO BE INSPECTED PER ASME SECTION VIII, DIV 1, APP'D, (EXCEPT WELDS FOR -6)

ALL WELDS TO BE PENETRANT INSPECTED PER NOTE 5

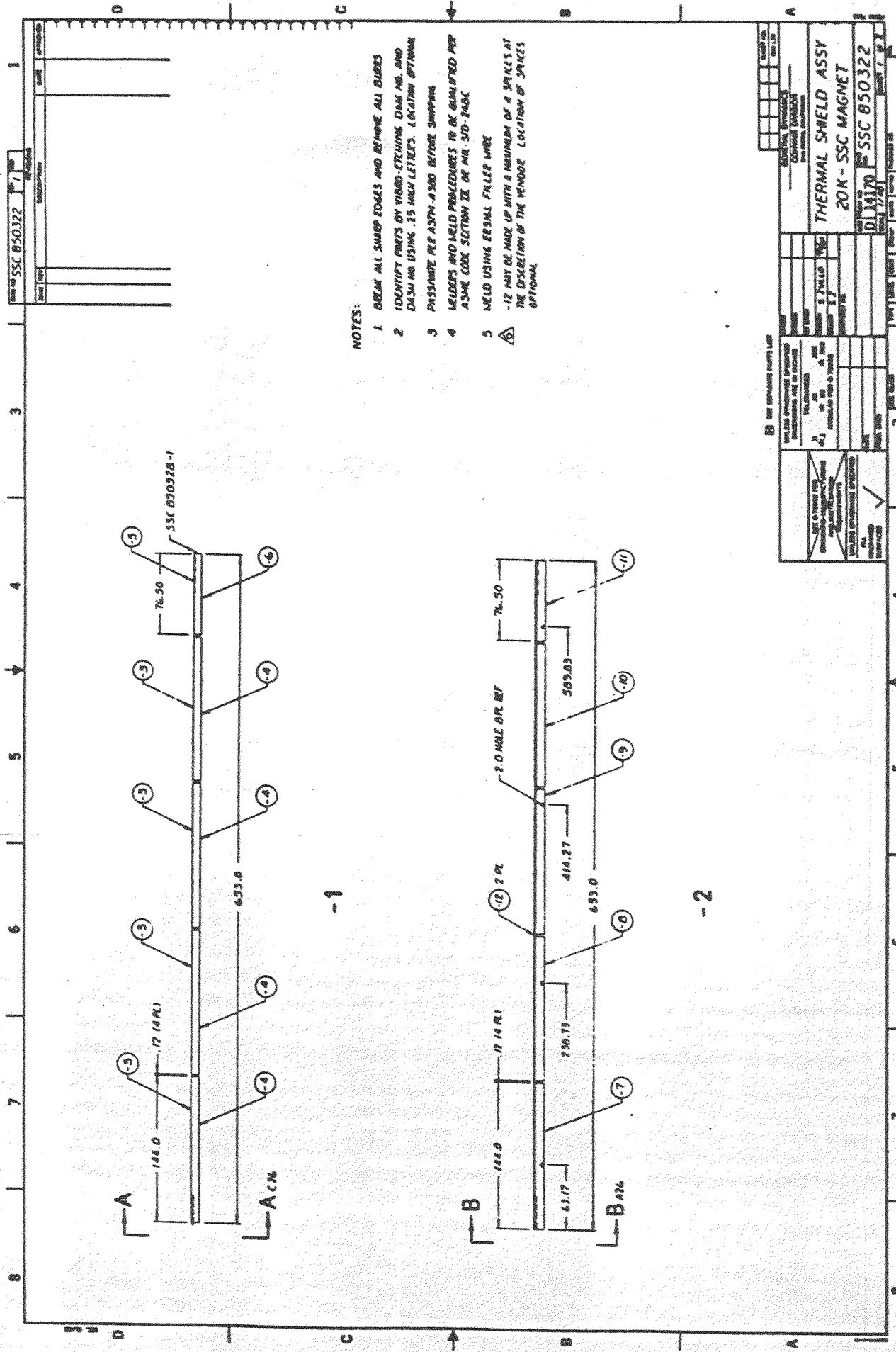
ALL WELDS TO BE BACK-GRADED TO SOUND METAL AND PENETRANT INSPECT PER NOTE 5

GENERAL SPECIFICATIONS
 CONTRACT NUMBER
 DRAWING NUMBER
 SHEET NUMBER

PROJECT
 TITLE
 DATE
 SCALE
 DRAWN BY
 CHECKED BY
 APPROVED BY

SSC 850321

A-A
SCALE: 1/2



-1

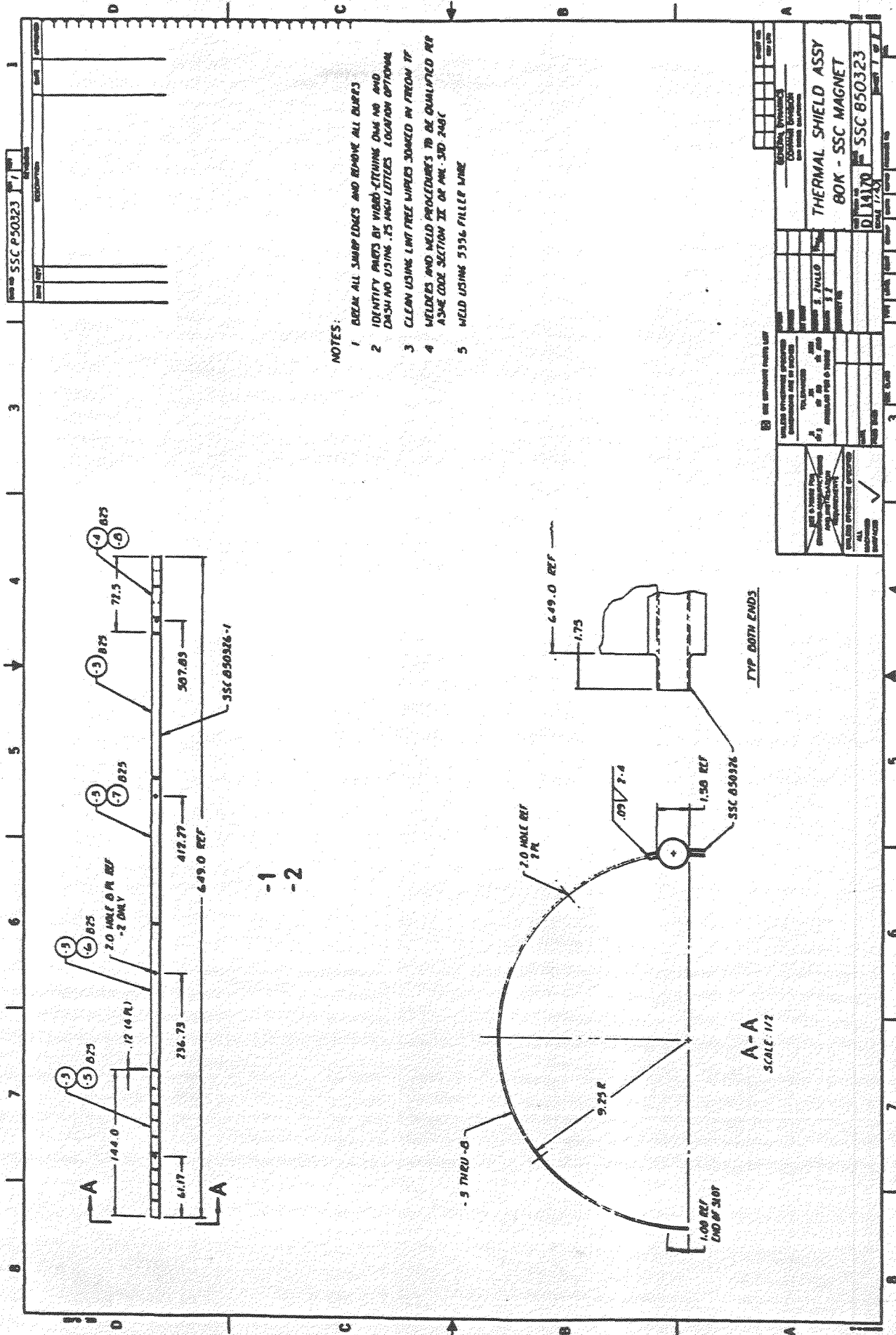
-2

NOTES:

1. BREAK ALL SHARP EDGES AND REMOVE ALL BURRS
 2. IDENTIFY PARTS BY VIDEO-ETCHING Dwg NO. AND DASH NO USING .15 MILL LETTERS. LOCATION OPTIONAL
 3. PASSWIRE PER ASTM-A580 BEFORE SHIPPING
 4. WELDS AND WELD PROCEDURES TO BE QUALIFIED PER ASME CODE SECTION IX OF MR. SD-348C
 5. WELD USING ERSBAL FILLER WIRE
- ⚠️ -12 MAY BE MADE UP WITH A MINIMUM OF 4 SPIKES AT THE DISCRETION OF THE WENODE LOCATION OF SPIKES OPTIONAL

Part No	SSC 850322	Rev	1
Part Name	Thermal Shield	Quantity	
Part Description		Material	
Part Drawing		Part Status	

USE APPROVED PARTS LIST VERIFY APPROVED PARTS LIST FOR ALL PARTS USE APPROVED PARTS LIST FOR ALL PARTS		PART NO PART NAME PART STATUS
USE APPROVED PARTS LIST VERIFY APPROVED PARTS LIST FOR ALL PARTS USE APPROVED PARTS LIST FOR ALL PARTS	PART NO PART NAME PART STATUS	PART NO PART NAME PART STATUS
THERMAL SHIELD ASSY 20K - SSC MAGNET D14170 SSC 850322		



NOTES:

- 1 BREAK ALL SHARP EDGES AND REMOVE ALL BURRS
- 2 IDENTIFY PARTS BY VIDEO-CHECKING ONE NO AND DIMS AND USING .75 MESH SIZES LOCATION OPTIONAL
- 3 CLEAN USING LAMP FREE WIPERS SOAKED IN FREON 1F
- 4 WELDERS AND WELD PROCEDURES TO BE QUALIFIED PER ASME CODE SECTION IX OR AWS STD 248C
- 5 WELD USING 5556 FILLER WIRE

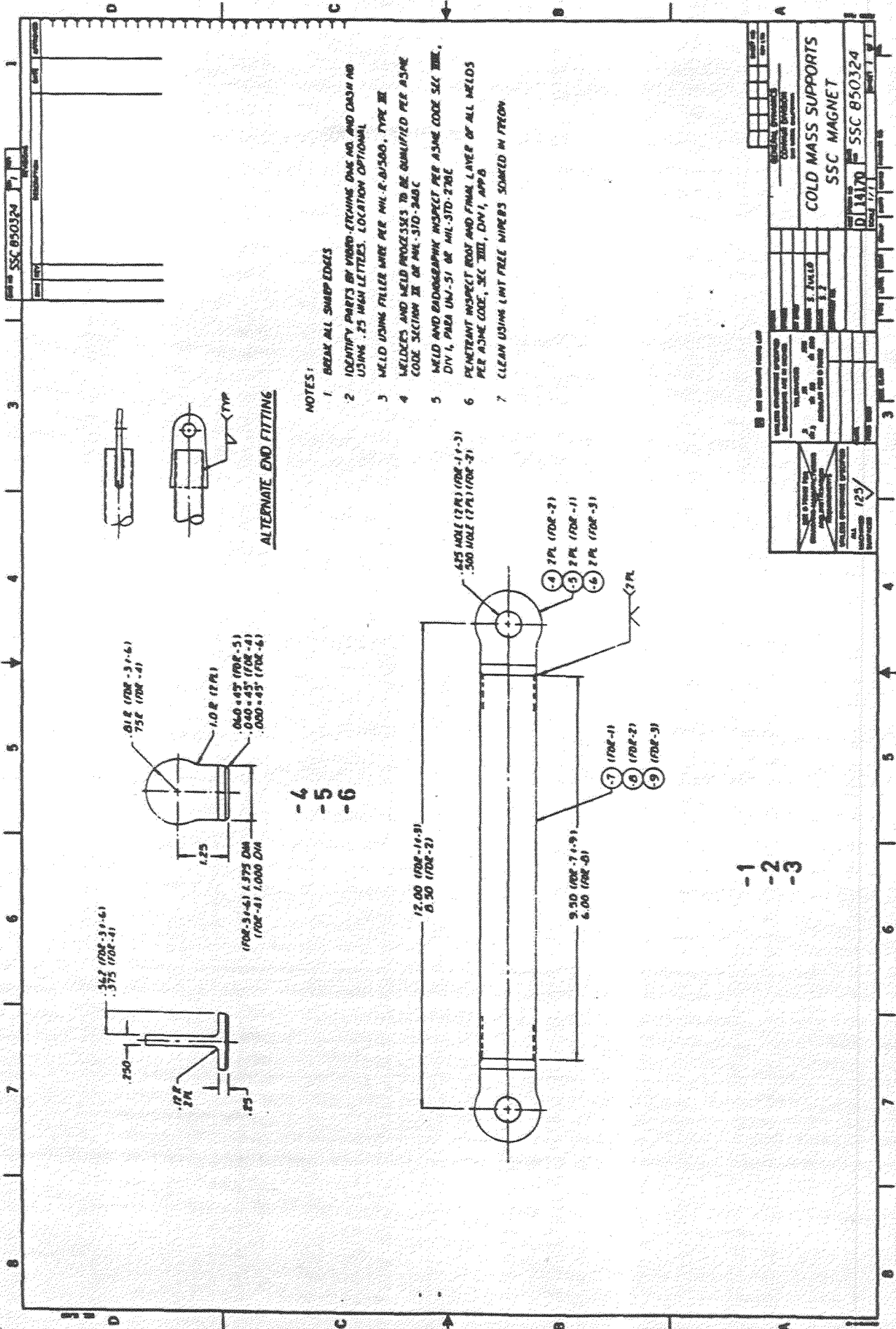
-1
-2

TYP BOTH ENDS

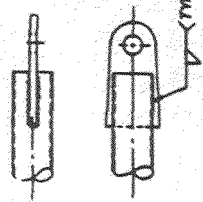
A-A
SCALE: 1/2

SSC P50323		REV	DATE	APPROVED
REV		DESCRIPTION	DATE	APPROVED
REV		DESCRIPTION	DATE	APPROVED
REV		DESCRIPTION	DATE	APPROVED
REV		DESCRIPTION	DATE	APPROVED

SEE SUPPLEMENT DRAWING FOR UNLESS OTHERWISE SPECIFIED DIMENSIONS ARE IN INCHES DECIMALS ARE TO BE TO 2 PLACES UNLESS OTHERWISE NOTED ANGLES TO NEAREST 5'		TYPICAL PART NUMBER 17-33
ALL DIMENSIONS UNLESS OTHERWISE SPECIFIED ARE TO BE TO 2 PLACES UNLESS OTHERWISE NOTED		TYPICAL PART NUMBER 17-33
THERMAL SHIELD ASSY BOK - SSC MAGNET		TYPICAL PART NUMBER 17-33
SSC P50323		TYPICAL PART NUMBER 17-33



ALTERNATE END FITTING



NOTES:

1. BREAK ALL SHARP EDGES
2. IDENTIFY PARTS BY MICRO-ETCHING DIA NO. AND DATE IN NO USING .25 HIGH LETTERS. LOCATION OPTIONAL
3. WELD USING FILLER WIRE PER MIL-R-61500, TYPE III
4. WELDERS AND WELD PROCESSES TO BE QUALIFIED PER ASME CODE SECTION IX OF MIL-STD-246C
5. WELD AND RADIOGRAPHY INSPECT PER ASME CODE SEC III, DIV 1, PARA UW-51 OR MIL-STD-228E
6. PENETRANT INSPECT ROOT AND FINAL LAYER OF ALL WELDS PER ASME CODE, SEC III, DIV 1, APP B
7. CLEAN USING LINT FREE WIPEES SOAKED IN PERON

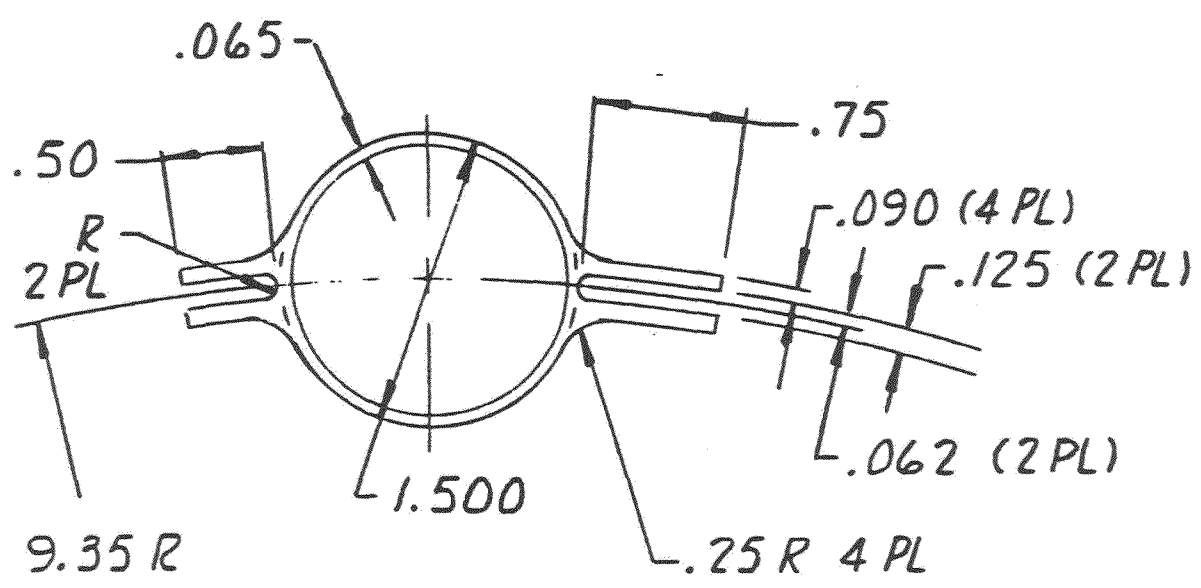
-4
-5
-6

-1
-2
-3

SSC 850324		REV		DATE	
COLD MASS SUPPORTS		SSC 850324		REV 1	
SSC MAGNET		REV 1		DATE	
DESIGNED BY		CHECKED BY		DATE	
DRAWN BY		APPROVED BY		DATE	
MATERIAL		QUANTITY		DATE	
FINISH		TOLERANCES		DATE	
TOLERANCES		SURFACE FINISH		DATE	
WELDING		INSPECTION		DATE	
PAINT		MARKING		DATE	
PACKAGING		STORAGE		DATE	
SHIPPING		RECEIVING		DATE	
DISPOSITION		REWORK		DATE	
REVISIONS		APPROVALS		DATE	
125		ALL DIMENSIONS IN INCHES		DATE	

A-23

REVISIONS			
LTR	DESCRIPTION	DATE	APPROVED



MATL: 6061-T6 AL ALY, QQ-A-200/16

SHEET	DASH NO.	LTR										

REVISION LETTER

SHEET CONTROL (READ UP)

ASSOCIATED LIST REQD. SEE DOCUMENT SAME NO. PREFIXED PLD FOR PARTS LIST ULD FOR USAGE LIST

SEE 0-70902 FOR STD MANUFACTURING AND INSTALLATION REQUIREMENTS

SEE 0-70914 FOR ABBREVIATION, CODE AND SYMBOL REQUIREMENTS

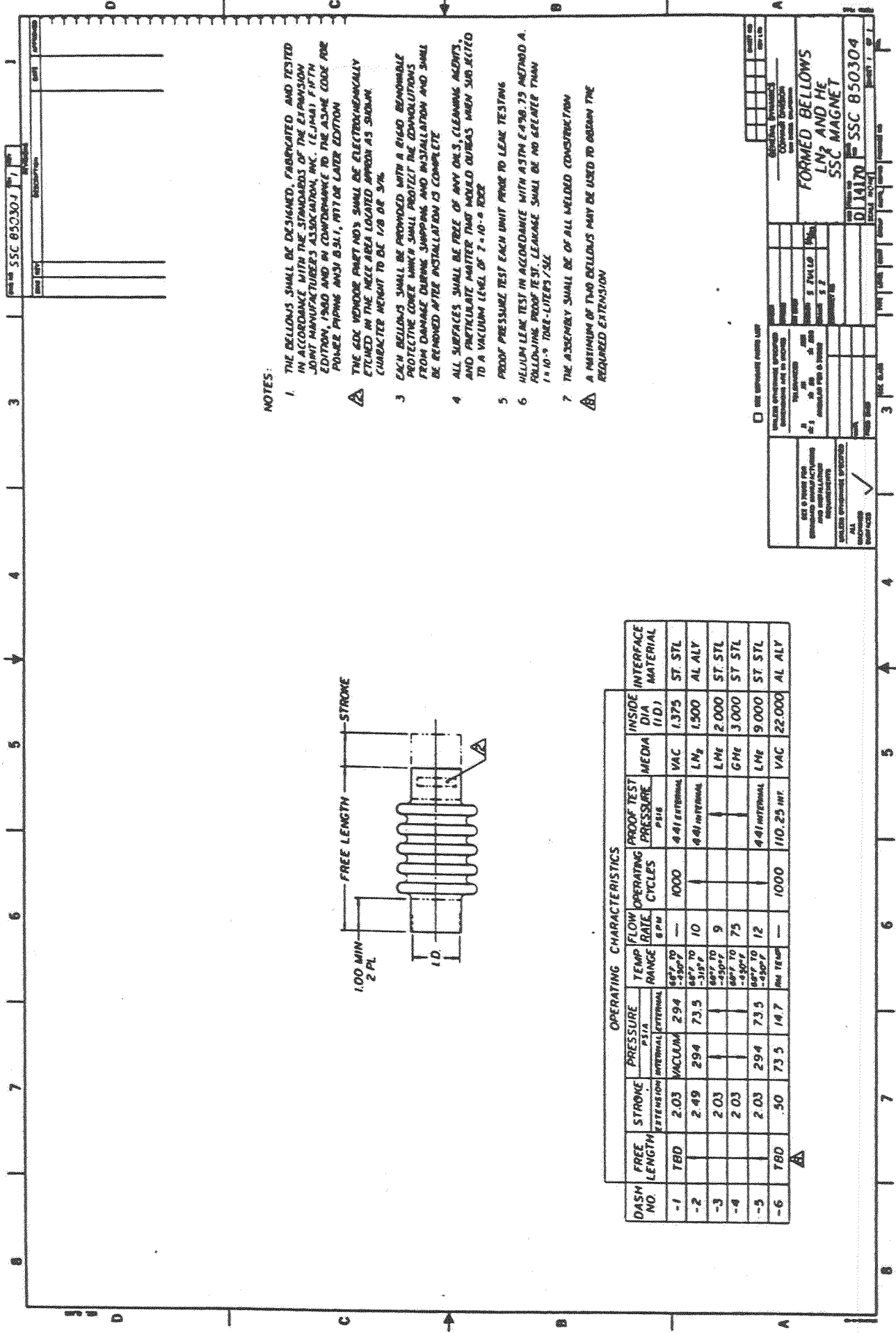
	GR ENGR
	DESIGN S. ZULLO
	DRAWN S. Z.
MATL	CONTRACT NO.
PROD. ENGR	
CHECK	
STRESS	

CONVAIR DIVISION OF GENERAL DYNAMICS
SAN DIEGO, CALIFORNIA

TUBE - EXTRUDED SHAPE

SIZE	CODE IDENT	DRAWING NO.
A	14170	SSC 850327
SCALE	NONE	REL
SHEET 1 OF 1		

PACKAG



NOTES:

1. THE BELLOWS SHALL BE DESIGNED, FABRICATED AND TESTED IN ACCORDANCE WITH THE STANDARDS OF THE EXPANSION JOINT MANUFACTURERS ASSOCIATION, INC. (EJMA) FIFTH EDITION, 1960 AND IN CONFORMANCE TO THE ASME CODE FOR POWER PIPING ANSI B.31.1, M11 OR LATER EDITION.
2. THE END WINDUP PART NO'S SHALL BE ELECTROCHEMICALLY ETCHEN IN THE NEAR AREA LOCATED APPROX AS SHOWN. CHARACTER HEIGHT TO BE 1/8 OR 3/16.
3. EACH BELLOWS SHALL BE PROVIDED WITH A RIGID BENDABLE PROTECTIVE COVER WHICH SHALL PROTECT THE CONJUNCTIONS FROM DAMAGE DURING SHIPPING AND INSTALLATION AND SHALL BE REMOVED AFTER INSTALLATION IS COMPLETE.
4. ALL SURFACES SHALL BE FREE OF ANY OILS, CLEANING AGENTS, AND PARTICULATE MATTER THAT WOULD OUBRAS WHEN SUBJECTED TO A VACUUM LEVEL OF 2 x 10⁻⁴ TORR.
5. PROOF PRESSURE TEST EACH UNIT PRIOR TO LEAK TESTING.
6. HELIUM LEAK TEST IN ACCORDANCE WITH ASTM E 498.75 METHOD A. FOLLOWING PROOF TEST. LEAKAGE SHALL BE NO GREATER THAN 1 x 10⁻⁵ TORR-LITERS/SEC.
7. THE ASSEMBLY SHALL BE OF ALL WELDED CONSTRUCTION.

▲ A MINIMUM OF TWO BELLOWS MAY BE USED TO OBTAIN THE REQUIRED EXTENSION

OPERATING CHARACTERISTICS

DASH NO.	FREE LENGTH	STROKE EXTENSION	PRESSURE PSIA		TEMP RANGE	FLOW RATE GPM	OPERATING CYCLES	PROOF TEST PRESSURE PSIA	MEDIA	INSIDE DIA (I.D.)	INTERFACE MATERIAL
			INTERNAL	VACUUM							
-1	TBD	2.03	294	294	86°F TO -150°F	—	1000	4.41 INTERNAL	VAC	1.375	ST. STL
-2		2.49	294	294	86°F TO -150°F	10		4.41 INTERNAL	LM ₂	1.500	AL ALY
-3		2.03			86°F TO -150°F	9			LM ₂	2.000	ST. STL
-4		2.03			86°F TO -150°F	75			GM ₂	3.000	ST. STL
-5		2.03	294	294	86°F TO -150°F	12		4.41 INTERNAL	LM ₂	9.000	ST. STL
-6	TBD	.50	73.5	147	PM ₂ TEMP	—	1000	110.25 INT.	VAC	22.000	AL ALY

☐ USE APPROXIMATE WEIGHT LIST

SEE DRAWING FOR DIMENSIONS AND MATERIALS REQUIREMENTS

ALL UNLESS OTHERWISE SPECIFIED

FORMED BELLOWS
LM₂ AND HE
SSC MAGNET

SSC 850304

10/14/70

PARTS LIST

0-70916 REQUIRED FOR ABBREVIATION, CODE AND SYMBOL INTERPRETATION

CONVAIR DIVISION OF GENERAL DYNAMICS
SAN DIEGO, CALIFORNIA

PDA **PL SSC 850205** REV LTR

TITLE **MLI BLANKETS ~ SSC MAGNET** PADR RELEASE DATE CODE IDENT NO **14170** SH **1** OF **1** SWS

DOC TYPE DOC OPT DOC CONT GROUP **673-2** REPRO CODE CONTRACT NO. UNDIM DWG
 DRAFTSMAN DESIGNER **2/5 35 GR ENGR S. ZULLO** STRESS PROD. ENGR MATERIAL CHECKER

DISTRIBUTION CODE PACKAGE NO. NOTE SYMBOL: * D - DOCUMENT NO. G - GENERAL NOTE M - MATERIAL N - REF DESIG U - USAGE DATA
 E - END ITEM L - LIMIT R - NOMENCLATURE T - TYPE DESIG/VALUE V - VENDOR ITEM

REQUIREMENTS PER ASSY/INSL	UNIT OF MEAS	FIND NO.	CODE IDENT NO.	PART OR IDENTIFYING NUMBER	NOMENCLATURE OR DESCRIPTION	ZONE		NOTE SYM *	NOTES
						L	R		
-2	-1			-1	BLANKET				
				-2	BLANKET				
2	2	LAYER		-3	EXTERIOR LAYER			M	LAMINATE COMPOSED OF .25 MIL MIN. TO 1.0 MIL MAX TYPE S ALUMINIZED MYLAR, .6 OZ/SQYD DACRON SCRIM (12x6 LENO WEAVE) AND .50 MIL MIN TO 1.0 MIL MAX TYPE S ALUMINIZED MYLAR, BONDED TOGETHER WITH A THERMOPLASTIC POLYESTER ADHESIVE. THE ALUMINIZED SURFACES OF THE MYLAR ARE EXPOSED BOTH SIDES
19	29	LAYER		-4	SEPARATOR NET			M	40 DENIER DACRON NET, NOMINAL 53 MESHES PER SQ IN, 6.6 MIL THK, .18 OZ PER SQ YD; SCAURED WITH HEAT-SET RESINLESS FINISH
18	28	LAYER		-5	REFLECTOR			M	.25 MIL MIN TO 1.0 MIL MAX MYLAR, TYPE S, ALUMINIZED BOTH SIDES
AR	AR			-6	LAYER TIE-DOWN			M	VENDOR OPTION. GDC APPROVAL REQ'D

APPENDIX B

EDDY CURRENT DURING
MAGNET DISCHARGE

Report Number SSC-LBL-306-RWB
1 May 1985

B.1 INTRODUCTION. Eddy current analysis is presented in this report in Section 3 and this appendix contains the listing, a sample of data input and a sample of data output. The analysis is based on the assumption that shield self-field is negligible to the magnet external field.

B.2 PROGRAM LISTING.

```

10 CLS
20 DIM B(50,50),CUR(50,50),SAFE(50,50)
30 DIM KURH(50,50),KURV(50,50)
40 REM read plate width and length
50 HEAD$="                I N P U T   D A T A   "
60 PRINT:PRINT:PRINT:PRINT
70 HEAD1$="      Enter Shield Width      ="
80 HEAD2$="      Enter Shield Length     ="
90 HEAD4$="      Enter Shield Diameter   ="
100 HEAD5$="      ENTER SHIELD THICKNESS ="
110 HEAD6$="      Enter Shield Resistivity="
120 PRINT HEAD1$;:INPUT"";WEDTH
130 PRINT HEAD2$;:INPUT"";LENTH
140 PRINT HEAD4$;:INPUT"";DIAMETER
150 PRINT HEAD5$;:INPUT"";THICK
160 PRINT HEAD6$;:INPUT"";RESIS
170 INPUT"";DUMMY#
180 READ BA
190 REM READ NUMBER OF GRIDS
200 CLS
210 HEADER$="      " x      y      J(x)      J(y)      Fr      Ftheta      Fz"
220 PRINT HEADERS#
230 LPRINT HEADERS#
240 PRINT
250 READ MW,ML:DW=WEDTH/MW:DL=LENTH/ML
260 RW=DW*RESIS/DL/THICK:RL=DL*RESIS/DW/THICK
270 READ ERR#
280 FOR I=1 TO MW:FOR J=1 TO ML:GOSUB 830:B(I,J)=DL*DW*BE
290 SAFE(I,J)=1
300 NEXT J:NEXT I
310 REM
320 CUR(1,1)=(B(1,1)+CUR(1,2)*RW+CUR(2,1)*RL)/(1.5*RL+1.5*RW)
330 FOR I=2 TO MW-1
340 CUR(I,1)=(B(I,1)+CUR(I+1,1)*RL+CUR(I-1,1)*RL+CUR(I,2)*RW)/(1.5*RW+2*RL)
350 NEXT I
360 CUR(MW,1)=(B(MW,1)+CUR(MW,2)*RW+CUR(MW-1,1)*RW)/(1.5*RL+1.5*RW)
370 FOR J=2 TO ML-1
380 CUR(1,J)=(B(1,J)+CUR(2,J)*RL+CUR(1,J-1)*RW+CUR(1,J+1)*RW)/(1.5*RL+2*RW)
390 FOR I=2 TO MW-1
400 CUR(I,J)=(B(I,J)+CUR(I-1,J)*RW+CUR(I+1,J)*RW+CUR(I,J-1)*RL+CUR(I,J+1)*RL)/
2*RL+2*RW)
410 NEXT I
420 CUR(MW,J)=(B(MW,J)+CUR(MW-1,J)*RW+CUR(MW,J-1)*RL+CUR(MW,J+1)*RL)/(1.5*RL+2*
RW)
430 NEXT J
440 CUR(1,ML)=(B(1,ML)+CUR(1,ML-1)*RL+CUR(2,ML)*RW)/(1.5*RL+1.5*RW)
450 FOR I=2 TO MW-1
460 CUR(I,ML)=(B(I,ML)+CUR(I+1,ML)*RL+CUR(I-1,ML)*RL+CUR(I,ML-1)*RW)/(1.5*RW+2*
L)
470 NEXT I
480 CUR(MW,ML)=(B(MW,ML)+CUR(MW-1,ML)*RL+CUR(MW,ML-1)*RW)/(1.5*RW+1.5*RL)
490 SUM=0

```

```

500 FOR I=1 TO MW:FOR J=1 TO ML
510 SUM=SUM+(CUR(I,J)-SAFE(I,J))^2:SAFE(I,J)=CUR(I,J)
520 NEXT J
530 NEXT I
540 SUM=SQR(SUM/MW/ML)
550 IF SUM > ERRR GOTO 310
560 REM shield currents
570 FOR I=1 TO MW
580 KURV(I,1)=CUR(I,1):NEXT I
590 FOR I=1 TO ML:KURH(1,I)=CUR(1,I):NEXT I
6600 FOR J=0 TO ML
610 FOR I=1 TO MW
620 KURV(I,J+1)=CUR(I,J+1)-CUR(I,J)
630 NEXT I
640 NEXT J
650 FOR J=1 TO ML
660 FOR I=0 TO MW
670 KURH(I+1,J)=CUR(I+1,J)-CUR(I,J)
680 NEXT I
690 NEXT J
700 FOR J=1 TO ML+1
710 X=(J-1)*DL
720 ANGEL=.5*(.5*LENTH-ABS(J-.5*ML)*DL)/DIAMETER
730 BR=BA*COS(ANGEL):BTH=BA*SIN(ANGEL)
740 FOR I=1 TO MW+1
750 Y=(I-1)*DW
760 FR=BTH*KURV(I,J):FTHETA=BR*KURV(I,J):FZ=BR*KURH(I,J)
770 PRINT USING" ##.## ##.## #####.## #####.## ####.## ####.## ####.##
;X,Y,KURH(I,J),KURV(I,J),FR,FTHETA,FZ
780 LPRINT USING" ##.## ##.## #####.## #####.## ####.## ####.## ####.##
";X,Y,KURH(I,J),KURV(I,J),FR,FTHETA,FZ
790 NEXT I
800 PRINT
810 NEXT J
820 END
830 ANGEL=.5*(.5*LENTH-ABS(J-.5*ML)*DL)/DIAMETER
840 BR=BA*COS(ANGEL)
850 RETURN

```

B.3 DATA INPUT SAMPLE.

```

Enter Shield Width      =? .39
Enter Shield Length     =? .39
Enter Shield Diameter   =? .4
ENTER SHIELD THICKNESS =? .0025
Enter Shield Resistivity=? 5e-7

```

B.4 AN OUTPUT SAMPLE.

x	y	J(x)	J(y)	Fr	Ftheta	Fz
0.00	0.00	23.57	23.57	1.12	23.55	23.55
0.00	0.04	8.23	31.80	1.51	31.76	8.22
0.00	0.08	5.60	37.40	1.78	37.36	5.60
0.00	0.11	3.51	40.91	1.94	40.86	3.50
0.00	0.15	1.70	42.60	2.02	42.56	1.70
0.00	0.19	0.02	42.62	2.02	42.58	0.02
0.00	0.23	-1.66	40.96	1.94	40.91	-1.66
0.00	0.27	-3.48	37.48	1.78	37.44	-3.48
0.00	0.30	-5.59	31.89	1.51	31.85	-5.59
0.00	0.34	-8.24	23.65	1.12	23.62	-8.23
0.00	0.38	-23.65	0.00	0.00	0.00	-23.62
0.04	0.00	31.76	8.19	0.78	8.15	31.62
0.04	0.04	11.42	11.38	1.08	11.37	11.37
0.04	0.08	7.89	13.67	1.30	13.61	7.86
0.04	0.11	4.97	15.14	1.44	15.07	4.95
0.04	0.15	2.42	15.86	1.50	15.79	2.41
0.04	0.19	0.03	15.87	1.51	15.80	0.03
0.04	0.23	-2.37	15.16	1.44	15.10	-2.36
0.04	0.27	-4.94	13.71	1.30	13.64	-4.92
0.04	0.30	-7.88	11.42	1.08	11.37	-7.84
0.04	0.34	-11.43	8.22	0.78	8.19	-11.38
0.04	0.38	-31.87	0.00	0.00	0.00	-31.73
0.08	0.00	17.31	5.54	0.79	5.49	17.31
0.08	0.04	13.70	7.82	1.11	7.74	13.56
0.08	0.08	9.59	9.52	1.35	9.42	9.49
0.08	0.11	6.09	10.63	1.51	10.53	6.03
0.08	0.15	2.97	11.19	1.59	11.07	2.94
0.08	0.19	0.03	11.19	1.59	11.08	0.03
0.08	0.23	-2.91	10.65	1.51	10.54	-2.88
0.08	0.27	-6.05	9.54	1.36	9.45	-5.99
0.08	0.30	-9.58	7.85	1.11	7.77	-9.48
0.08	0.34	-13.71	5.56	0.79	5.51	-13.58
0.08	0.38	-37.44	0.00	0.00	0.00	-37.06
0.11	0.00	40.74	3.44	0.65	3.37	40.01
0.11	0.04	15.15	4.89	0.92	4.80	14.88
0.11	0.08	10.70	6.00	1.13	5.90	10.51
0.11	0.11	6.83	6.75	1.27	6.63	6.71
0.11	0.15	3.34	7.12	1.34	6.99	3.28
0.11	0.19	0.04	7.12	1.34	6.99	0.03
0.11	0.23	-3.28	6.76	1.28	6.63	-3.22
0.11	0.27	-6.79	6.02	1.14	5.91	-6.66
0.11	0.30	-10.69	4.91	0.93	4.82	-10.49
0.11	0.34	-15.17	3.45	0.65	3.39	-14.90
0.11	0.38	-40.89	0.00	0.00	0.00	-40.15
0.15	0.00	42.40	1.66	0.39	1.61	41.21
0.15	0.04	15.87	2.37	0.56	2.31	15.42
0.15	0.08	11.26	2.92	0.69	2.84	10.94
0.15	0.11	7.20	3.30	0.78	3.20	7.00
0.15	0.15	3.53	3.48	0.82	3.39	3.43
0.15	0.19	0.04	3.48	0.82	3.39	0.04
0.15	0.23	-3.46	3.30	0.78	3.21	-3.36
0.15	0.27	-7.16	2.93	0.69	2.85	-6.96
0.15	0.30	-11.24	2.38	0.56	2.31	-10.92
0.15	0.34	-15.89	1.66	0.39	1.62	-15.44
0.15	0.38	-42.55	0.00	0.00	0.00	-41.36
0.19	0.00	42.47	0.07	0.01	0.07	41.71
0.19	0.04	15.89	0.09	0.02	0.09	15.60
0.19	0.08	11.27	0.10	0.02	0.10	11.06
0.19	0.11	7.21	0.10	0.02	0.10	7.08
0.19	0.15	3.53	0.11	0.02	0.11	3.47

0.19	0.27	-7.16	0.09	0.02	0.09	-7.04
0.19	0.30	-11.25	0.08	0.02	0.08	-11.05
0.19	0.34	-15.90	0.06	0.01	0.06	-15.62
0.19	0.38	-42.62	0.00	0.00	0.00	-41.85
0.23	0.00	40.89	-1.58	0.22	-1.57	40.47
0.23	0.04	15.20	-2.27	-0.32	-2.25	15.05
0.23	0.08	10.73	-2.80	-0.40	-2.77	10.61
0.23	0.11	6.85	-3.16	-0.45	-3.13	6.78
0.23	0.15	3.55	-3.35	-0.48	-3.31	3.31
0.23	0.19	0.03	-3.35	-0.48	-3.32	0.03
0.23	0.23	-3.29	-3.17	-0.45	-3.14	-3.26
0.23	0.27	-6.81	-2.82	-0.40	-2.79	-6.74
0.23	0.30	-10.72	-2.28	-0.32	-2.26	-10.61
0.23	0.34	-15.22	-1.60	-0.23	-1.58	-15.06
0.23	0.38	-41.02	0.00	0.00	0.00	-40.60
0.27	0.00	37.48	-3.41	-0.32	-3.39	37.31
0.27	0.04	13.76	-4.85	-0.46	-4.83	13.70
0.27	0.08	9.63	-5.95	-0.56	-5.92	9.59
0.27	0.11	6.11	-6.69	-0.63	-6.66	6.09
0.27	0.15	2.98	-7.05	-0.67	-7.02	2.97
0.27	0.19	0.03	-7.06	-0.67	-7.03	0.03
0.27	0.23	-2.93	-6.70	-0.64	-6.67	-2.92
0.27	0.27	-6.08	-5.97	-0.57	-5.94	-6.05
0.27	0.30	-9.62	-4.87	-0.46	-4.85	-9.57
0.27	0.34	-13.77	-3.43	-0.33	-3.41	-13.71
0.27	0.38	-37.59	0.00	0.00	0.00	-37.42
0.30	0.00	31.93	-5.55	-0.26	-5.54	31.89
0.30	0.04	11.48	-7.83	-0.37	-7.82	11.47
0.30	0.08	7.94	-9.52	-0.45	-9.51	7.93
0.30	0.11	5.00	-10.64	-0.51	-10.63	4.99
0.30	0.15	2.43	-11.19	-0.53	-11.18	2.42
0.30	0.19	0.02	-11.20	-0.53	-11.18	0.02
0.30	0.23	-2.39	-10.65	-0.51	-10.64	-2.38
0.30	0.27	-4.97	-9.55	-0.45	-9.54	-4.97
0.30	0.30	-7.92	-7.86	-0.37	-7.85	-7.92
0.30	0.34	-11.49	-5.57	-0.26	-5.57	-11.48
0.30	0.38	-32.02	0.00	0.00	0.00	-31.78
0.34	0.00	23.70	-8.23	0.00	-8.23	23.70
0.34	0.04	3.28	-11.43	0.00	-11.43	3.28
0.34	0.08	5.64	-13.73	0.00	-13.73	5.64
0.34	0.11	3.53	-15.20	0.00	-15.20	3.53
0.34	0.15	1.71	-15.92	0.00	-15.92	1.71
0.34	0.19	0.01	-15.93	0.00	-15.93	0.01
0.34	0.23	-1.66	-15.22	0.00	-15.22	-1.66
0.34	0.27	-3.51	-13.76	0.00	-13.76	-3.51
0.34	0.30	-5.63	-11.47	0.00	-11.47	-5.63
0.34	0.34	-8.28	-8.26	0.00	-8.26	-8.26
0.34	0.38	-23.76	0.00	0.00	0.00	-23.76
0.38	0.00	0.00	-23.70	1.13	-23.62	0.00
0.38	0.04	0.00	-31.96	1.52	-31.94	0.00
0.38	0.08	0.00	-37.62	1.79	-37.57	0.00
0.38	0.11	0.00	-41.14	1.95	-41.10	0.00
0.38	0.15	0.00	-42.85	2.03	-42.80	0.00
0.38	0.19	0.00	-42.86	2.04	-42.81	0.00
0.38	0.23	0.00	-41.16	1.96	-41.14	0.00
0.38	0.27	0.00	-37.68	1.79	-37.63	0.00
0.38	0.30	0.00	-32.04	1.52	-32.01	0.00
0.38	0.34	0.00	-23.76	1.13	-23.73	0.00
0.38	0.38	0.00	0.00	0.00	0.00	0.00